

Institut für Biomedical Engineering
Abteilung für Medizintechnik und Regenerative Medizin

**Ultraviolet A/Riboflavin Crosslinked Collagen and
Multiple Bioactive Ion Capsules for Enhanced Bone
Tissue Engineering**

**Thesis submitted as a requirement to fulfill the degree
of “Doctor of Philosophy” in *Experimental Medicine*
(PhD)**

**at the
Faculty of Medicine
Eberhard Karls Universität
Tübingen**

presented by

Fan, Lu

2025

Dean: Professor Dr. B. Pichler

1st reviewer: Professor Dr. K. Schenke-Layland

2nd reviewer: Professor Dr. U. Rothbauer

Date of oral examination: 18.11.2024

Table of Contents

Abbreviations	iii
List of Figures and Tables	viii
1. Introduction.....	1
1.1 Collagen and Bone.....	2
1.1.1 Collagen in Native Bone Tissue.....	2
1.1.2 Bone and Bone Defects.....	4
1.1.3 Bone Repair and Healing.....	6
1.2 Bone Tissue Engineering	8
1.2.1 The Development of Bone Tissue Engineering	8
1.2.2 Key Factors for Successful Bone Tissue Engineering	9
1.2.3 Advanced Strategies in Bone Tissue Engineering	11
1.3 Collagen as a Scaffold for Supporting Bone Regeneration	13
1.4 Collagen Crosslinking Techniques	14
1.5 Ultraviolet A and Riboflavin Crosslinking.....	18
1.6 Bioactive Substances for Improving Biofunctionalities of Collagen-based Scaffolds.....	21
1.6.1 Strategies for Bioactive Integration in Collagen-based Scaffolds	21
1.6.2 Bioactive Ions as Functional Enhancers in Collagen-Based Scaffolds.....	23
1.7 Objectives	25
2. Results	29
2.1 Evaluation of Injectable Composite Material Comprising Biphasic Bone Substitutes and Crosslinked Collagen.....	29
2.1.1 Summary and Major Findings.....	29
2.1.2 Personal Contribution	31

2.2	Deciphering UVA/Riboflavin Collagen Crosslinking: A Pathway to Improve Biomedical Materials	42
2.2.1	Summary and Major Findings.....	42
2.2.2	Personal Contribution	44
2.3	Encapsulated Vaterite-Calcite CaCO ₃ Particles Loaded with Mg ²⁺ and Cu ²⁺ Ions with Sustained Release Promoting Osteogenesis and Angiogenesis.	60
2.3.1	Summary and Major Findings.....	60
2.3.2	Personal Contribution	62
3.	Discussion and Outlook	80
3.1	Refining UVA/R Crosslinking Process for Specific Collagen Systems	80
3.2	Unraveling the Mechanisms of UVA/R Collagen Crosslinking.....	83
3.3	Impact of UVA/R Crosslinking on Collagen Matrix Properties	86
3.4	UVA/R vs. Chemical Crosslinking: A Comparative Analysis	88
3.5	Bioactive Ion Encapsulation System for Enhancing Osteogenesis and Angiogenesis.....	90
3.6	Outlook.....	94
4.	Summary	97
5.	Zusammenfassung.....	99
6.	References	101
7.	Declaration.....	117
8.	Author Contribution	118
9.	Acknowledgements.....	121
10.	Appendix	124
10.1	Ethical Statement	124
10.2	Proof of Author Contribution Agreement	124

Abbreviations

$^1\text{O}_2$	singlet oxygen
$^3\text{R}^*$	triplet activate state riboflavin
ACC	amorphous calcium carbonate
ALP	alkaline phosphatase
ALPL	alkaline phosphatase (gene)
APTES	(3-aminopropyl)triethoxysilane
BBS	biphasic bone substitutes
BGLAP	bone gamma-carboxyglutamate protein; osteocalcin (gene)
BGs	bioactive glasses
BMBF	Federal Ministry of Education and Research
BMP-2	bone morphogenetic protein-2
BMPs	bone morphogenetic proteins
BrdU	bromodeoxyuridine
BS	bone substitutes
BTE	bone tissue engineering
CCK-8	cell counting kit-8
CD	circular dichroism
Col	non-crosslinked collagen
COL1A1	collagen type I alpha 1 chain (gene)
COL1A2	collagen type I alpha 2 chain (gene)
CSC	China Scholarship Council
DAS	dialdehyde starch

DHT	dehydrothermal treatment
DOPA	3,4-dihydroxy-L-phenylalanine
DSC	differential scanning calorimetry
ECM	extracellular matrix
EDC	1-ethyl-3-(3-dimethylaminopropyl)carbodiimide
EDS	energy dispersive X-Ray analysis
FDA	United States Food and Drug Administration
FITC	fluorescein isothiocyanate
G'	storage modulus
G''	loss modulus
GAG	glycosaminoglycan
GAPDH	glyceraldehyde 3-phosphate dehydrogenase (gene)
GPC	gel permeation chromatography
HA	hydroxyapatite
HAc	acetic acid
HIF1A	hypoxia-inducible factor 1-alpha (gene)
HO ₂ '	hydroperoxyl radical
HPLC	high-performance liquid chromatography
ICP-OES	inductive coupled plasma-optical emission spectroscopy
LbL	layer by layer
LC-MS	liquid chromatography-mass spectrometry
LVER	linear viscoelastic range
MAPK/ERK	mitogen-activated protein kinase/ extracellular signal-regulated kinase

MMP1	matrix metalloproteinase 1
MRM	multiple reaction monitoring
MSCs	mesenchymal stem cells
NC	negative control
NHS	N-Hydroxysuccinimide
OPN	osteopontin
PAH	poly(allylaminehydrochloride)
PBS	phosphate-buffered saline
PC	positive control
PCA	principal component analysis
PCL	polycaprolactone
P-col	porcine skin-derived collagen
PEI	polyethyleneimine
PEM	polyelectrolyte multilayer
PLA	polylactic acid
PLGA	poly(lactic-co-glycolic acid)
PMNs	polymorphonuclear leukocytes
pNPP	p-nitrophenyl phosphate
PSS	poly(sodium 4-styrene-sulfonate)
QCM	quartz crystal microbalance
R	ground state riboflavin
R*	excited state riboflavin
RANKL	receptor activator of nuclear factor kappa-B ligand
R-col	rat tail-derived collagen

RGD	arginyl-glycyl-aspartic acid
RH	general structure representing a hydrogen donor
ROS	reactive oxygen species
R _{ox}	oxidized form of riboflavin
RUNX2	runt-related transcription factor 2 (gene)
SDS-PAGE	sodium dodecyl-sulfate polyacrylamide gel electrophoresis
SEC	size exclusion chromatography
SHG	second harmonic generation
TGF- β	transforming growth factor-beta
T _m	denaturation temperature
UV	ultraviolet
UVA/R	ultraviolet A and riboflavin
VEGF	vascular endothelial growth factor
VEGFA	vascular endothelial growth factor (gene)
Wnt	Wingless-related integration site
xCol	crosslinked collagen
Xcol_EDC/NHS	EDC/NHS crosslinked collagen
Xcol_Genipin	genipin crosslinked collagen
Xcol_UVA/R	UVA and riboflavin crosslinked collagen
XTT	methoxynitrosulfophenyl-tetrazolium carboxanilide
β -TCP	β -tricalcium phosphate
ΔD	dissipation change
Δf	frequency shift

ΔH	enthalpy change
Δm	mass of adsorbed polyelectrolyte

List of Figures and Tables

Figure 1. Hierarchical structure of type I collagen fiber and human bone.....	2
Figure 2. The illustration of bone healing stages after a fracture.....	6
Figure 3. The key factors contributing to successful bone tissue engineering (BTE), highlighting the importance of material properties, biological factors, and cellular interactions in the development of effective bone scaffolds.....	11
Figure 4. Mechanisms of representative collagen chemical crosslinking.....	14
Figure 5. Mechanisms of representative enzymatic crosslinking methods.....	15
Figure 6. Representative physical crosslinking mechanisms.....	16
Figure 7. Chemical structures and distribution of promising sites of UVA/R crosslinking in porcine type I collagen.....	19
Figure 8. Excitation of riboflavin (under UVA irradiation) and the two possible reaction mechanisms.....	20
Figure 9. The multifaceted roles of various ions across processes like immunoregulation, osteoinduction, osteogenesis, angiogenesis and tissue vascularization in bone healing and tissue engineering.....	24
Figure 10. Flowchart or project methodology, progression, and outcomes.....	27
Table 1. Frequently applied bioactive ions in bone healing: effective concentrations and material ion release profiles.....	92

CHAPTER 1

INTRODUCTION

1. Introduction

Collagen, a fundamental building block of the mammal body, was named from the Greek word "κόλλα" in the late 16th century, meaning glue, reflecting its role in binding tissues together in the body (Mosleh et al., 2023). A breakthrough in the understanding of collagen came with the work of G.N. Ramachandran in the 1950s, who first discovered the structure for collagen, known as "Madra's triple helix" (Ramachandran and Kartha, 1955). Following Ramachandran's discovery, there has been extensive research on collagen, leading to a deeper understanding of its various types, functions, and roles in the human body. In particular, type I collagen in bones provides mechanical strength and plays a crucial role in healing and regenerating bone tissue. Current research is delving deeper into the expansive realm of collagen, aiming to enhance our knowledge of the fundamental biological and chemical characteristics, alongside its processing and medical applications. The exploration continues to extend the applications in regenerative medicine and its involvement of collagen in various diseases. The ongoing studies not only seek to expand our understanding of collagen's intrinsic properties but also to explore innovative ways to harness its potential in medical and therapeutic contexts. In bone tissue engineering (BTE), collagen's significance transcends mere structural support; it is instrumental in mineralization and guiding the cellular processes crucial for bone healing and remodeling.

1.1 Collagen and Bone

1.1.1 *Collagen in Native Bone Tissue*

In the bone matrix, collagen, especially type I, accounts for 90% of the non-mineralized components and is essential to bone structure and function (Thompson and Hing, 2004). Arrays of tropocollagen molecules (300 nm long, 1.25 nm wide, mass 285 kDa), each consisting of three left-handed chain assemblies, are carefully arranged in collagen fibrils and fibers (Shoulders and Raines, 2009). As illustrated in **Figure 1**, these chains are stabilized by hydrogen bonds that are rich in amino acids such as glycine, proline, and

hydroxyproline, bounded together in a right-handed triple helix. The repeating of G-X-Y sequences is crucial for the formation of the triple helix (Mogilner et al., 2002), providing structural stability and flexibility necessary for the bone to resist mechanical stress (Kramer et al., 1999). Groups of five tropocollagen molecules are organized into microfibrils by a $\frac{3}{4}$ stagger, parallel array. Collagen microfibrils form naturally into fibrils and fibers, stretching up to a centimeter long and a millimeter thick, and are distinguished by a 67 nm banding pattern known as the D-period (Shoulders and Raines, 2009). The organization of these collagen fibers varies within the bone: larger fibers align parallel in the outer cortical layer, while smaller, crisscrossing fibers predominate in the inner cancellous layer (Georgiadis et al., 2016). Hydroxyapatite nanocrystals, contributed by osteoblasts to the collagen fibers, form the composite bone matrix, enhancing mechanical properties like impact resistance and load distribution (Fan et al., 2023b).

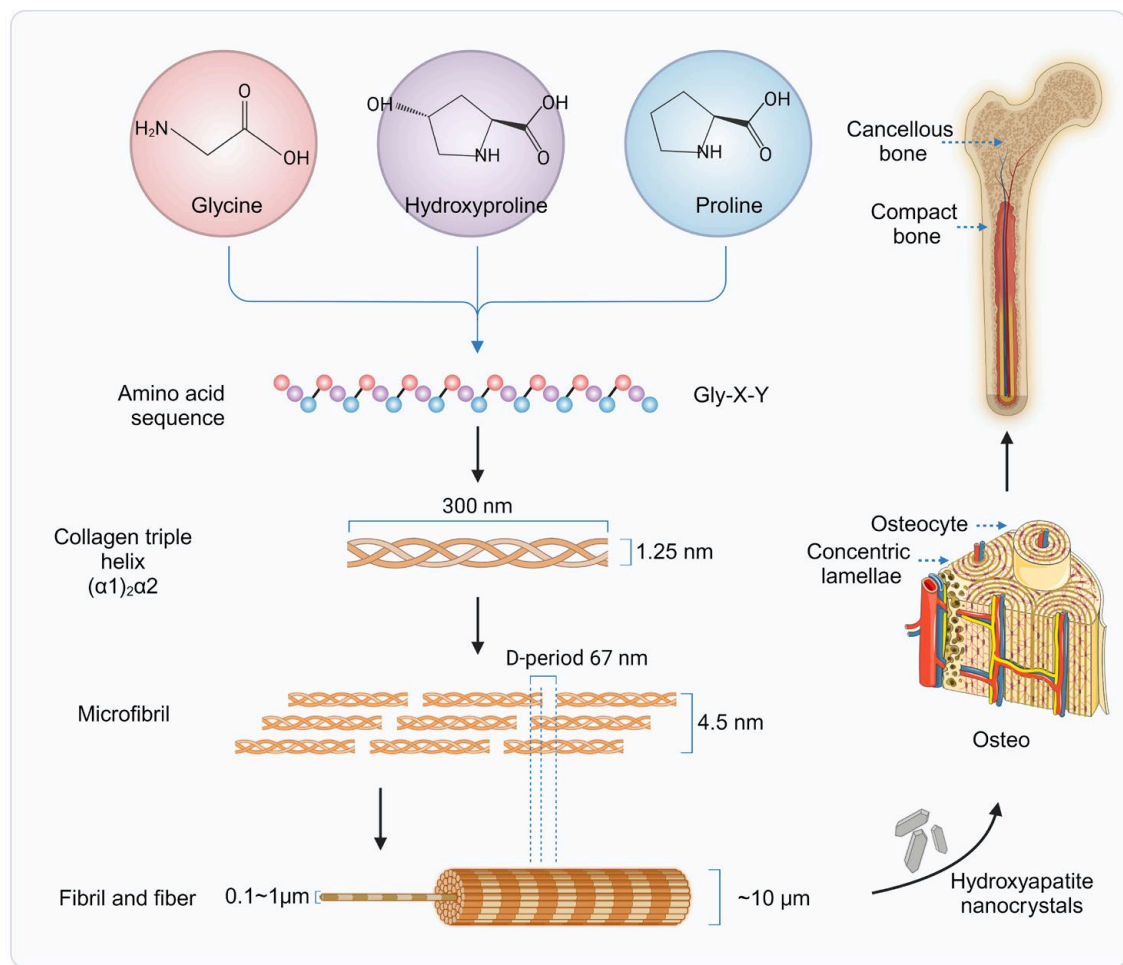


Figure 1. Hierarchical structure of type I collagen fiber and human bone. This schematic diagram was graphically processed based on our previous study (Fan et al., 2023b). Graphic elements were generated by *Servier Medical Art* (provided by *Servier*, licensed under a *Creative Commons Attribution 4.0 Unported License*) and *Biorender.com*.

Beyonds providing the mechanical strength and framework necessary for bone integrity, type I collagen also engages in critical interactions with bone cells such as mesenchymal stem cells (MSCs), osteoblasts and osteoclasts, playing pivotal role in bone biological dynamics. These interactions are facilitated through integrin binding sites on the collagen molecules, notably through sequences like RGD and GFOGER, which promote cell adhesion, migration, and signaling pathways crucial for bone formation and remodeling (Taubenberger et al., 2010, Wojtowicz et al., 2010). While direct binding sites for growth factors and cytokines on type I collagen are less defined, the collagen matrix plays an indirect yet pivotal role in modulating the activity of these signaling molecules. The degradation of collagen, for instance, can release matrix-bound growth factors, thus influencing their concentration and activity in the bone microenvironment (Minor and Coulombe, 2020). Moreover, the mechanical properties of the collagen matrix, influenced by its density and organization, contribute to the regulation of cellular behavior through mechanotransduction pathways (Zhou et al., 2021). This intricate interaction network is vital for maintaining the balance between bone formation and resorption, with collagen's structural and biochemical properties collectively orchestrating bone remodeling and repair processes. The inherent properties of collagen in native bone underscore its potential in BTE.

1.1.2 Bone and Bone Defects

The human skeletal system, a marvel of natural engineering, is predominantly and averagely composed of 206 bones, a dynamic and complex tissue that serves multiple critical functions (Hart et al., 2020). Beyond providing structural support and protection for internal organs, bones are vital for movement, mineral storage, and housing bone marrow, which is essential for blood cell production (Su et al., 2019). Bone's remarkable ability to repair and regenerate itself is a testament to its complexity, involving a sophisticated interplay of cells,

signaling molecules, and the extracellular matrix, primarily type I collagen (Lin et al., 2020b).

The regenerative capabilities of bone, though remarkable, are not limitless. Large or complex bone defects—stemming from trauma, tumor resections, congenital anomalies, or diseases such as osteoporosis—present significant challenges, often surpassing the bone's natural capacity for healing and leading to conditions like non-union or delayed healing (Szwed-Georgiou et al., 2023). Such bone defects constitute a major global health concern, impacting millions annually. Notably, it is estimated that worldwide, over 2 million bone grafting procedures are performed each year, with approximately half a million of these occurring in the United States, predominantly for orthopedic and dental applications (Gillman and Jayasuriya, 2021). In Germany, osteoporosis prevalence stands at 8% among women and 2% among men over the age of 45, with the country housing more than 6.3 million osteoporosis patients (Andrich et al., 2021). Meanwhile, over 160 million individuals in China are affected by osteoporosis, according to the Chinese Center for Disease Control and Prevention (Cheng et al., 2021).

These statistics emphasize the critical demand for innovative solutions in bone repair and healing. The challenge extends to finding effective approaches that can accommodate the intricate dynamics of bone regeneration, catering to the varying severities and types of bone damage encountered clinically. This necessity drives the pursuit of advanced strategies in BTE and regenerative medicine aimed not just at filling defects but at actively promoting the regenerative processes inherent to the bone. Research is increasingly focusing on understanding the mechanisms underlying bone repair and how these can be supported or enhanced through intervention. This includes exploring the roles of various biomaterials, bioactive molecules, and cellular therapies in facilitating bone regeneration, with an emphasis on ensuring compatibility with the body's natural healing processes and minimizing the risk of rejection or complications. Optimizing these approaches for practical application holds the promise of significantly improving therapeutic outcomes for individuals suffering

from bone-related ailments, thereby enhancing their quality of life and addressing a crucial global health issue.

1.1.3 Bone Repair and Healing

The natural process of bone repair and healing is a finely tuned physiological event, showcasing the body's remarkable ability to regenerate. This process is a sophisticated orchestration of biological events, typically occurs in several distinct but overlapping stages (Guo and DiPietro, 2010) (**Figure 2**):

- **Hemostasis and inflammation:** immediately following a fracture or bone injury, blood vessels rupture, leading to the formation of a hematoma (blood clot). The resultant hypoxic environment within the hematoma is crucial for cell activation, migration, and differentiation. Beyond serving as a provisional three-dimensional matrix for repair cells, hematoma also releases cytokines and growth factors, triggering an inflammatory response that is crucial for initiating the healing process (Schell et al., 2017).
- **Soft callus formation:** within a few days post-injury, fibroblasts and MSCs populate the fracture site, replacing hematoma with fibrin-rich granulation tissue, primarily composed of collagen and fibrocartilage. This granulation tissue not only provides a conducive microenvironment for angiogenesis and chondrogenesis, essential for soft callus formation at the fracture site ends but also sets the stage for subsequent endochondral ossification (Guo and DiPietro, 2010).
- **Hard callus formation:** MSCs gradually differentiate into osteoblasts, initiating intramembranous ossification and mineralization within soft callus to form hard callus. Hard callus is significantly more biomechanically stable than its soft counterpart, serves to tightly bridge the bone defect ends, making the latter stage to the repair phase (Maruyama et al., 2020).
- **Bone remodeling:** commencing 3 to 4 weeks post-fracture and potentially spanning several years, this final stage of bone defect healing involves both the resorption and formation of bone by osteoclasts and

osteoblasts, in accordance with Wolff’s law, which states that bone remodels in response to the mechanical loads it experiences. This remodeling process is pivotal for restoring the bone’s full biomechanical stability, ultimately reshaping the bone back to its original structure and strength as well as the restoration of the bone’s functionality (Rowe et al., 2018).

While the bone’s natural repair mechanisms are adept at managing small fractures and injuries, their efficiency significantly wanes when faced with larger or more complex defects. Furthermore, certain pathological conditions, such as osteoporosis, diabetes mellitus type II, autoimmune disorder like rheumatoid arthritis, and the natural aging process can drastically impair or completely halt the spontaneous healing process (Hoff et al., 2017). Orthopedic surgery is often challenged by segmental bone defects, non-unions, and compound fractures, which present complex issues including substantial bone loss, compromised blood supply, heightened risk of infection, and the critical need for precise stabilization (Adamczyk et al., 2020). These multifaceted challenges highlight the crucial need for advanced medical interventions, which typically encompass bone grafting, surgical stabilization, and, in instances of infection, prompt antibiotic treatment and surgical debridement to prevent further complications.

In response to these challenges, BTE emerges as a pivotal field, offering innovative solutions for bone defect repair.

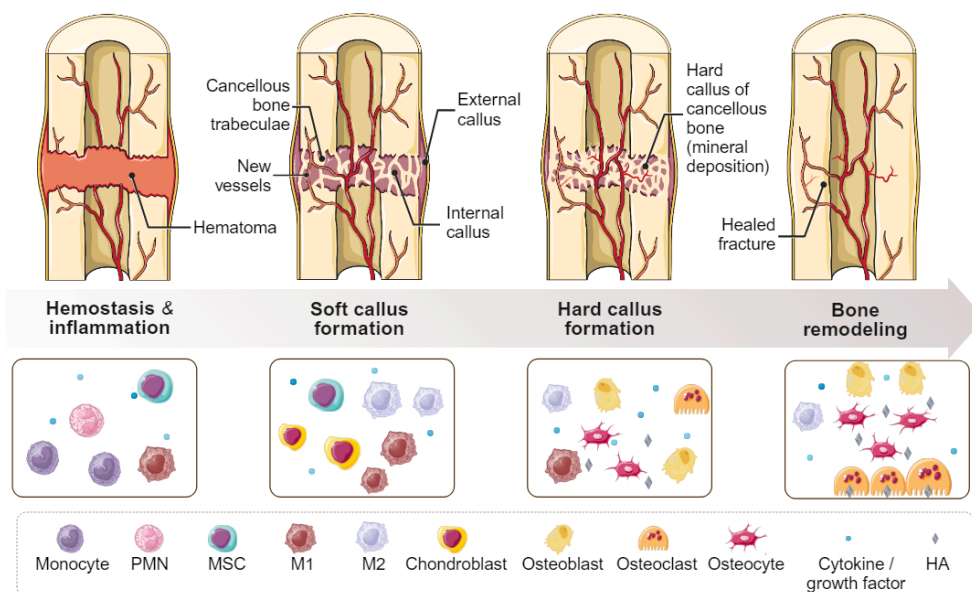


Figure 2. The illustration of bone healing stages after a fracture: **(1)** Hemostasis & inflammation phase: immediately after the fracture, blood vessels are damaged leading to a hematoma, which provides a matrix for new tissue. Various cell types like monocytes, polymorphonuclear leukocytes (PMNs), and mesenchymal stem cells (MSCs) migrate to the area, marking the beginning of the inflammatory phase. **(2)** Soft callus formation: as inflammation subsides, fibrocartilaginous callus forms. MSCs differentiate into chondroblasts forming a soft callus. This is also where macrophages play a role in both the inflammatory response (M1) and tissue repair (M2). **(3)** Hard callus formation: osteoblasts create new bone, converting the soft callus into a hard callus, while osteoclasts resorb excess bone. During this stage, hydroxyapatite (HA), a mineral essential for bone strength, is deposited. **(4)** Bone remodeling: the final stage where the structure of the bone is refined. Osteoclasts and osteoblasts work together to remodel the hard callus into mature lamellar bone, with osteocytes maintaining the bone matrix and hydroxyapatite providing strength and rigidity. This schematic diagram was graphically processed based on previous studies (Pfeiffenberger et al., 2021, Wang and Yeung, 2017). Graphic elements were generated by *Servier Medical Art* (provided by Servier, licensed under a *Creative Commons Attribution 4.0 Unported License*) and *Biorender.com*.

1.2 Bone Tissue Engineering

1.2.1 The Development of Bone Tissue Engineering

The journey of BTE is a testament to humanity's enduring quest to mend what nature struggles to repair on its own. Tracing its origins to the 17th century, the field's rudimentary beginnings were marked by the pioneering efforts of Dutch surgeon Job Van Meekeren (Raymond J Fonseca, 2017). In those early days, the concept and practice of bone repair were primitive, relying on basic surgical techniques and a limited understanding of bone regeneration and healing processes. As centuries unfolded, BTE underwent transformative growth, fueled by an ever-deepening comprehension of bone biology, alongside the advent of novel materials and the seamless integration of burgeoning technologies into the fabric of medical practice.

The 20th century, in particular, heralded a watershed moment for BTE, marked by the introduction of biocompatible materials designed to act as scaffolds, thereby laying the groundwork for the growth of new bone tissue (Zhu et al., 2021, Desai and Hubbell, 1991). This era saw researchers embark on a quest to explore an array of substances—ranging from natural and synthetic polymers to ceramics and composites—in pursuit of the ideal amalgam of durability, flexibility, and biocompatibility (Desai and Hubbell, 1991, Dillow and Tirrell, 1998). In the present day, BTE stands as a vibrant interdisciplinary field

that merges biomaterials, living cells, and bioactive molecules to create constructs that do more than merely support—they actively facilitate the genesis of new bone (Alonzo et al., 2021). By adeptly mimicking the natural environment of bone, these engineered tissues are tailored to enhance the integration and proliferation of new bone cells, thus presenting a formidable challenge to the constraints of conventional bone repair methodologies.

1.2.2 Key Factors for Successful Bone Tissue Engineering

Achieving success in BTE is contingent upon a multidisciplinary fusion of insights from biology, materials science, engineering, and medicine. It hinges on several key factors that govern the interaction between biomaterials and the biological environment. These factors are crucial in ensuring the successful integration of engineered scaffolds with native bone tissue, facilitating bone repair and regeneration. The ensuing sections delineate the pivotal factors instrumental to the triumph of BTE endeavors (**Figure 3**):

- **Initial cell response:** the surface properties of the material, including its chemistry (bioactive chemical groups, e.g., -OH, -COOH, -NH₂), topography and roughness (micro- and nano-scale), can influence initial cell attachment and behavior (Anselme et al., 2011). This includes the attachment of osteoprogenitor cells and their subsequent proliferation and differentiation into osteoblasts (Anselme et al., 2011). The efficacy of biomaterials such as collagen, with its excellent cell-binding properties, is crucial for supporting a more robust and well-integrated bone formation.
- **Osteoconduction:** a process in which a scaffold or structure facilitates the growth of new bone tissue by providing a surface on which bone-forming cells can migrate, adhere and form new bone (Di Silvio and Jayakumar, 2009). It essentially acts as a guide for the natural bone growth process and facilitates the scaffold's amalgamation with the adjacent bone tissue (Zhu et al., 2022). Materials designed to be osteoconductive, such as calcium phosphates and collagen, provide a scaffold that has similar composition and structure to native bone, supporting the growth of new bone tissue from the edges of the existing

bone into the scaffold (Zhu et al., 2022). The porosity of the material is crucial, allowing for cell and blood vessel infiltration, which is essential for the integration of the new bone with the existing bone (Spece et al., 2020).

- **Osteoinduction:** a process that stimulates stem cells to differentiate into bone-forming cells, culminating in the creation of new skeletal tissue (Albrektsson and Johansson, 2001). This process is crucial for bone healing and regeneration, especially in areas where bone is not naturally present. Biomaterials can be engineered to be osteoinductive by incorporating biological factors like BMPs and bioactive cations that stimulate the differentiation of MSCs into bone-forming cells (Oliveira et al., 2021). This early induction of osteogenesis is vital for ensuring that new bone tissue forms and integrates effectively with the host bone.
- **Biodegradation rate:** the optimal biodegradation rate for a scaffold should align with the pace of new bone growth, guaranteeing that the scaffold supports the regenerative process effectively. This ensures that the scaffold provides support during the early stages of healing but gradually transfers the load to the newly formed bone, facilitating integration. While collagen is a favored material due to its natural properties, it tends to degrade too quickly, potentially compromising scaffold stability before adequate bone formation. Synthetic polymers like polycaprolactone (PCL) and poly(lactic-co-glycolic acid) (PLGA) offer the advantage of greater stability and regulated biodegradation, ensuring they support bone growth without compromising structural integrity too early (Makadia and Siegel, 2011). However, these synthetic options often elicit a less favorable initial cellular response compared to collagen (Kyriakides et al., 2022), highlighting a critical area for material optimization in BTE.
- **Mechanical properties:** the congruence of a material's mechanical traits with those of the host bone is crucial for effective integration. Materials like bioactive glasses (BGs) and reinforced composites are scrutinized for their capability to align with bone's mechanical characteristics, which

helps prevent issues such as stress shielding or scaffold overload (Bellucci et al., 2015).

- **Vascularization:** materials like certain bioactive ceramics with proper porosity and mechanical strength are being extensively researched to promote angiogenesis and the formation of new blood vessels, ensure that the newly formed tissue is well-nourished and oxygenated, which is crucial for the survival of bone cells and the integration process (Wang et al., 2022).
- **Immunogenicity:** the use of biocompatible materials like collagen and alginate, known for their minimal response, is crucial, as inflammation can hinder the healing and integration processes (Ketabat et al., 2017).

These elements collectively underscore the complexity and multidisciplinary nature of BTE, highlighting the intricate balance between material properties and biological responses required to achieve successful outcomes in bone repair and regeneration.

1.2.3 Advanced Strategies in Bone Tissue Engineering

Following the delineation of key factors crucial for the success of BTE, the past decades have seen the emergence of advanced strategies that significantly enhance bone healing and regeneration. Central to these advancements are the contributions of materials science, which have led to the development of scaffolds that are biocompatible, osteoconductive, and, in some cases, osteoinductive (Oliveira et al., 2021). These scaffolds are essential for bone cells to infiltrate, proliferate, and differentiate, successfully replicating the intricate structure and function of natural bone (Gillman and Jayasuriya, 2021). Collagen-based scaffolds, in particular, have been highlighted for their compatibility with the organic component of the bone matrix, facilitating a conducive environment for cell attachment and the seamless integration of newly formed bone tissue (Fan et al., 2023b).

Furthermore, the strategic inclusion of bioactive ions, growth factors, and stem cell therapy within BTE constructs taps into the biological mechanisms of bone regeneration (Perez et al., 2015, Oliveira et al., 2021). Steering the

transformation of MSCs into osteoblasts and orchestrating the release of osteogenic factors, these approaches significantly bolster the regenerative potential of BTE constructs. As the field progresses, the synergy between innovative materials and these advanced technologies is paving the way for personalized, patient-specific treatments. Such methodologies promise to navigate the complexities of bone repair, providing superior outcomes and an enhanced quality of life for patients.

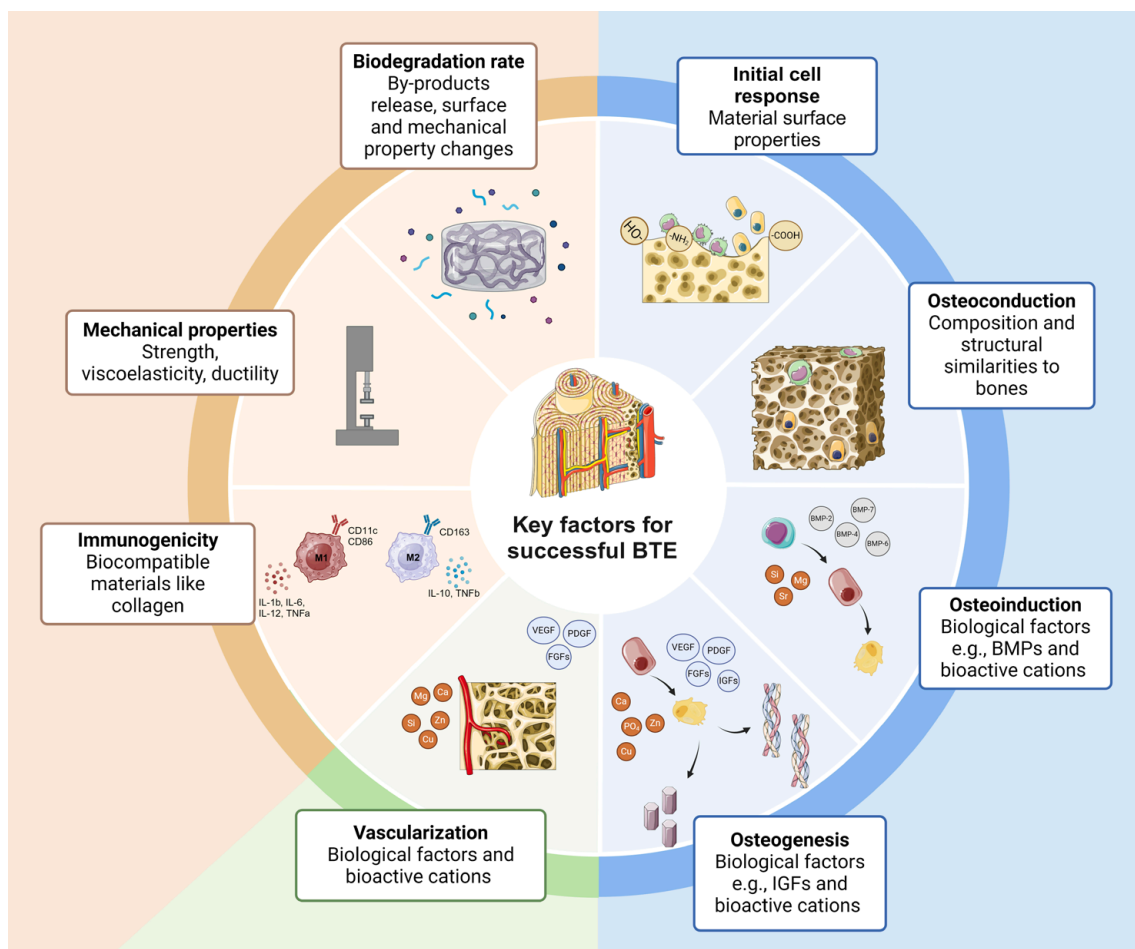


Figure 3. The key factors contributing to successful bone tissue engineering (BTE), highlighting the importance of material properties, biological factors, and cellular interactions in the development of effective bone scaffolds. Those critical factors include initial cell response, osteoconduction, osteoinduction, osteogenesis, vascularization, biodegradation, mechanical properties, and immunogenicity. Graphic elements were generated by *Servier Medical Art* (provided by *Servier*, licensed under a *Creative Commons Attribution 4.0 Unported License*) and *Biorender.com*.

1.3 Collagen as a Scaffold for Supporting Bone Regeneration

Collagen, as a scaffold material, stands at the forefront of supporting bone regeneration, embodying the convergence of natural biomimicry and engineering ingenuity. This protein, fundamental to the structure of the extracellular matrix, has been harnessed in BTE for its unparalleled biocompatibility and its intrinsic ability to enhance cell attachment, growth, and differentiation.

The strategic utilization of collagen scaffolds in BTE leverages not only the material's native structural characteristics but also its biochemical properties that are conducive to bone formation and healing (Li et al., 2021b). Collagen provides a physiologically familiar environment for bone cells, enhancing the scaffold's integration with the surrounding bone tissue and promoting effective bone regeneration. This integration is critical in applications ranging from filling small bone defects to facilitating the repair of substantial skeletal discontinuities, where the scaffold's role in guiding tissue growth becomes invaluable (Oosterlaken et al., 2021).

Another compelling attribute of collagen is its abundant availability from a wide range of sources, including bovine, porcine, and marine organisms, which provides a versatile foundation for scaffold development. Porcine-derived collagen, in particular, is preferred in BTE for its exceptional biocompatibility and low disease transmission risk, closely mirroring human collagen's amino acid composition, structure and functionality (Sharifi et al., 2019). Moreover, advancements in fabrication techniques have significantly enhanced the design and utility of collagen-based materials. Methods like lyophilization, electrospinning, and 3D bioprinting have been employed to create scaffolds with optimized porosity, mechanical strength, and architectural precision (Spece et al., 2020, Montalbano et al., 2021).

Nonetheless, the inherent physical and biochemical properties of collagen, on another hand, result in the limitations and challenges for collagen scaffolds' application. Collagen is naturally susceptible to enzymatic degradation by collagenases and other proteolytic enzymes present in the body,

as well as hydrolytic degradation (Bhagwat and Dandge, 2018). This causes rapid degradation rate of collagen, which can compromise scaffold stability before adequate bone formation. The fabrication techniques employed also directly affect the scaffold's mechanical properties and degradation behavior. Furthermore, while providing excellent matrices for cell attachment and proliferation due to their biocompatibility and bioactivity, collagen scaffolds do not inherently possess osteoinductive properties—essential for successful bone regeneration (Cunniffe and O'Brien, 2011).

To address these challenges, research has been directed towards crosslinking methods to enhance scaffold durability and mechanical strength. Additionally, strategies that incorporate bioactive substances for osteoinduction and agents to promote osteogenesis and angiogenesis are being explored to overcome collagen's biological limitations, thereby stimulating bone formation and vascularization, and enhancing the scaffold's regenerative potential.

1.4 Collagen Crosslinking Techniques

The evolution of collagen crosslinking techniques encapsulates a remarkable journey of scientific innovation, primarily aimed at optimizing collagen's utility in biomedical applications. Initially, traditional chemical crosslinking agents like formaldehyde and glutaraldehyde was prevalent, driven by the demand for durable collagen-based materials in medical implants and sutures (Cheung et al., 1985). However, growing concerns regarding cytotoxicity and long-term biocompatibility steered research towards alternative crosslinking methods, including enzymatic and natural agents. This progression has paralleled an enhanced understanding of collagen's molecular structure and the body's inherent crosslinking mechanisms. Below is a summary of different crosslinking methods along with their respective benefits and obstacles:

Chemical crosslinking commonly involves carbodiimide (e.g., 1-Ethyl-3-(3-dimethylaminopropyl)carbodiimide in combination with N-Hydroxysuccinimide, EDC/NHS), or another plant-derived crosslinker, genipin (**Figure 4**). These agents offer high crosslinking efficiency, improved stability, mechanical strength, and a controlled degradation rate. Nonetheless, despite

reduced cytotoxicity compared to glutaraldehyde, there remains a risk of residual chemicals in the collagen matrix, potentially leading to adverse biological responses (Islam et al., 2021). Moreover, excessive crosslinking or the use of certain chemical crosslinkers can alter collagen's natural structure, impacting cell and tissue interactions (Zhang et al., 2022b). Therefore, research is ongoing to develop more natural-derived agents, like dialdehyde starch (DAS), silane coupling agents (e.g., APTES), tannic acid, and other polyphenols, for effective crosslinking without compromising biocompatibility (Oryan et al., 2018).

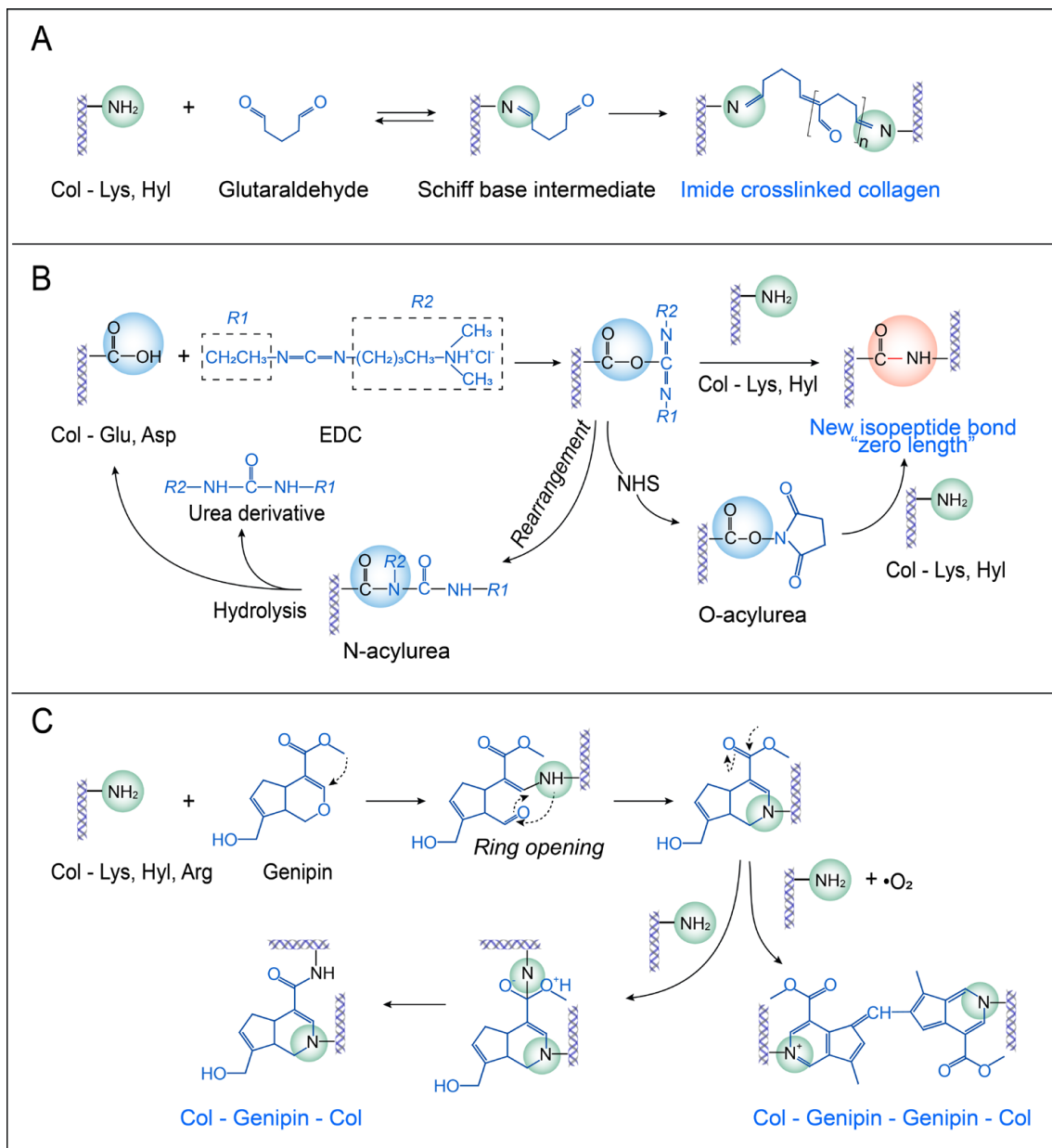


Figure 4. Mechanisms of representative collagen chemical crosslinking. **(A)** Glutaraldehyde crosslinking leads to imide crosslink formation (Olde Damink et al., 1995). **(B)** EDC/NHS mediated crosslinking results in a stable “zero length” isopeptide bond (Pieper et al., 2000). **(C)** Genipin-induced crosslinking through ring opening and subsequent crosslink formation (Butler et al., 2003).

Enzymatic crosslinking in collagen utilizes enzymes like transglutaminase, lysyl oxidase, tyrosinase, and laccase, offering significant advantages such as biocompatibility and a reduced likelihood of triggering immune responses, along with enabling controlled, uniform crosslinking (Adamiak and Sionkowska, 2020a) (**Figure 5**). However, this method encounters challenges including the high costs associated with enzymes, their sensitivity to environmental factors that can affect stability and activity, and the difficulty in achieving an optimal balance between crosslink density and the preservation of collagen's natural properties (Adamiak and Sionkowska, 2020a).

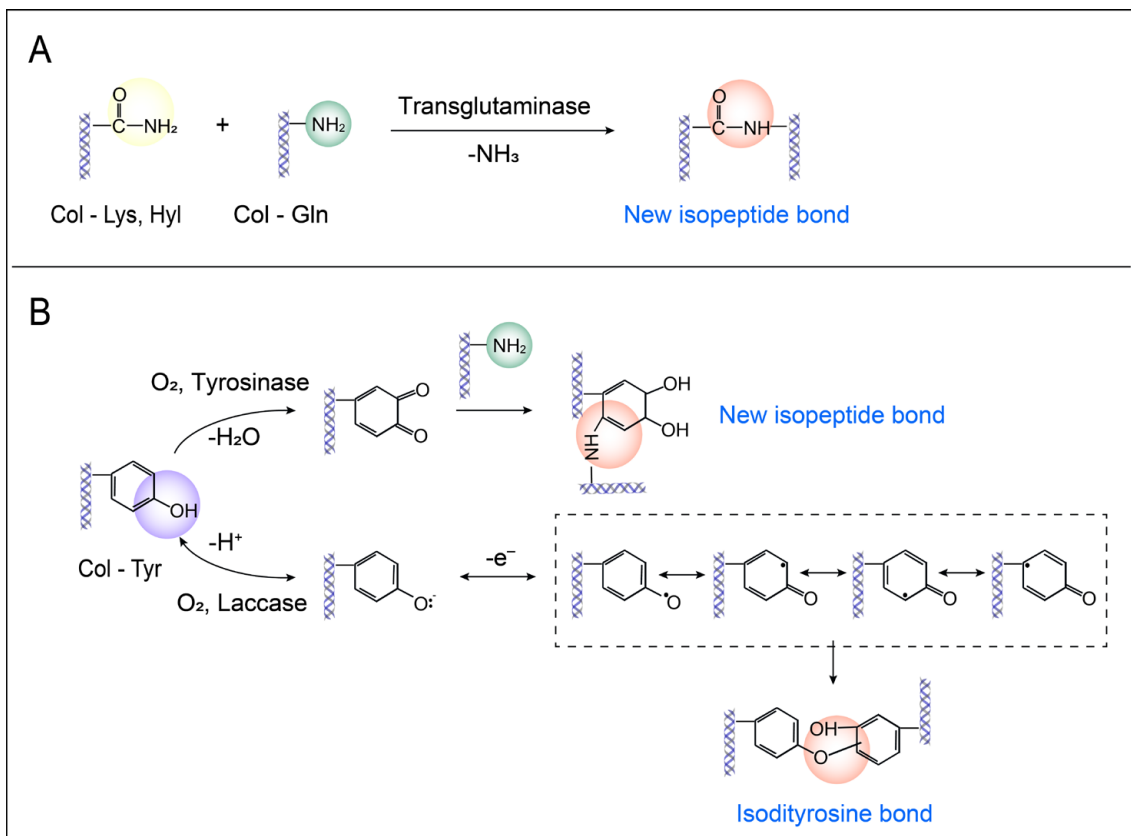


Figure 5. Mechanisms of representative enzymatic crosslinking methods. **(A)** Collagen crosslinking via transglutaminase, catalyzing the formation of an isopeptide bond between lysine and glutamine residues (Greenberg et al., 1991). **(B)** Oxidative collagen crosslinking, with tyrosinase or laccase enzymes, induces the formation of isopeptide and isodityrosine bonds, respectively (Jus et al., 2011).

Physical crosslinking techniques for collagen, encompassing dehydrothermal treatment (DHT), lyophilization, and various irradiation methods such as UV, gamma, and electron beam rays, offer a safer approach without addition of cytotoxic crosslinker (**Figure 6**). These methods are not only efficient and cost-effective, but also capable of creating porous structures advantageous for tissue engineering applications (Zhang et al., 2012). However, they pose challenges in balancing crosslinking efficiency against the potential risk of damaging collagen structure (Adamiak and Sionkowska, 2020a). Achieving the desired levels of strength and durability without compromising the integrity of collagen remains a critical area of focus in these physical crosslinking processes.

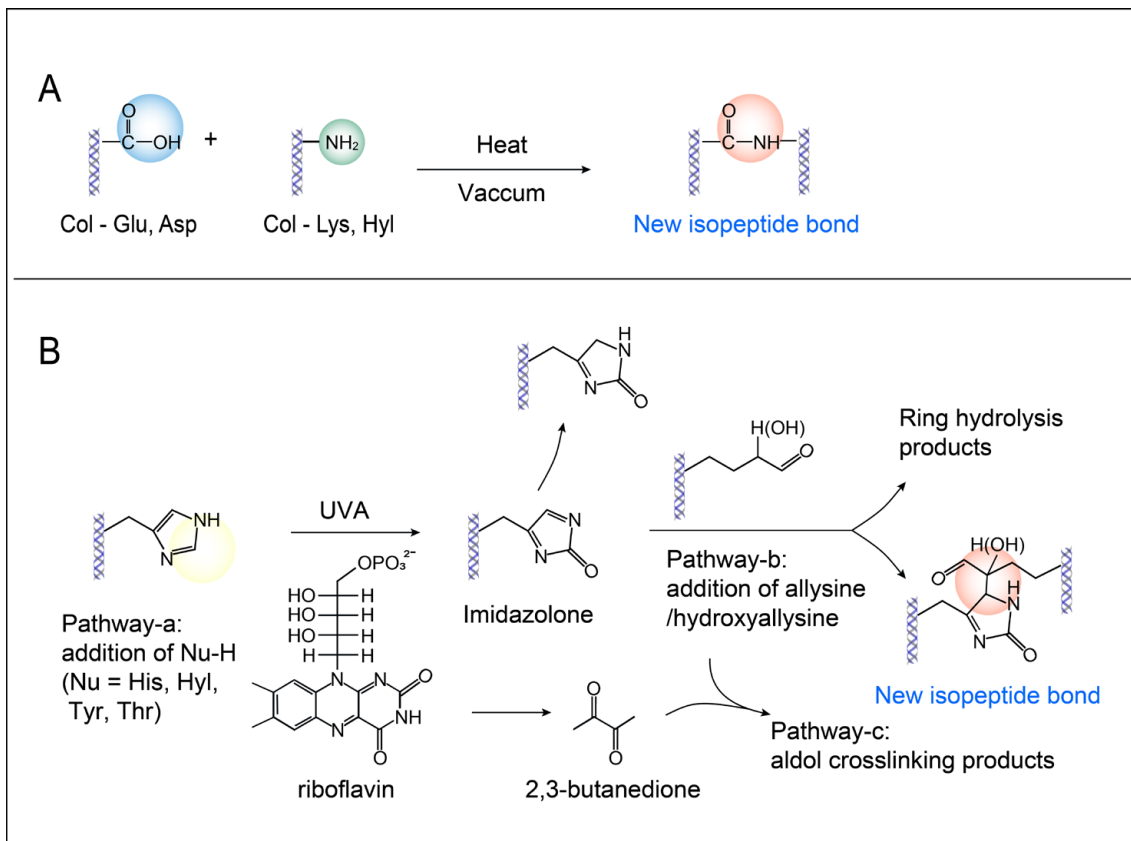


Figure 6. Representative physical crosslinking mechanisms. **(A)** DHT crosslinking pprocess. (Yannas and Tobolsky, 1967) **(B)** Proposed UVA/riboflavin collagen crosslinking mechanisms: Pathway-a is singlet oxygen-dependent, which produces imidazolone. This short-lived intermediate can then react with an uncapped nucleophile (Nu). Pathway-b invokes endogenous carbonyls (allsine) as a nucleophile in a subsidiary $1O_2$ -dependent pathway. Pathway-c suggests that a self-activation product of riboflavin, 2,3-butanedione could react strongly with endogenous carbonyls (McCall et al., 2010).

In summary, while various crosslinking techniques have significantly advanced the functionality of type I collagen in tissue engineering, each method presents its unique set of benefits and challenges. Balancing efficiency, biocompatibility, and safety, while preserving collagen's intrinsic properties, remains a key focus of ongoing research. Among these diverse techniques, one particularly innovative method stands out for its unique approach and potential in specific applications: UVA and riboflavin crosslinking. This method has garnered significant interest in recent years, especially in the field of ophthalmology, and is now being explored for its applications in broader tissue engineering contexts.

1.5 Ultraviolet A and Riboflavin Crosslinking

Ultraviolet A and riboflavin (UVA/R) crosslinking technique, initially developed for keratoconus treatment in ophthalmology by Professor Theo Seiler and Dr. Eberhard Spoerl at Dresden University of Technology in Germany during the late 1990s, represented a pivotal advancement in non-invasive eye treatments (Spoerl et al., 1998). Their pioneering work utilized riboflavin, a naturally occurring vitamin B2, in conjunction with UVA light to fortify collagen fibers within the cornea, demonstrating a significant leap forward in eye care (Spoerl et al., 1998). Since its inception, the application of this method has broadened significantly, crossing into various medical fields. In tissue engineering, it has led to the development of innovative hydrogels designed to reduce postoperative adhesions, offering promising implications for enhancing recovery from laparoscopic surgeries (Wu et al., 2022). Additionally, UVA/R crosslinked acellular porcine cornea are under investigation as potential scaffolds for the Boston Keratoprosthesis, underscoring advances in biocompatibility and efficiency (Li et al., 2022). The technique has also paved the way for novel approaches in 3D bioprinting and organ-on-chip systems, showcasing the extensive and dynamic potential of UVA/R crosslinking across the spectrum of modern biomedical innovations (Lin et al., 2020c, Zandrini et al., 2022, Zhang et al., 2022a).

The UVA/R crosslinking technique, promising for its medical and engineering applications, is hindered by incomplete understanding of its underlying mechanisms, building up barriers to clinical adoption and technological advancement. Central to the debate are the crosslinking sites on collagen, and riboflavin's role in this photocrosslinking process. Some researchers advocate for a non-selective crosslinking approach (Uemura et al., 2019, Zhang et al., 2011), others identify specific amino acids—such as lysine, histidine, arginine, tyrosine, methionine, tryptophan, and phenylalanine (**Figure 7**)—as key sites for crosslinking (Yamauchi and Shiiba, 2008, Sharif et al., 2017, Gabriela and Iulia, 2019, Fuentes-Lemus et al., 2018). Regarding riboflavin, the predominant theory suggests that riboflavin acts as a photosensitizer, generating reactive oxygen species (ROS) that promote collagen oxidation and subsequent polymerization, a process supported by numerous studies (Uemura et al., 2019, Kopsachilis et al., 2013, Raiskup and Spoerl, 2013). However, alternative perspectives argue for a more complex photochemical process that is significantly influenced by the presence of oxygen and/or the duration of UVA exposure (McCall et al., 2010, Sel et al., 2014) (**Figure 8**). This divergence in understanding highlights the challenges in establishing standardized manufacturing protocols and poses difficulties for regulatory evaluations of medical devices utilizing this technology.

Bridging these scientific gaps is critical for advancing the application of UVA/R crosslinking in collagen-based technologies. Our study aims to delve into the fundamental mechanisms of UVA/R crosslinking, exploring both established and alternative theories to shed light on the complex interactions between collagen and riboflavin. Such insights are crucial for refining and enhancing the technique's effectiveness. Nevertheless, investigating these mechanisms within collagen proves challenging due to the dynamic nature of photochemical processes and the molecular complexity of collagen itself (Uemura et al., 2019, Wollensak et al., 2003, Spoerl et al., 2007). To dissect these complex mechanisms, advanced experimental setups and thorough analytical techniques are indispensable for accurately discerning the transient states and pathways involved in the process (Adamiak and Sionkowska, 2020b,

Lin, 2018, Subasinghe et al., 2018). Moreover, the variability in collagen's properties—affected by its source, type, processing methods, and environmental conditions—introduces additional complexities to the study, demanding a sophisticated and nuanced investigative approach (Pehrsson et al., 2021, Gu et al., 2019, Patel et al., 2018, Bielajew et al., 2020, Ali et al., 2022). A comprehensive understanding of these crosslinking dynamics is essential for fostering the acceptance and clinical integration of UVA/R crosslinking techniques, representing a significant leap in the fields of biomedical engineering and regenerative medicine.

In essence, the UVA/R crosslinking method is distinguished by its innovative utilization of naturally occurring components and its promising potential across various biomedical applications. Addressing its present limitations and challenges is imperative for unlocking its full potential in regenerative medicine and tissue engineering, paving the way for groundbreaking advancements in these fields.

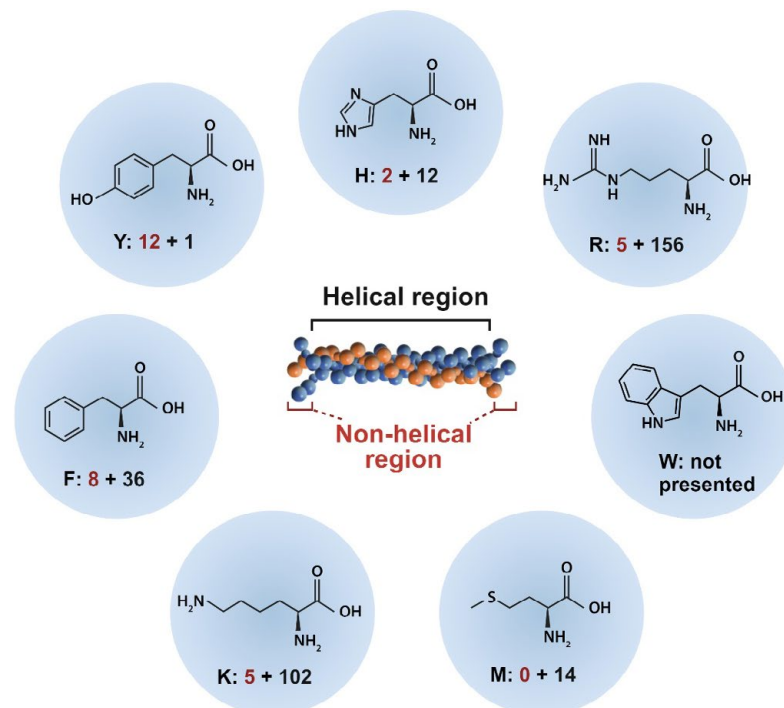


Figure 7. Chemical structures and distribution of promising sites of UVA/R crosslinking in porcine type I collagen. This figure illustrates the molecular structures of seven amino acids and quantifies their occurrence within the helical (marked in black) and non-helical regions (marked in red) of porcine type I collagen, referencing the amino acid sequence from Uniprot. Y (tyrosine), K (lysine), R (arginine), M (methionine), H (histidine), W (tryptophan, not present in porcine collagen type I), F (phenylalanine).

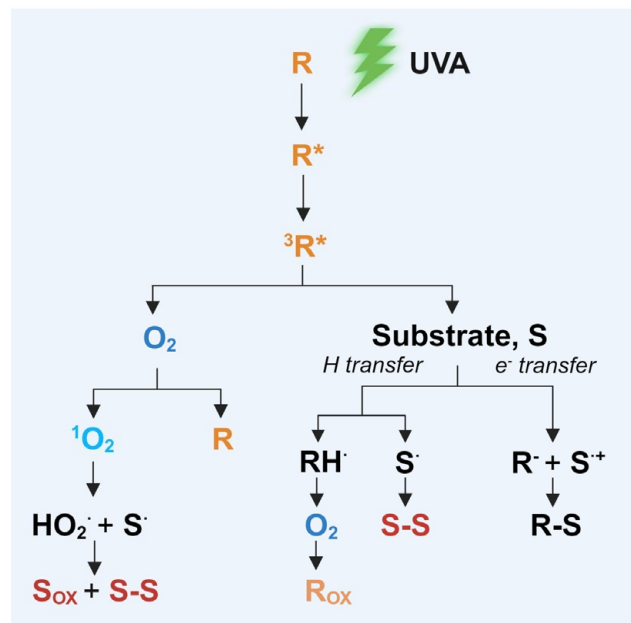


Figure 8. Excitation of riboflavin (under UVA irradiation) and the two possible reaction mechanisms (Raiskup and Spoerl, 2013, Kamaev et al., 2012)

1.6 Bioactive Substances for Improving Biofunctionalities of Collagen-based Scaffolds

Integrating a range of bioactive substances to elicit a more favorable biological response is a critical strategy of advancing collagen-based scaffolds for bone regeneration. These bioactive additives not only complement the intrinsic properties of collagen but also endow the scaffolds with the necessary signals to support and direct the complex cascade of bone healing and tissue formation.

1.6.1 Strategies for Bioactive Integration in Collagen-based Scaffolds

The enrichment of collagen-based materials with bioactive substances is a sophisticated approach aimed at elevating the regenerative capacity of scaffolds. A prevalent method involves embedding growth factors, such as BMPs, TGF- β , and VEGF, within collagen matrices (Toosi and Behravan, 2020). These factors substantially promote osteoinduction, stimulate osteogenesis, and facilitate angiogenesis, though their application necessitates careful control over release kinetics to mitigate high-dose side effects (Oliveira et al., 2021). Moreover, growth factors are typically expensive to produce and

purify, as well as difficult to maintain the stability, which limit their use in larger-scale applications (Gillman and Jayasuriya, 2021, Sarrigiannidis et al., 2021).

The strategic addition of minerals like hydroxyapatite or bioactive glasses, aim to replicate the inorganic phase of bone within collagen scaffolds, thus improving osteoconductivity and scaffold stiffness. However, achieving a uniform distribution of these minerals in the collagen matrix can be challenging, and there's a risk of altering the scaffold's biocompatibility and mechanical integrity (Wang et al., 2021).

Peptide functionalization is another targeted approach that mimics the biological signals of growth factors or matrix proteins by attaching bioactive peptides to the collagen substrate (Malcor and Mallein-Gerin, 2022). This method, while relatively more cost-effective compared to growth-factor delivery, demands an intricate understanding of peptide-collagen interactions and the stabilization of these bioactive peptides within physiological conditions (Luo and Kiick, 2017).

Other promising strategies like gene delivery systems, utilizing vectors embedded within the collagen matrix, introduce a transformative potential for in situ production of therapeutic molecules (Morshed et al., 2020). However, this innovation is met with intricate regulatory considerations and necessitates a thorough evaluation of vector safety (Hosseinkhani et al., 2023). Cell-seeding strategies directly infuse viable cells such as MSCs into collagen scaffolds, with the intent to enhance intrinsic biological activity and tissue integration. A significant challenge is ensuring cell survival and uniformity post-integration, coupled with a profound understanding of the ethical and regulatory frameworks governing cell-based therapies (Wu et al., 2018, Li et al., 2021a). Explorations into nanoparticle-mediated delivery systems have unveiled the potential for a sustained and controlled release of bioactive molecules (Edmundson et al., 2013). Nevertheless, the development of such systems must rigorously address concerns over nanoparticle toxicity and stability to ensure clinical viability (Fathi-Achachelouei et al., 2019).

In sum, while the incorporation of bioactive substances into collagen-based materials offers promising enhancements in BTE, it presents a complex

balance between efficacy and safety. These limitations underscore the need for alternative approaches that can provide a more harmonious integration with the collagen matrix while maintaining robust biofunctional activity.

1.6.2 Bioactive Ions as Functional Enhancers in Collagen-Based Scaffolds

The incorporation of bioactive ions into collagen-based scaffolds represents a cornerstone strategy in BTE due to their fundamental roles in promoting bone health and facilitating regeneration. Simple in integration yet profound in effect, these ions are instrumental in processes ranging from bone mineralization to intracellular signaling (Charbonnier et al., 2021) (**Figure 9**).

Calcium, for instance, the primary mineral component of bone, bolsters the osteoconductivity of collagen scaffolds and supports hydroxyapatite deposition, which is essential for bone mineralization (Hoveidaei et al., 2023). At the cellular level, it engages in signaling pathways such as the Wntless/Integrated (Wnt)/ β -catenin route, central to osteoblast differentiation and bone formation, and influences the release of growth factors and cytokines imperative for remodeling and repair (LaGuardia et al., 2023, Liu et al., 2023). Magnesium, another pivotal cation, stimulates bone cell activities and serves as an enzymatic cofactor, vital for the synthesis of nucleic acids and proteins. Its role extends to activating key pathways like mitogen-activated protein kinase/extracellular signal-regulated kinase (MAPK/ERK), further underpinning its contribution to bone formation and healing (Bosch-Rué et al., 2023, Luo et al., 2023). Meanwhile, copper is involved in synthesizing collagen and elastin, components critical for bone matrix structure and elasticity, by activating lysyl oxidase for crosslinking these proteins, thus enhancing the matrix's mechanical strength and resilience (Harris et al., 1980, Lin et al., 2020a). Furthermore, copper facilitates angiogenesis, essential during bone healing's initial stages, and modulates the immune response, indirectly influencing bone regeneration (Yoshida et al., 2023).

Compared to complex bioactive molecules, these ions offer a streamlined approach for scaffold integration, resulting in a uniform and economical

improvement of both mechanical and biological scaffold properties. Their intrinsic biocompatibility reduces the likelihood of adverse immune responses, a contrast to the potential complexities linked with growth factors (Su et al., 2023). Yet, challenges persist in achieving controlled and sustained ion release at therapeutic levels and ensuring even ion distribution—factors crucial for uniform scaffold performance and consistent regeneration outcomes. Moreover, the investigation into the synergistic effects of various ions introduces additional complexity.

To fully harness the regenerative potential of bioactive ions within collagen-based scaffolds, it is essential to develop advanced encapsulation and delivery systems capable of managing the intricate interactions and controlled release of these ions. A thorough comprehension of release kinetics and the synergistic interaction among multiple ions is imperative for maximizing their functional advantages. Addressing these technical complexities is key to ensuring that collagen scaffolds can effectively meet the multifaceted demands of modern BTE applications.

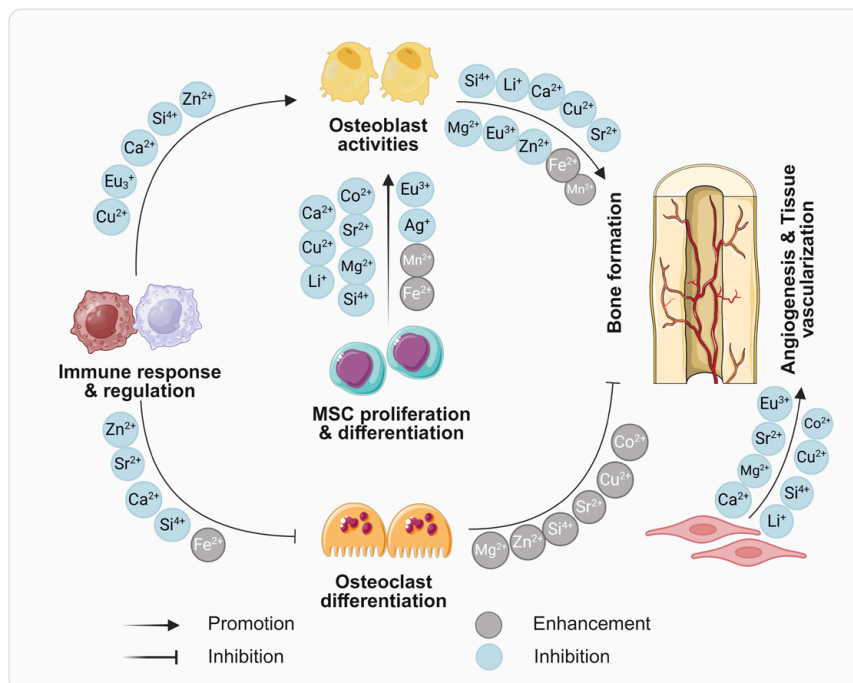


Figure 9. The multifaceted roles of various ions across processes like immunoregulation, osteoinduction, osteogenesis, angiogenesis and tissue vascularization in bone regeneration and tissue engineering. Ions that enhance the above processes are labeled as blue, while ions that show inhibition effect are labeled as grey (Zhao et al., 2023).

1.7 Objectives

Collagen, serving as an indispensable component in BTE, is crucial for effective bone defect healing and repair. The UVA/R crosslinking technique presents as a promising method to address the primary limitations of collagen scaffolds, including their degradation rate and mechanical properties, without compromising their biocompatibility. Moreover, the integration of controllable release system of bioactive ions could effectively improve the biofunctionalities of collagen-based scaffolds. However, several challenges and uncertainties remain in this field, which need to be addressed to translate these advancements into clinical benefits. To overcome these challenges, this project aims to fulfill the five main objectives below:

- **Advancing UVA/R collagen crosslinking process:** to identify and optimize the suitable parameters for UVA/R collagen crosslinking. This will include determining the optimal conditions for collagen preparation, riboflavin concentration, UVA irradiation intensity, and exposure time. The physicochemical properties of the crosslinked collagen matrix, such as stiffness, viscosity, and degradation rate, will be thoroughly evaluated to establish the feasibility and efficacy of this strategy.
- **Assessing UVA/R crosslinking against chemical methods:** to conduct a comparative analysis of UVA/R crosslinked collagen matrix with those crosslinked with two chemical methods (EDC/NHS and genipin). This will encompass assessing crosslinking efficiency, mechanical properties, thermal stability, degradation resistance in physiological and enzymatic environments, and biological properties including cytotoxicity, cell attachment, and proliferation.
- **Development of injectable composite material:** to develop an injectable composite material, combining UVA/R crosslinked collagen with a synthetic biphasic bone substitute. Manufacturing techniques will be established, and the material's properties, including the morphology of the collagen matrix, injectability, biocompatibility (material cytotoxicity, osteoblast proliferation), in vivo compatibility, and tissue response, will be examined.

- **Exploration of UVA/R crosslinking mechanism:** A key objective delves deeply into unraveling the intricacies of the UVA/R crosslinking process. This exploration is critical to enhancing our understanding of how this technique fundamentally alters the collagen matrix at a molecular level. This will focus on identifying primary crosslinking sites within the collagen structure using synthetic peptides, aiming to uncover where crosslinking occurs and its impact on the collagen matrix. Additionally, the investigation will delve into the riboflavin-mediated photochemical reactions, particularly understanding how UVA light and riboflavin interact to induce crosslinking in this process. Unraveling these mechanisms is crucial for refining the crosslinking technique and its application in tissue engineering.
- **Development of a bioactive ion encapsulation system:** to develop an advanced encapsulation system capable of delivering multiple bioactive ions, such as calcium, magnesium, and copper, enhancing the bioactivity of collagen-based scaffolds. This encapsulation system is designed to control the release of these ions steadily over time, which is critical for maintaining an optimal environment for bone regeneration.

To address these objectives and substantially advance the application of UVA/R crosslinked collagen in BTE, the methodology and progression of this project are depicted in **Figure 10**. This figure outlines the comprehensive approach of the study, with a primary focus on enhancing the mechanical strength and stability of collagen through UVA/R crosslinking. Additionally, it details the improvement of collagen-based materials' functionalities through the controlled release of multiple bioactive cations. These enhancements aim to increase the effectiveness of collagen-based scaffolds for tissue regeneration, moving these innovations closer to clinical application.

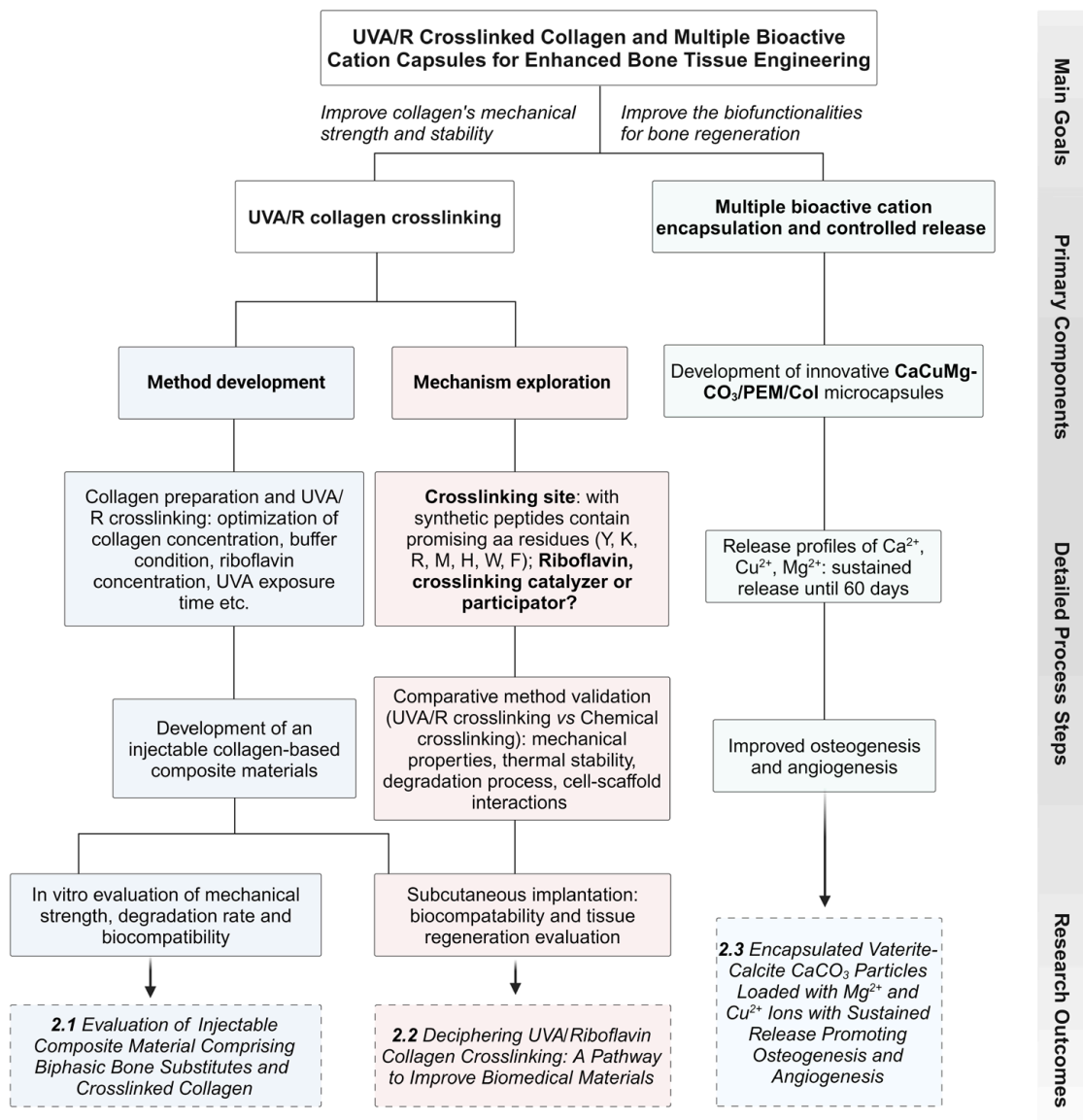


Figure 10. Flowchart of project methodology, progression, and outcomes. This diagram illustrates the comprehensive approach of the study, primarily focusing on the enhancement of collagen's mechanical strength and stability through UVA/R crosslinking, and the improvement of collagen-based material's functionalities via controlled release of multiple bioactive cations. The flowchart delineates the sequential steps, from developing collagen UVA/R crosslinking to decipher the sophisticated photocrosslinking mechanism, alongside the innovation of a bioactive cation encapsulation system, CaCuMg-CO₃/PEM/Col, leading to pivotal research outcomes: 2.1, 2.2, 2.3. These findings are elaborated upon Section 2. Results.

CHAPTER 2

RESULTS

2. Results

2.1 Evaluation of Injectable Composite Material Comprising Biphasic Bone Substitutes and Crosslinked Collagen

Fan, L., Ren, Y., Burkhardt, C., Jung, O., Schnettler, R., Barbeck, M., & Xiong, X. (2023). *Advanced Engineering Materials*, 25(19), 2300508.

2.1.1 Summary and Major Findings

Annually, millions of people around the globe suffer from bone defects, significantly impacting their life quality and functional abilities. Irregularly shaped bone defects pose substantial reconstructive challenges. This study in focus sought to create and evaluate an injectable material, composed collagen type I and bone substitutes, specifically tailored for irregularly shaped bone defects healing.

Drawing inspiration from the cornea crosslinking technique using ultraviolet A and riboflavin (UVA/R) for treating keratoconus, we established a photochemical crosslinking approach to functionalize the collagen matrix. This innovative composite is designed to adapt seamlessly to the unique contours and dimensions of bone defects, offering a personalized fit that enhances treatment efficacy. The photochemically crosslinked collagen matrix (xCol), as revealed through scanning electron microscopy (SEM), exhibits an interconnected, porous, and fibrous three-dimensional structure, which is advantageous for facilitating cell infiltration and enhancing material-cell interactions. Furthermore, rheological analysis indicated that the crosslinking process significantly enhanced storage modulus (G') of the material, while maintaining a consistent loss modulus (G''). These rheological characteristics are crucial for the injectability of collagen, ensuring the versatility as a biomaterial. Additionally, this structure provides an ideal extracellular matrix (ECM) microenvironment conducive to the activity of bone regeneration-related cells, such as osteoblasts and osteoclasts.

This study found that crosslinked collagen matrices (xCol) were significantly more resistant to degradation than non-crosslinked collagen (Col)

matrices. The Col matrices rapidly lost their structure within 24 hours, whereas xCol matrices better maintained their form. Notably, after 72 hours, the xCol samples preserved much of their shape, while the Col samples had completely disintegrated in PBS. GPC analysis showed a substantial molecular weight difference between the two, with xCol at 951 kD and Col at 565 kD, demonstrating the effectiveness of UVA and riboflavin crosslinking in stabilizing collagen structure during *in vitro* degradation.

To obtain the injectable composite material, the optimized collagen matrix was mixed with 0.005% riboflavin, then integrated with BBS materials, further treated using UVA irradiation. The BBS, comprising hydroxyapatite (HA) and β -tricalcium phosphate (β -TCP), served as the inorganic fraction. This composite underwent a controlled precipitation process, formed an interconnected porous network. The resulting composite material, incorporating the optimized crosslinked collagen matrix and BBS, demonstrated excellent injectability and stability.

Biocompatibility evaluations of this composite via XTT and BrdU assays on fibroblast and preosteoblast cultures indicated excellent compatibility, with over 80% cell viability and high metabolic activity. However, cell proliferation within the composite was up to 40% lower than in control media. This suggests that cell growth is subject to modulation by various signals within the composite environment. To comprehensively understand the material's potential in clinical applications, further studies focusing on cell differentiation and tissue regeneration processes are essential. Such investigations will provide deeper insights into the material's efficacy in supporting tissue healing and regeneration.

The findings from this study underscore that the developed collagen-based composite materials exhibit high biocompatibility, positioning them as promising candidates for use as injectable biomaterials in a variety of surgical procedures. This research represents a significant stride in the functionalization of collagen matrices for bone regeneration, offering a viable solution for managing complex bone defects. An area warranting further exploration is the mechanism underlying the photochemical UVA and riboflavin crosslinking

technique. Delving deeper into this process could lead to more controlled collagen crosslinking, achieving optimized biomechanical properties with a better equilibrium between stability and degradability. Such advancements would enhance the material's clinical applicability and effectiveness. Additionally, it is crucial to investigate the *in vivo* immunological response to these materials, particularly considering the potential risks associated with collagen derived from animal sources. Understanding the immune response in a live organism context will be essential for ensuring the safety and efficacy of these materials in clinical settings. This aspect of research will provide critical insights into the long-term viability and acceptance of these biomaterials in the human body, paving the way for their successful application in bone regeneration therapies.

2.1.2 Personal Contribution

My involvement in this research was multifaceted and substantial. I collaborated in the design of the experiments and actively participated in their execution. This included preparing samples, conducting rheological analysis, and carrying out degradation studies. Additionally, I was responsible for the comprehensive evaluation of all the experimental results, as well as writing and revision of the manuscript.

Evaluation of Injectable Composite Material Comprising Biphasic Bone Substitutes and Crosslinked Collagen

Lu Fan, Yanru Ren, Claus Burkhardt, Ole Jung, Reinhard Schnettler, Mike Barbeck,* and Xin Xiong*

Bone tissue engineering has emerged as a promising approach to regenerate bone tissue, and injectable biomaterials have shown potential for bone regeneration applications due to their ease of administration and ability to fill irregularly shaped defects. This study aims to develop and characterize an injectable composite material comprising biphasic bone substitutes (BBS) and crosslinked porcine collagen type I for bone regeneration applications. The collagen is crosslinked via a UVA-riboflavin crosslinking strategy and evaluated by testing the physicochemical properties, including the rheological behavior, dynamic storage modulus (G') and loss modulus (G''), and in vitro degradation process. The results show that the crosslinked collagen (xCol) exhibits suitable physicochemical properties for injectability and improved viscoelasticity and degradation resistance. Furthermore, xCol is then combined with BBS in a predetermined ratio, obtaining the injectable composite material. The biocompatibility of the materials is evaluated in vitro by XTT and BrdU assays on fibroblasts and preosteoblasts. The results demonstrate that the composite material is biocompatible and supporting pre-osteoblasts proliferation. In conclusion, the injectable composite material BBS-xCol has promising physicochemical and biological properties for bone regeneration applications. Further studies are warranted to evaluate its efficacy in vivo and optimize its composition for clinical translation.

bone tissue and overcome the limitations of current clinical approaches.^[4,5,7]

Injectable biomaterials have shown potential for bone regeneration applications due to their ease of administration and ability to fill irregularly shaped defects, such as cleft palate, orbital floor fracture, mandibular defect, vertebral compression fracture, and complex tibial plateau fracture.^[6,8–10] The injectable materials can be easily delivered to the defect site using minimally invasive procedures, such as percutaneous injection or catheterization.^[11] This can reduce surgical trauma, shorten the recovery time, and improve patient comfort.^[11] The ability of filling irregular shaped defects makes injectable materials can conform to the shape and size of the bone defect, providing a customized fit that can improve the effectiveness of the treatment.^[5] Moreover, they can promote the recruitment and proliferation of bone-forming cells,^[12] accelerate the formation of new bone tissue, and enhance the integration of the implant with the surrounding bone.^[13]


Several materials have been investigated for use in injectable bone regeneration materials, including hydrogels,^[8,11,14] ceramics,^[11] polymers,^[9,15] alginate,^[16] and platelet-rich plasma.^[17] However, many of them are still limited in mechanical strength, rapid degradation, and risk of infection.^[5] Besides those materials, increasing attention has been focused on collagen type I, which is a natural protein component of the extracellular matrix and has been used in bone regeneration applications due to its biodegradability and ability to support cell attachment

1. Introduction

Bone defects and injuries resulting from trauma,^[1,2] tumors,^[1,3] infections,^[3,4] or congenital abnormalities^[1,5] can significantly impact patients' quality of life and functional abilities. Current clinical approaches for bone regeneration, such as autografts and allografts, have limitations of limited availability, donor site morbidity, and risk of disease transmission.^[6] Bone tissue engineering has emerged as a promising approach to regenerate

L. Fan, C. Burkhardt, X. Xiong
NMI Natural and Medical Sciences Institute at the University of Tübingen
Markwiesenstr. 55, 72770 Reutlingen, Germany
E-mail: xin.xiong@nmi.de

L. Fan
Institute of Biomedical Engineering, Department of Medical Technologies
and Regenerative Medicine, Medical Faculty
Eberhard Karls University of Tübingen
Silcherstr. 7/1, 72076 Tübingen, Germany

 The ORCID identification number(s) for the author(s) of this article can be found under <https://doi.org/10.1002/adem.202300508>.

DOI: 10.1002/adem.202300508

Y. Ren, O. Jung, M. Barbeck
Clinic and Policlinic for Dermatology and Venereology
University Medical Center Rostock
Stempelstraße 13, 18057 Rostock, Germany
E-mail: mike.barbeck@med.uni-rostock

R. Schnettler
University Medical Center
Justus Liebig University of Giessen
Ludwigstraße 23, 35390 Gießen, Germany

M. Barbeck
BerlinAnalytix GmbH
Ullsteinstraße 108, 12109 Berlin, Germany

and proliferation.^[18] Moreover, the mechanical strength and resistance to degradation of collagen can be enhanced via various crosslinking processes, such as chemical crosslinking with glutaraldehyde and carbodiimides.^[18–21] Compared with chemical crosslinking methods, the physical crosslinking with ultraviolet-A (UVA) and riboflavin offers several advantages, particularly in terms of biocompatibility, mechanical properties, and tissue integration.^[22,23] In addition, biphasic bone substitutes (BBS) are a mixture of hydroxyapatite (HA) and β -tricalcium phosphate (β -TCP) which can well mimic the composition and structure of autologous bone.^[24] They are a commonly used bone substitute material for osseous repair and have shown excellent biocompatibility and osteoconductivity.^[25] The combination of crosslinked collagen and BBS is a promising direction of developing injectable materials. However, there is a need for further research to improve the physicochemical properties and stability of collagen and optimize the composition of the composite material and to evaluate its efficacy and safety.^[26]

Therefore, this study aims to develop and evaluate an injectable composite material comprising BBS and crosslinked collagen for bone regeneration applications, as shown in **Figure 1**. The porcine skin-derived collagen type I was cross-linked using UVA and riboflavin, and evaluated with physicochemical properties, including the rheological behavior, dynamic storage modulus (G'), and loss modulus (G''), recorded with a stress-controlled rheometer and in vitro degradation process measured with gel permeation chromatography/size exclusion chromatography (GPC/SEC). Furthermore, the biological properties of the synthesized composite material BBS-xCol were

evaluated in vitro to assess the potential of the material for bone regeneration in vivo. The ultimate goal of this study is to evaluate the safety and efficacy of the developed injectable material and to prepare it for further clinical applications.

2. Experimental Section

2.1. Material Preparation

2.1.1. Collagen Matrix Preparation

The homogenization process of the porcine skin-derived collagen was optimized based on the protocol described in our previous publication.^[27] Briefly, the frozen split skin was defrosted at 4 °C overnight and then rinsed in double-deionized water (ddH₂O) at the concentration of 3.2:1 (w/w). Then the mixture of split skin and ddH₂O was agitated using a paddle mixer (IKA Digital 20, IKA Works, Inc., Wilmington, NC, USA) at 100 rpm for 1 h and pre-homogenized at 700 rpm for 3 h. The pH value was adjusted to 3.2, and the suspension was left overnight at room temperature before further processing. After that, the collagen suspension was treated in a water bath at 65 °C for 10 min, then immediately homogenized with an IKA Ultra-Turrax homogenizer (IKA Works, Inc.) (about 12 000 rpm) for 1 min, and further filtered via a Buchner Funnel. Finally, a foaming paddle was used to foam the filtered suspension for 2 h, and riboflavin (ROTH, 9607.1) was added into collagen suspension in the last 15 min of the 2 h, producing liquid collagen foam with protein concentrations around 40 mg mL⁻¹.

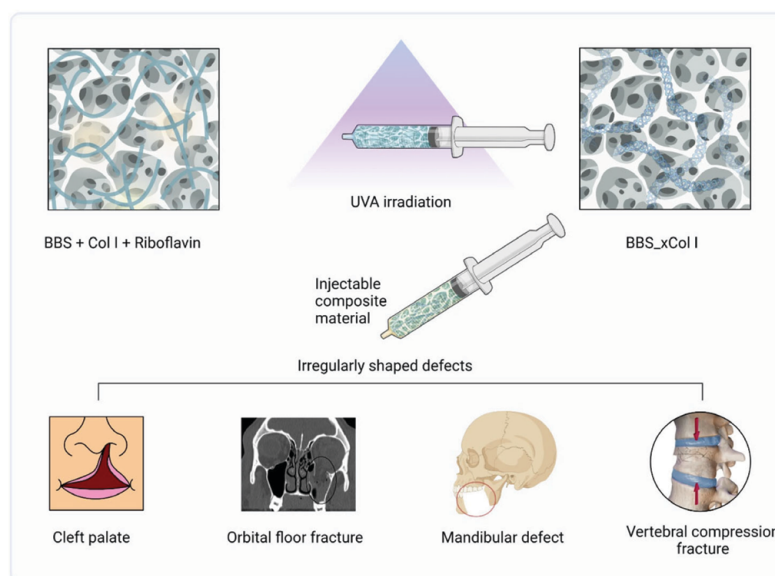


Figure 1. Schematic illustration of this simple, efficient, and safe preparation process of injectable composite material comprising BBS and UVA/riboflavin crosslinked collagen matrix and the applications of the injectable composite material.

2.1.2. Crosslinking Under UVA Irradiation

The homogenized collagen suspensions mixed with a series of concentration of riboflavin (R): 0.001%, 0.005%, 0.01%, 0.05%, 0.1% were transformed into Petri dishes with a smooth thin surface. The Petri dishes were then placed into a UVA lamp box with a wavelength of 365–370 nm and an irradiance of 3–9 mW cm⁻² for 10 min. The crosslinked collagen (xCol) samples were collected and further characterized with rheological analysis and degradation evaluation, with the noncrosslinked collagen as control.

2.1.3. Combination of Collagen and BBS

The biphasic bone substitute (BBS) material *maxresorb* (Botiss biomaterials GmbH, Berlin, Germany) composed of 60% hydroxyapatite (HA) und 40% β -tricalcium phosphate (β -TCP) was applied as the basis inorganic material in this study.^[28] The manufacturing process of *maxresorb* included a controlled precipitation process of aqueous solutions of calcium and phosphate as well as subsequent cold isostatic pressing into mechanically stable objects. This process resulted in an interconnecting porous system with defined pore diameters ranging from 200 to 800 μ m, as well as micropores of 1–10 μ m.^[28,29]

The optimized xCol with 0.005% riboflavin was chosen to be combined with BBS for the synthesis of injectable composite material. Briefly, the homogenized collagen with 0.005% riboflavin was immediately mixed with BBS particles at the ratio of 1:9 (w/w) in a sterilized Petri dish and then quickly transferred into a syringe (1 mL). Similarly, the syringe was placed into the UVA lamp box for crosslinking. Overall, it is a very simple, efficient, and safe process, which also saves the material sterilization step.

2.2. Material Characterization

2.2.1. Morphological Characterization of Collagen Matrices with Scanning Electron Microscopy (SEM)

The noncrosslinked collagen (Col) and UVA/riboflavin cross-linked collagen (xCol) samples were characterized using a Zeiss scanning electron microscopy (SEM) instrument (1540XB CrossBeam, Zeiss) with a high-resolution GEMINI field-emission column operating at a very low acceleration voltage. The instrument was equipped with a thermally assisted Schottky field-emission gun, which allowed for a controlled and precise emission of electrons at a very low-energy speed. Furthermore, the SEM setup included a Canion focused ion beam (FIB) system with a gallium metal-ion source installed at an angle of 54° to the electron beam. This FIB system allowed for precise sample preparation and manipulation, enabling cross-sectional analysis and the ability to obtain high-resolution images. The collagen samples were prepared for SEM analysis by rapidly freezing them at liquid nitrogen, preserving their native structure, and preventing sample degradation. The SEM analysis of the Col and xCol samples provided detailed information about their surface morphology, microstructure, organization, and integrity.

2.2.2. Morphological Characterization of BBS with Fluorescence Microscope

For the visualization of BBS material, fluorescence microscope (KEYENCE BZ-X800, KEYENCE GmbH, Neu-Isenburg, Germany) was applied. The fluorescence microscope provided high-resolution images, allowing for detailed observation of the morphology and interconnecting porous system of fluorescein isothiocyanate (FITC)-labeled BBS.

2.2.3. Rheological Characterization via Amplitude Sweep

The dynamic storage modulus (G') and loss modulus (G'') of collagen samples were measured using a stress-controlled rheometer (Anton Paar MCR 302) equipped with a 50 mm-diameter stainless steel cone and plate with a cone angle of 1° and a truncation gap of 103 μ m. Dynamic shear–strain–amplitude sweeps (DSS) were performed at a constant oscillation frequency (ω) of 10 rad s⁻¹ to record G' and G'' using xCol samples with different concentrations of riboflavin and a control group, noncross-linked collagen. Four replicates were used for each sample. The DSS test was carried out by increasing the strain amplitude from 0.1% to 100% at a constant temperature of 23 °C. The storage and loss moduli were recorded during the test, and the flow point of each sample was determined as the point of intersection between the storage and loss moduli. The loss factor ($\tan\delta$) was calculated using Equation (1), where G'' and G' represent the loss and storage moduli, respectively.

$$\tan\delta = \frac{G''}{G'} \quad (1)$$

2.2.4. In vitro Collagen Degradation Evaluated via Gel Permeation Chromatography (GPC)

The in vitro degradation of collagen matrix was carried out by incubating the samples in phosphate-buffered saline (PBS, 1x) solution in 37 °C with a gentle agitation at 60 rpm. After 72 h' incubation, the supernatants with degrades were collected via centrifugation, further evaluated using the gel permeation chromatography (GPC) system. The GPC measurements provided information about the molecular weight changes of the collagen samples during the degradation process, which is an important parameter for assessing the stability and suitability of the material for bone regeneration applications. The GPC was carried out using an Agilent Infinity II 1260 series HPLC system equipped with quaternary pump, a refractive index detector (RI – 101, Shodex), multiangle light scattering detector (DAWN HELEOS II; Wyatt), and a column packed with a highly porous modified silica particle (PSS, Proteoma). The samples were diluted in an appropriate solvent (20% Acetonitrile in PBS) and injected into the column. The separation was based on the size of the molecules as they passed through the column and were eluted in order of decreasing molecular weight. For determination of molecular weight distribution, first a calibration with a standard molecule of known molecular weight was performed. The eluent was passed through the column, and the molecular weight

distribution of the sample was determined by comparing the retention time to that of standard molecules of known molecular weight.

2.3. Cell Culture

The L929 mouse fibroblast cell line and MC3T3 mouse preosteoblast cell line, purchased from the European Collection of Cell Cultures, ECACC (Salisbury, UK), were used for in vitro biological evaluation of the synthesized injectable composite material. The cells were cultured in Dulbecco's Modified Eagle Medium (DMEM) supplemented with 10% fetal bovine serum (FBS) and 1% penicillin-streptomycin (PS) in a humidified incubator at 37 °C with 5% CO₂, and 95% humidity.

2.4. Cell Viability Tests

The cell viability tests were conducted in accordance with the standard protocol of the DIN EN ISO 10993-5: 2009/-12: 2012, by determining the metabolic activity of the cells after exposure to the extracts of the materials and controls. RM-A materials, which included polyurethane film with 0.1% zinc diethyldithiocarbamate (ZDEC) (Hatano Research Institute, Food and Drug Safety Center, Hadano, Japan), were used as positive control. Grade 5 titanium plates were applied as a negative control. The cells treated with culture medium served as the medium control group. Each group was conducted with 3 replicates. The percentage of cell viability was calculated by comparing the absorbance values of the treated cells to those of the control cells. A viability percentage above 70% was considered noncytotoxic.

First, the BBS_xCol and BBS_Col composite materials, Col, positive control (PC), and negative control (NC) were extracted by soaking in culture medium for 24 h at 37 °C, with a gentle agitation at 60 rpm. Then, the extracts were sterilized by filtering through a 0.22 µm filter. To assess cell viability, L929 and MC3T3 cells were seeded in 96 well plates at a density of 10⁴ cells well⁻¹ and incubated for 24 h. Then, the culture medium was replaced with the extracts of the materials and controls and incubated for 24 h.

2.4.1. XTT Assay

The Sodium 3,3'-[1(phenylamino)carbonyl]-3,4-tetrazolium]-3-is(4-methoxy-6-nitro) Benzene Sulfonic acid Hydrate (XTT)-assay kit (Roche Diagnostics, Mannheim, Germany) was used for this measurement. Initially, the electron coupling reagent was mixed with the XTT labeling reagent in a ratio of 1:50. Next, 50 µL of this mixture was added to the cells and incubated for 4 h in standard cell culture conditions. Subsequently, the absorbance of 100 µL aliquots transferred into a new 96 well plate was measured using a scanning multiwell spectrophotometer (ELISA reader) equipped with filters for 450 and 650 nm.

2.4.2. BrdU Assay

Bromdesoxyuridin (BrdU) ELISA (Roche Diagnostics, Mannheim, Germany) was applied for the analysis. To perform

the BrdU assay, the cells were coincubated with BrdU for 2 h under standard cell culture conditions. The cells were then fixed with the FixDenat reagent at room temperature and afterward treated with anti-BrdU peroxidase (POD) antibody for 1 h. The cells were washed three times for 5 min each before adding tetramethylbenzidine (TMB) to react with the substrate for 20 min at room temperature. The reaction was stopped by adding 25 µL of 1 M H₂SO₄. The absorbance was measured at 450 and 690 nm using a scanning multiwell spectrophotometer (ELISA reader) with a filter.

2.5. Statistical Analysis

By the paired T-test and the analysis of variance (ANOVA), which is an extension of the T-test, data were statistically analyzed. An LSD posthoc assessment followed to compare groups using GraphPad Prism software (Version 9.0.0, GraphPad Software Inc., La Jolla, USA). The intra- (#) and interindividual (*) statistical differences were defined by three significance levels. If P-values were less than 0.05 (#/*P < 0.05), the difference were considered as significant. High significant were considered, if the p-values were less than 0.01 (##/***P < 0.01) or less than 0.005 (###/****P < 0.005) or less than 0.001 (####/*****P < 0.001). Using GraphPad Prism software, the data were represented as average values and standard deviation.

3. Results

3.1. Morphological Characterization

The morphological characterizations depicted in Figure 2 provide valuable insights into the structural properties of collagen matrices without UVA/R crosslinking, biphasic bone substitute (BBS) material, and the composite material consisting of BBS and crosslinked collagen (BBS_xCol). SEM images (Figure 2A, B) clearly highlight the distinctions between noncrosslinked and crosslinked collagen matrices. These images reveal the effects of the crosslinking process on the compactness, fiber organization, and the formation of the porous microstructures within the xCol matrix. Fluorescence microscopy (Figure 2C) confirms the successful labeling of BBS material with FITC, enabling the visualization of the distribution of BBS and its interconnected porous system within the material. Additionally, photographic images (Figure 2D) visually showcase the distinct appearances of the injectable noncrosslinked collagen matrix, crosslinked collagen matrix, BBS, and the composite BBS_xCol material. Overall, these characterizations in Figure 2 provide a comprehensive illustration of the microscopic and macroscopic structures of collagen matrices and BBS material.

3.2. Physicochemical Characterization

3.2.1. Rheological Behavior of Collagen Matrix

The results of shear–stress–amplitude sweeps of collagen samples are shown in Figure 3 and 4. The limit of the linear viscoelastic (LVE) region is first determined. The LVE region indicates

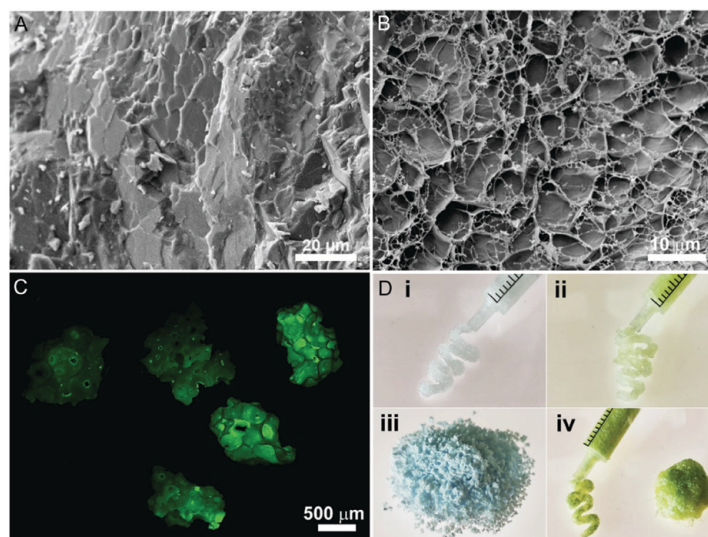


Figure 2. Morphological characterizations of collagen matrix, BBS material, and composite material. A) Cryo-SEM images of noncrosslinked collagen matrix and B) UVA/R crosslinked collagen matrix. C) Fluorescence microscopy image of FITC-labeled BBS. D) Photographic images of noncrosslinked collagen matrix. i), crosslinked collagen matrix (ii), BBS (iii), and the composite material composed of BBS and crosslinked collagen matrix (iv).

the range in which the test can be carried out without destroying the structure of the sample, which is depicted on the left side of the diagrams in Figure 3; the range starts from the lowest strain values.^[30] In the LVE region, the dynamic storage modulus (G') and loss modulus (G'') of all the collagen samples without crosslinking showed constant values, the so-called plateau values, the statistical analyses of which are also shown in Figure 4C,D. Among those, xCol_0.001% R and xCol_0.005% R showed significantly higher G' and G'' values, indicating higher elasticity and viscosity. After leaving the LVE region, the curves showed a gradually dropping G' values and increasing G'' values, indicating a gradual breakdown of the superstructure, which formed a consistent, 3D network. As shown in Figure 4A,B, after the LVE region, the curves of xCol_0.001% R and xCol_0.005% R were over other groups, suggesting a higher sample stiffness and strength (G'), and viscoelasticity. Moreover, all the samples showed overall similar yield point ($t_f = 10\%$), which is the value of the shear stress at the limit of LVE region. However, the cross-linked collagen matrix showed higher flow point ($G' = G''$; $t_f > 100\%$) than the noncrosslinked collagen ($t_f = 100\%$), indicating the lower tendency of the xCol to brittle fracturing.

Additionally, the loss factor ($\tan \delta$) can be calculated from G' and G'' , which describes the ratio of the energy dissipated to the energy stored during deformation. A lower value of $\tan \delta$ indicates more elastic properties, while a higher value suggests more viscous behavior. As shown in Figure 4E, all the samples showed a gel-like solid state, with $\tan \delta < 1$. The groups of xCol_0.001% R and xCol_0.005% R showed significantly lower $\tan \delta$ values compared with noncrosslinked collagen; especially the xCol_0.005% R group showed overall the lowest ($P < 0.001$).

3.2.2. Degradation Study with Gel Permeation Chromatography (GPC)

The visual changes observed during the in vitro degradation process of collagen samples in PBS buffer at 37 °C are illustrated in Figure 5A. The noncrosslinked collagen sample exhibited a significant loss of original geometry after only 24 h, whereas the crosslinked collagen samples displayed better shape retention. After 72 h, xCol_0.001% R and xCol_0.005% R still retained some of their original geometry, while the noncrosslinked collagen matrix became completely dissolved in the PBS buffer. Although the other crosslinked collagen samples (xCol_0.01% R, xCol_0.05% R, xCol_0.1% R) also showed some loss of the original shape, some pieces still remained after 72 h.

The solutions collected after incubating for 72 h were subjected to GPC measurements (Figure 5B). The results indicated that a considerable difference in molecular weight (Mw) between the solutions was obtained from crosslinked and noncrosslinked collagen samples. Among the crosslinked collagen groups, xCol_0.005% R exhibited the highest Mw of 951 kD, while the noncrosslinked collagen showed only 565 kD. These findings suggest that crosslinking plays a critical role in the structure integrity of collagen under in vitro degradation conditions.

3.3. Biological Evaluations

3.3.1. XTT assay for Cell Viability

According to the XTT assay, the viability of L929 fibroblasts was assessed and results showed that all groups including Col,

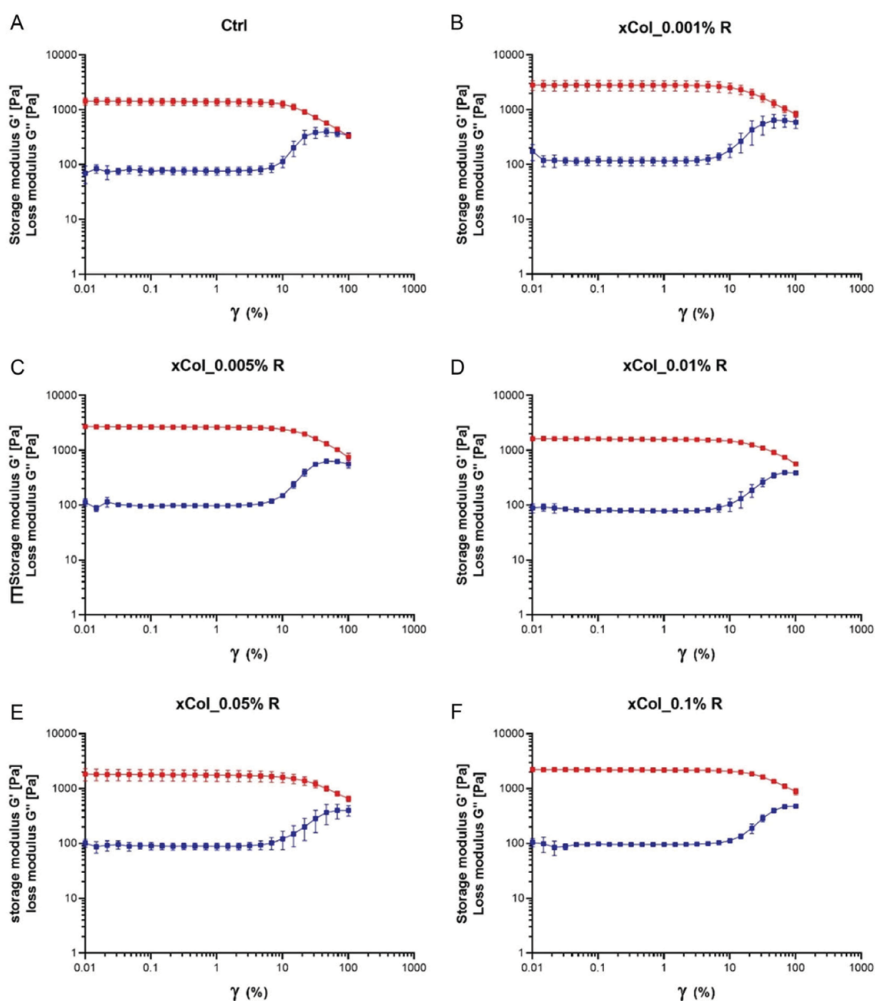


Figure 3. A) Amplitude sweeps for comparison of noncrosslinked collagen and crosslinked collagen prepared with different concentration of riboflavin (R): B–F) 0.001%–0.1%, at 23 °C, $\omega = 10 \text{ rad s}^{-1}$. (mean \pm SD, $n = 4$).

BBS_Col, and BBS_xCol exhibited a cell viability higher than 70% of medium control, without significant difference observed (Figure 6A). The group of Col showed higher cell viability compared to the medium control, whereas the BBS_Col and BBS_xCol groups exhibited similar viability to the medium control. There was also no significant difference among those three material groups. Among the three material groups, there was no significant difference. However, the results obtained from MC3T3 preosteoblasts showed a different trend (Figure 6B). The Col and BBS_Col groups demonstrated cell viability lower than 70% of the medium control, while the BBS_xCol group showed significantly higher cell viability, which was comparable to the medium control. This indicates that BBS_xCol has better

biocompatibility and is more suitable for use in bone tissue engineering applications.

3.3.2. BrdU assay for proliferation

In Figure 7A, the BrdU assay results showed that the L929 fibroblasts had high viability when cultured with the Col group, which was comparable to the medium control, and acceptable viability with BBS_Col and BBS_xCol groups. The BBS_Col and BBS_xCol groups exhibited lower cell viability compared to the Col group. However, in the case of MC3T3 preosteoblasts, the BrdU assay indicated significantly lower cell viability in

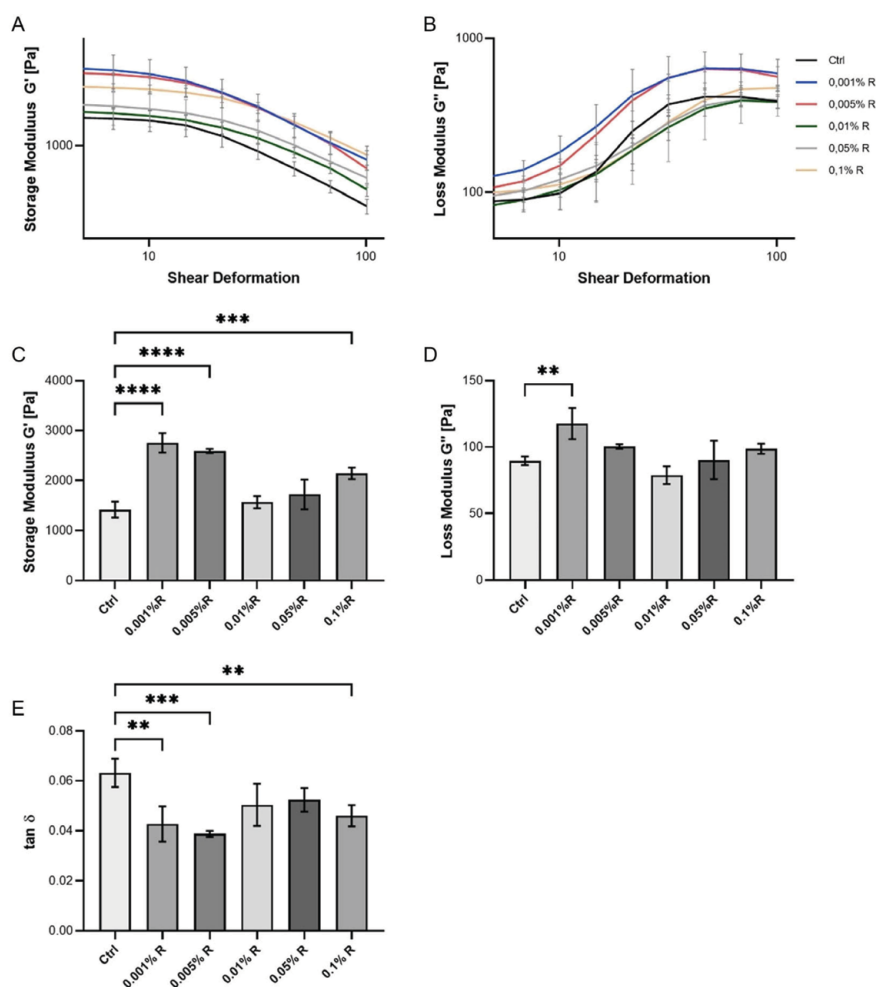


Figure 4. A,B) Dynamic storage modulus (G') and loss modulus (G'') change after leaving the LVE region. C,D). The G' values and G'' values recorded in the plateau LVE region. E). The loss factor ($\tan \delta$) calculated from G' and G'' values. (mean \pm SD, $n = 4$; Paired T-test, ** $P < 0.01$, *** $P < 0.001$, **** $P < 0.0001$, indicated that there was a significant difference of values in comparison to control).

the material groups compared to the medium control (Figure 7B). These findings suggest that the different materials may have varying effects on cell viability depending on the cell type. Further investigation is needed to determine the specific factors that contribute to the observed differences in cell viability.

4. Discussion

Collagen and collagen gels have been extensively studied as matrix and coating for cell culture and diverse clinic applications. As indicated by Funaki 2017,^[31] at a concentration of above 0.5%

of collagen, the solution forms a gel with a density much lower than that found in normal tissues. Density can be increased by up to 20% by compressing the collagen gel, mimicking the density of cartilage and dermis. The compression results from the reduction of the fluid content from the collagen gel.^[32] Another option is to crosslink the collagen either with collagen or with other polymers. As shown in Figure 2A,B, the SEM images provide visual evidence of the structural modifications induced by the crosslinking process in the collagen matrix. These results not only highlight the effectiveness of the crosslinking treatment but also underscore its potential impact on the overall properties and functionalities of the collagen-based materials. The enhanced compactness is further corroborated by the finding in

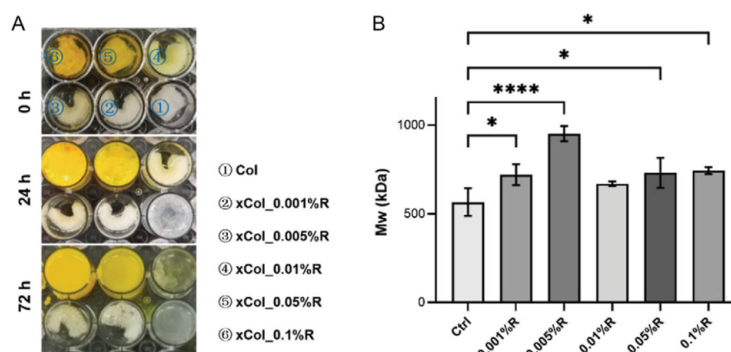


Figure 5. In vitro degradation process of collagen samples in PBS buffer at 37 °C. A) Photographs taken at 0, 24, and 72 h during the degradation process. B) The gel permeation chromatography (GPC) measurements of the supernatant collected after 72 h of degradation. (mean \pm SD, $n = 4$; Paired T-test, $*P < 0.05$, $**P < 0.01$, $***P < 0.001$, $****P < 0.0001$, indicated that there was a significant difference of values in comparison to control).

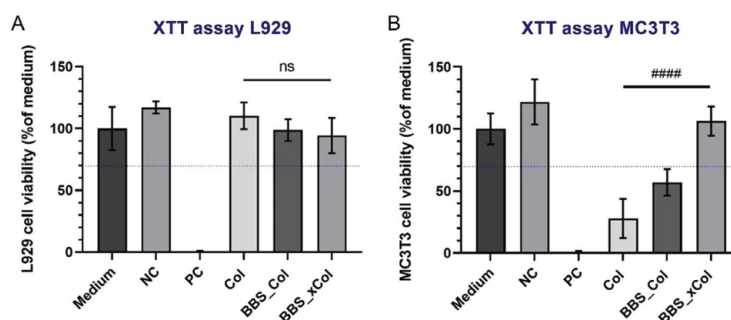


Figure 6. Cytocompatibility results of Col, BBS_Col, BBS_xCol via XTT assay using A) L929 fibroblasts and B) MC3T3 preosteoblasts. (The dotted blue lines show the respective thresholds that should not be undershot; mean \pm SD, $n = 6$; One-way ANOVA test, ns: $P > 0.05$, #### $P < 0.0001$).

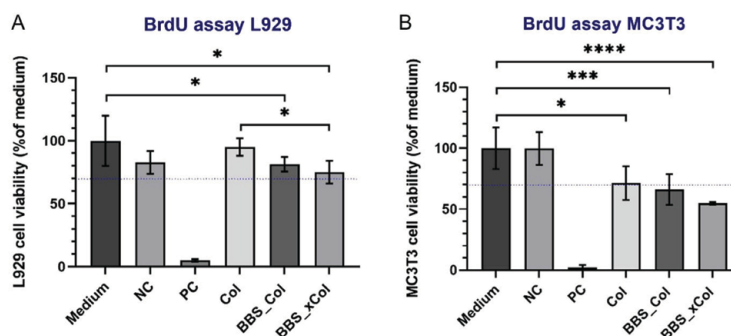


Figure 7. Cytocompatibility results of Col, BBS_Col, BBS_xCol via BrdU assay using A) L929 fibroblasts and B) MC3T3 preosteoblasts. (The dotted blue lines show the respective thresholds that should not be undershot; mean \pm SD, $n = 6$; One-way ANOVA test, $*P < 0.05$, $****P < 0.0001$).

Figure 2B, where the crosslinked collagen displays more fiber structure compared to its noncrosslinked counterpart. Moreover, the formation of a porous microstructure within the crosslinked collagen matrix, as evidenced by the SEM images, is indicative of the interconnectivity of the collagen network. The presence of

these pores might offer potential advantages such as increased surface area and enhanced cell infiltration, which are crucial for tissue regeneration and biomaterial integration.

Microenvironment and its stiffness have a crucial role by cellular responses including adhesion, differentiation, and

proliferation. As reported by Engler, osteoblasts may differentiate better in a gel/matrix with higher stiffness for example the polyacrylamide gel exceeding 10 kPa stiffness.^[32,33] Therefore, in the present study, the elastic-viscous properties of collagen matrices are the focus of physical characterization. The elasticity of a material, or the energy stored during deformation, is described by the storage modulus, while the viscosity, or the energy dissipated during deformation, is described by the loss modulus. The intersection of G' and G'' on a shear deformation plot identifies the flow point. Materials with a higher flow point require more force to initiate flow. A higher storage modulus (G') indicates a higher material stiffness. The loss factor $\tan \delta$ is an indicator for elastic properties. If a material has a higher G' and smaller G'' , the resulting $\tan \delta$ will be lower and a value near zero indicates ideal-elastic behavior. When the storage modulus values are higher than the loss modulus values, the material is referred to as a viscoelastic solid. As shown in the Figure 4C, the crosslinking process resulted in an increase in G' , indicating an increase in the elastic properties. Samples containing 0.001%, 0.005%, and 0.01% riboflavin exhibited the highest increase, exceeding 1000 Pa, while samples containing 1% riboflavin showed the lowest increase. These findings suggest that excessive crosslinker amounts may not improve the crosslinking reaction and the resulting degree of crosslinking. G'' showed only slight changes before and after the crosslinking indicating that the viscosity of the collagen matrix did not change significantly. These properties are important for the injection purposes of collagen matrices and ensure their potential as a versatile biomaterial for injectable implants.

Interestingly, when the collagen foams were stored at 4 °C for 24 h, the measurements were compared within the limit of the LVEs to ensure that no material degradation occurred, which could potentially introduce artifacts into the data.^[30] Additionally, the samples behave in a more predictable and consistent manner. Following storage modulus, the noncrosslinked collagen had a mean G' limit of 1417 ± 187 Pa. In contrast, the crosslinked collagen displayed a G' limit range of 2592 ± 594 Pa to 3178 ± 594 Pa, depending on the concentration of riboflavin used for crosslinking. The G'' values of the crosslinked collagen containing 0.001%, 0.005%, and 0.01% riboflavin did not exhibit a significant difference from the noncrosslinked collagen, while the other samples showed apparent differences. These results confirmed the previous analyses that the crosslinking process with certain concentration of riboflavin increased the elasticity and stability of collagen, as evidenced by the increase in G' , without affecting the viscosity or reducing the resistance to deformation, as indicated by the lack of change in G'' . In addition, the $\tan \delta$ values also support the use of crosslinked collagen containing 0.001% and 0.005% riboflavin as they resulted in the lowest $\tan \delta$ values of 0.043 (SD = 0.017) and 0.039 (SD = 0.001), indicating a higher proportion of viscoelastic properties.

The incorporation of the biphasic bone substitute (BBS) material into the collagen-based composite offers a compelling opportunity to enhance its mechanical properties and stability. Previous studies have highlighted the exceptional properties of BBS,^[34,35] further supporting its attractiveness as a component for reinforcing the composite material. In this study, our primary focus has been on characterizing the mechanical properties and degradation resistance as a representative for the mechanical

properties of the composite. This approach allows us to evaluate the overall performance of the composite material, considering the significant role of collagen in determining its mechanical characteristics.

To achieve the integration of collagen into the porous BBS, the adsorption of collagen on differently charged surfaces was investigated via a quartz crystal microbalance (QCM) and measurements of δ -potential in our previous studies.^[36] Our findings indicated that collagen can be stably adsorbed on both negatively and positively charged surfaces because of its amphipathic nature. Therefore, the negatively charged BBS used in this study favored the adsorption of collagen under the specific process conditions with a net positive charge. In the present study, the XTT assay and BrdU assay were utilized to comprehensively evaluate the cytocompatibility of the prepared injectable composite material BBS_xCol, BBS_Col, and Col. By combining these two assays, it is possible to gain a more comprehensive understanding of the cytotoxicity of the biomaterial, as they measure different aspects of cell viability. The proliferation rate of both tested cell lines demonstrated a comparable trend across all tested materials, as depicted in the Figure 7, indicating that integration of crosslinked collagen into BBS did not significantly affect cell viability. The slightly decreased viability of the cells is a temporary effect due to the addition of differently prepared collagen and crosslinked collagen. Further studies are necessary to assess the efficacy of the developed composite material in vivo and to optimize its composition for potential clinical translation. In particular, the inclusion of advanced imaging techniques and intelligent computational analysis could provide valuable insights into the interfacial interactions and cellular responses within the material both in vitro and in vivo.^[37]

5. Conclusion

In this study, a novel injectable material comprising crosslinked collagen and BBS was developed and characterized for its functionality. The collagen matrices without UVA/riboflavin crosslinking were analyzed using a rheometer and a GPC system. The results showed that collagen crosslinked with 0.001% and 0.005% riboflavin exhibited significantly higher stability and elasticity. Biocompatibility of the collagen-BBS and crosslinked collagen-BBS composites was assessed using XTT and BrdU assays in fibroblast and preosteoblast cultures. The results revealed that the new materials demonstrated good biocompatibility, with over 80% cell viability. The XTT assay also showed high metabolic activity in the cells. However, proliferation rates in BBS_Col and BBS_xCol were up to 40% lower than the control samples and culture media, indicating that regulation of the proliferation rate varies depending on different signals and cannot be simply categorized as good or bad. Overall, the findings indicate that the developed BBS_Col and BBS_xCol composite materials are highly biocompatible and have potential for use as an injectable biomaterial in various surgical procedures.

Acknowledgements

L.F. acknowledges the support of the China Scholarship Council (CSC, no. 202008500143). This work was supported by the Federal Ministry of

Education and Research (BMBF, Germany, FKZ: 13GW0400A, C and 13GW0430B) and the State Ministry of Baden-Württemberg for Economic Affairs, Labor, and Tourism (FKZ: 35-4223.10/22).

Conflict of Interest

The authors declare no conflict of interest.

Author Contributions

R. S., M.B., and X.X.: conducted conceptualization. L.F., M.B., X.X.: conducted methodology. X.X., L.F., and M.B.: conducted validation. L.F., Y.R.R., and X.X.: conducted formal analysis. L.F. O. J.: conducted investigation. O.L., R. S., M.B., and X.X.: took care of resources. L.F., C.B., and X.X.: took care of data curation. L.F.: took care of writing the original draft. L.F., M.B., X.X.: took care of writing the review and editing. L.F. took care of visualization. X.X.: took care of supervision. M. B. and X.X.: took care of project administration. O. J., M.B., and X.X.: took care of funding acquisition. All authors have read and agreed to the published version of the manuscript.

Data Availability Statement

The data that support the findings of this study are available from the corresponding author upon reasonable request.

Keywords

biocompatibility, biphasic bone substitutes, crosslinking, injectable material, physicochemical properties, porcine collagen I

Received: April 11, 2023

Revised: June 23, 2023

Published online:

- [1] M. G. Raucci, U. D'Amora, A. Ronca, L. Ambrosio, *Adv. Healthcare Mater.* **2020**, *9*, 2000349.
- [2] F. Chamieh, A.-M. Collignon, B. R. Coyac, J. Lesieur, S. Ribes, J. A. Llorens, A. Nicoletti, D. Letourneur, M.-L. Colombier, *Sci. Rep.* **2016**, *6*, 38814.
- [3] X. Zhao, H. Ma, H. Han, L. Zhang, J. Tian, B. Lei, Y. Zhang, *Mater. Today Bio* **2022**, *16*, 100336.
- [4] G. E. DeCesare, F. W. B. Deleyiannis, J. E. Losee, *Semin. Plast. Surg.* **2009**, *23*, 119.
- [5] J. D. Kretlow, S. Young, L. Klouda, M. Wong, A. G. Mikos, *Adv. Mater.* **2009**, *21*, 3368.
- [6] G. Fernandez de Grado, L. Keller, Y. Idoux-Gillet, Q. Wagner, A.-M. Musset, N. Benkirane-Jessel, F. Bornert, D. Offner, *J. Tissue Eng.* **2018**, *9*, 2041731418776819.
- [7] X. Huang, Y. Ge, B. Yang, Q. Han, W. Zhou, J. Liang, M. Li, X. Peng, B. Ren, B. Yang, *Bioact. Mater.* **2021**, *6*, 4568.
- [8] W. Wang, K. W. K. Yeung, *Bioact. Mater.* **2017**, *2*, 224.
- [9] M. B. Dreifke, N. A. Ebraheim, A. C. Jayasuriya, *J. Biomed. Mater. Res., Part A* **2013**, *101*, 2436.
- [10] S. Lam, J. Kuether, A. Fong, R. Reid, *Craniofacial Trauma Reconstruction* **2015**, *8*, 159.
- [11] P. Bertsch, M. Diba, D. J. Mooney, S. C. G. Leeuwenburgh, *Chem. Rev.* **2022**, *123*, 834.
- [12] C. Laomeephol, H. Ferreira, S. Kanokpanont, J. A. Luckanagul, N. M. Neves, S. Damrongsakkul, *Biomater. Transl.* **2022**, *3*, 213.
- [13] H. Zhou, C. Liang, Z. Wei, Y. Bai, S. B. Bhaduri, T. J. Webster, L. Bian, L. Yang, *Mater. Today* **2019**, *28*, 81.
- [14] P. Maturavongsadit, W. Wu, J. Fan, I. B. Roninson, T. Cui, Q. Wang, *Biomater. Transl.* **2022**, *3*, 152.
- [15] M. Liu, X. Zeng, C. Ma, H. Yi, Z. Ali, X. Mou, S. Li, Y. Deng, N. He, *Bone Res.* **2017**, *5*, 1.
- [16] S. J. Bidarra, C. C. Barrias, P. L. Granja, *Acta Biomater.* **2014**, *10*, 1646.
- [17] Y. Zhang, F. Xing, R. Luo, X. Duan, *Front. Med.* **2021**, *8*, 676033.
- [18] C. L. Wu, S. S. Lee, C. H. Tsai, K. H. Lu, J. H. Zhao, Y. C. Chang, *Aust. Dent. J.* **2012**, *57*, 207.
- [19] L. Fan, Y. Ren, S. Emmert, I. Vučković, S. Stojanovic, S. Najman, R. Schnettler, M. Barbeck, K. Schenke-Layland, X. Xiong, *Int. J. Mol. Sci.* **2023**, *24*, 3744.
- [20] Y.-H. Jiang, Y.-Y. Lou, T.-H. Li, B.-Z. Liu, K. Chen, D. Zhang, T. Li, *Am. J. Transl. Res.* **2022**, *14*, 1146.
- [21] Y. Li, Y. Liu, R. Li, H. Bai, Z. Zhu, L. Zhu, C. Zhu, Z. Che, H. Liu, J. Wang, *Mater. Des.* **2021**, *210*, 110049.
- [22] A. Hoyer, F. Raikup-Wolf, E. Spörl, L. E. Pillunat, *Der Ophthalmologe* **2009**, *106*, 133.
- [23] H. Hatami-Marbini, S. M. Jayaram, *Invest. Ophthalmol. Visual Sci.* **2018**, *59*, 764.
- [24] D. Jelusic, M. L. Zirk, T. Fienitz, D. Plancak, I. Puhar, D. Rothamel, *Clin. Oral Implants Res.* **2017**, *28*, e175.
- [25] D. Sieger, T. Korzinskas, O. Jung, S. Stojanovic, S. Wenisch, R. Smeets, M. Gosau, R. Schnettler, S. Najman, M. Barbeck, *Int. J. Mol. Sci.* **2019**, *20*, 1969.
- [26] E.-U. Lee, D.-J. Kim, H.-C. Lim, J.-S. Lee, U.-W. Jung, S.-H. Choi, *Biomater. Res.* **2015**, *19*, 1.
- [27] O. Jung, M. Barbeck, L. U. Fan, F. Korte, C. Zhao, R. Krastev, S. Pantermehl, X. Xiong, *In Vivo* **2023**, *37*, 320.
- [28] P. Weiss, O. Gauthier, J. M. Boulter, G. Grimandi, G. Daculsi, *Bone* **1999**, *25*, 675.
- [29] M. Barbeck, O. Jung, R. Smeets, M. Gosau, R. Schnettler, P. Rider, A. Houshmand, T. Korzinskas, *In Vivo* **2020**, *34*, 557.
- [30] G. M. Thomas, *Applied Rheology*, Anton Paar GmbH, Austria, **2018**.
- [31] M. Funaki, P. A. Janmey, *Biology and Engineering of Stem Cell Niches*, **2017**, p. 363–373.
- [32] R. A. Brown, *Exp. Cell Res.* **2013**, *319*, 2460.
- [33] A. J. Engler, S. Sen, H. L. Sweeney, D. E. Discher, *Cell* **2006**, *126*, 677.
- [34] B. Trajkovski, M. Jaunich, W.-D. Müller, F. Beuer, G.-G. Zafropoulos, A. Houshmand, *Materials* **2018**, *11*, 215.
- [35] X. Zhang, H. Tainen, H. J. Haugen, *Med. Biol. Eng. Comput.* **2019**, *57*, 311.
- [36] L. Fan, F. Körte, A. Rudt, O. Jung, C. Burkhardt, M. Barbeck, X. Xiong, *Front. Bioeng. Biotechnol.* **2022**, *10*, 983988.
- [37] F. Peng, S. Jeong, G. Gonzalez, H. Marks, A. Ho, E. Roussakis, P. B. Kraledat, P. Hansen, C. L. Evans, *Adv. Funct. Mater.* **2021**, *31*, 2009229.

2.2 Deciphering UVA/Riboflavin Collagen Crosslinking: A Pathway to Improve Biomedical Materials

Fan, L., Jung, O., Herrmann, M., Shirokikh, M., Stojanovic, S., Najman, S., Körte, F., Xiong, X., Schenke-Layland, K., & Barbeck, M. (2024). *Advanced Functional Materials*, 2401742.

2.2.1 Summary and Major Findings

Since its initial application in the 1990s for treating keratoconus, collagen crosslinking using ultraviolet A rays and riboflavin (UVA/R) has significantly evolved, gaining prominence in the development of innovative hydrogels, scaffolds, and implants across various biomedical domains. Building on the findings of our previous study (section 2.1), where UVA/R crosslinking demonstrated its potential in enhancing biomechanical properties and stability of an injectable composite material, this study delves deeper into the intricacies of the UVA/R crosslinking process.

Despite its widespread application, the precise mechanism underlying UVA/R collagen crosslinking has remained an area of active research and debate, with several aspects yet to be fully understood. Recognizing the need for a deeper understanding and the imperative for a refined manufacturing process for collagen functionalization, this study aimed to unravel the UVA/R collagen crosslinking process. The focus was primarily on identifying the primary sites of crosslinking within collagen using synthetic peptides and exploring the pathways of riboflavin-mediated photochemical crosslinking.

In this study, seven synthetic peptides representing key amino acids—tyrosine, lysine, arginine, methionine, histidine, tryptophan, and phenylalanine—were employed to pinpoint specific sites of crosslinking in the UVA/riboflavin collagen crosslinking process. Liquid chromatography–mass spectrometry (LC-MS) analysis revealed that covalent crosslinking linkages occurred exclusively in tyrosine-containing peptides following UVA/R treatment. Additionally, di-tyrosine formation was observed in UVA/R crosslinked collagen hydrolysates. Considering the tyrosine residue content in porcine type I collagen's protein sequence, the crosslinking efficiency of tyrosine within the collagen matrix was

estimated to be at least 14.3%. This evidence of di-tyrosine in hydrolyzed UVA/R crosslinked collagen underscores the unique role of tyrosine in the crosslinking process, confirming its practical significance in collagen matrices. Moreover, our study reveals riboflavin's dual role in collagen crosslinking as both photosensitizer and substrate. Investigation into the ratios of tyrosine to riboflavin in both peptide and collagen systems showed a positive correlation between crosslinking efficacy and lower riboflavin concentrations, inversely proportional at higher concentrations. For example, in collagen, increased storage modulus was observed at lower riboflavin concentrations, which declined sharply at higher levels. A theoretical kinetic model inspired our discovery: the crosslinking efficiency is markedly sensitive to riboflavin concentration, particularly in environments with consistent oxygen availability. Riboflavin initially acts as a photosensitizer, generating reactive oxygen species for crosslinking, predominantly at tyrosine residues. At higher concentrations, riboflavin's participation in the reaction diminishes crosslinking efficiency, suggesting an intricate balance between riboflavin concentration and collagen matrix properties. Our findings identify tyrosine as the primary site for collagen crosslinking in UVA/riboflavin processes, with an estimated crosslinking efficiency of at least 14.3% within the collagen matrix. Additionally, it reveals riboflavin's dual role as both a photosensitizer and a competitor in collagen crosslinking, where its concentration critically influences the crosslinking efficacy and mechanical properties of the collagen matrix.

Raman spectroscopy's molecular fingerprinting highlighted differences in collagen crosslinked by UVA/R and EDC/NHS methods, underscoring tyrosine's critical role in UVA/R crosslinking, and lysine and hydroxylysine in EDC/NHS crosslinking. These spectroscopic insights also suggest Raman spectroscopy as a promising technique for guiding collagen functionalization in advanced biomedical applications.

Comparative analysis of UVA/R and chemical crosslinkers (EDC/NHS and genipin) on collagen matrices showed UVA/R's comparable efficacy through size exclusion chromatography (SEC) analysis of collagenase-degraded matrices. UVA/R crosslinked collagen matrices exhibited a cleaner

profile with less fragmentation, suggesting a safer in vivo profile. Rheological analysis, differential scanning calorimetry (DSC), and degradation evaluations revealed that UVA/R crosslinked collagen (Xcol_UVA/R) offers an optimal balance of stiffness, flexibility, stability, and degradability. This highlights its potential for developing collagen-based scaffolds in regenerative medicine.

In vitro cytotoxicity tests underscored Xcol_UVA/R's superior performance, supporting cell survival and proliferation. In contrast, the non-crosslinked collagen scaffold, despite being biocompatible, lacked structural integrity for effective cell-material interaction. Lower cell viability on Xcol_EDC/NHS and Xcol_Genipin scaffolds raised concerns about their cytotoxicity, highlighting the comparative advantage of Xcol_UVA/R in supporting cellular activities.

The histological assessment of subcutaneous implants demonstrates UVA/riboflavin crosslinking's effectiveness in enhancing collagen matrices' biostability and integration. The initial acute immune response, indicated by the presence of pro-inflammatory macrophages, transitions towards an anti-inflammatory profile in the BS-Xcol_UVA/R group, suggesting a conducive environment for tissue repair. These findings support the potential of UVA/R crosslinked collagen in influencing the immune environment favorably.

The findings from these investigations lay a robust foundation for the innovative design and application of collagen-based biomaterials, advancing biomedical technology and opening new scientific horizons with wide-reaching implications. These insights pave the way for further exploration into the use of photochemically crosslinked biomaterials in tissue engineering and regenerative medicine. Understanding the underlying mechanisms of these observations is crucial for fully harnessing their potential in clinical settings, particularly for achieving controlled immune responses essential for the successful integration and functionality of implants.

2.2.2 Personal Contribution

My role was integral in the experiment's conceptualization and execution, encompassing most of the in vitro experiments like SDS-PAGE, CD

spectroscopy, rheological characterizations, DSC analysis, and cytotoxicity tests. SEM, Raman spectroscopy, and LC-MS analysis were conducted with colleagues' guidance. I also prepared samples for in vivo implantation, although animal experiments were performed by colleagues. Furthermore, I was responsible for the thorough evaluation and presentation of all experimental results, along with the writing and revision of the manuscript.

Deciphering UVA/Riboflavin Collagen Crosslinking: A Pathway to Improve Biomedical Materials

Lu Fan, Ole Jung, Markus Herrmann, Marina Shirokikh, Sanja Stojanovic, Stevo Najman, Fabian Körte, Xin Xiong, Katja Schenke-Layland,* and Mike Barbeck

Collagen crosslinking employing ultraviolet A rays and riboflavin (UVA/R) has emerged as a pivotal technique in clinical therapies, especially in ophthalmology since the 1990s. Despite its clinical adoption, the lack of clarity of the detailed mechanism and the imperative for a refined manufacturing process necessitates further investigation. This study advances the understanding of UVA/R crosslinked collagen, concentrating on identifying the primary crosslinking sites using seven synthetic peptides and exploring the pathways of riboflavin-mediated crosslinking. The results demonstrate that tyrosine residues are key crosslinking sites, and riboflavin plays a dual role as both a catalyst and a competitive inhibitor in the crosslinking process. Furthermore, the UVA/R crosslinked collagen matrix exhibits a more harmonious balance between stability and degradability compared with chemically crosslinked collagen matrices, coupled with superior mechanical properties and augmented biocompatibility. In vivo experiments further validate its excellent biocompatibility, reduced tissue inflammation, and promotion of tissue regeneration. The research provides crucial insights into collagen crosslinking mechanisms, paving the way for the development of sophisticated collagen-based biomaterials tailored for biomedical applications.

bone grafts, and regeneration, ophthalmology, cardiovascular, and neural tissue engineering.^[1–3] To optimize the functionality of the collagens, mainly collagen type I (collagen), in these applications, crosslinking is often imperative, enhancing its mechanical properties, biostability, biocompatibility, and other functionalities.^[4–6] Among the various crosslinking techniques, ultraviolet A rays and riboflavin (UVA/R) crosslinking stands out as a particularly promising technique, having been approved for clinical use in ophthalmological therapy since the early 1990s.^[7] This inherent convenience and safety hold tremendous potential for expanding collagens' application landscape across diverse biomedical fields.^[8,9] The realm of UVA photocrosslinking is rapidly advancing, revealing promising applications across medical disciplines.^[10] Its utility now extends to creating innovative hydrogels aimed at minimizing postoperative adhesions, which has potential to revolutionize laparoscopic surgery recovery.^[11]

Moreover, UVA/R crosslinked acellular porcine cornea are being evaluated as a potential scaffold for Boston Keratoprosthesis, reflecting significant strides in biocompatibility and efficiency.^[12,13] This technique's application has diversified, with

1. Introduction

Collagens have been extensively utilized in various biomedical fields as functional biomaterials, including wound healing,

L. Fan, M. Herrmann, M. Shirokikh, F. Körte, X. Xiong, K. Schenke-Layland
NMI Natural and Medical Sciences Institute at the University Tübingen
Markwiesenstr. 55, 72770 Reutlingen, Germany
E-mail: katja.schenke-layland@uni-tuebingen.de

L. Fan, K. Schenke-Layland
Institute of Biomedical Engineering
Department for Medical Technologies and Regenerative Medicine
Medical Faculty
Eberhard Karls University Tübingen
Silcherstr. 7/1, 72076 Tübingen, Germany

O. Jung, M. Barbeck
Clinic and Policlinic for Dermatology and Venereology
University Medical Center Rostock
Strempelstraße 13, 18057 Rostock, Germany

S. Stojanovic, S. Najman
Department of Cell and Tissue Engineering
Scientific Research Center for Biomedicine
Faculty of Medicine
University of Niš
Blvd. Dr Zorana Djindjica, Niš 18108, Serbia
S. Stojanovic, S. Najman
Department of Biology and Human Genetics
Faculty of Medicine
University of Niš
Blvd. Dr Zorana Djindjica, Niš 18108, Serbia

 The ORCID identification number(s) for the author(s) of this article can be found under <https://doi.org/10.1002/adfm.202401742>

© 2024 The Authors. Advanced Functional Materials published by Wiley-VCH GmbH. This is an open access article under the terms of the [Creative Commons Attribution-NonCommercial](https://creativecommons.org/licenses/by-nc/4.0/) License, which permits use, distribution and reproduction in any medium, provided the original work is properly cited and is not used for commercial purposes.

DOI: 10.1002/adfm.202401742

groundbreaking methods like the glutaraldehyde-free preparation for cardiac implants,^[14] meniscus tissue engineering,^[15] controlled drug delivery device,^[16] and extends its influence into cutting-edge research domains including 3D bioprinting^[17,18] and organ-on-a-chip systems, showcasing the dynamic potential of UVA/R crosslinking in modern biomedical engineering.^[19–22]

Despite these promising applications, the mechanism underlying UVA/R crosslinking remains an area of ongoing research and debate. Many studies suggest that riboflavin functions primarily as a photocatalyst generating reactive oxygen species (ROS) to induce collagen oxidation and polymerization.^[9,23,24] Alternative theories propose that this is a much more complex photochemical process, which is oxygen and/or UVA exposure-dependent.^[25,26] Debates also exist regarding the specific crosslinking sites on collagen molecules, with some asserting non-selectivity,^[9,27] while others point to amino acids like lysine, histidine, arginine, tyrosine, or methionine.^[28–31] These differing viewpoints on UVA/R crosslinking mechanisms underscore a lack of comprehensive understanding, presenting challenges in standardizing manufacturing processes and in the regulatory evaluation of medical devices. To address these knowledge gaps and potentially increase applications using collagen, our study investigates the fundamental principles of UVA/R crosslinking. By exploring alternative mechanistic explanations and unraveling the intricate interactions between collagen and riboflavin, we provide valuable insights that will contribute to the refinement and optimization of UVA/R crosslinking techniques. However, investigating the crosslinking mechanism in collagen presents significant challenges due to the dynamic photochemical processes and collagen molecular complexity.^[9,32,33] To unravel these detailed mechanisms, advanced experimental techniques and comprehensive analytical methods are required to identify and characterize the transient intermediates and pathways accurately.^[34–36] Additionally, the variability in collagen's physical and chemical properties, influenced by the collagen source, type, processing, and environmental factors add layers of difficulty to these studies, necessitating a nuanced approach to fully understand the crosslinking process.^[37–41]

In our study, we adopted an innovative experimental framework, synthesizing seven synthetic peptides representing crucial potential crosslinking sites on collagen, focusing on amino acid residues such as tyrosine (Y), lysine (K), arginine (R), methionine (M), histidine (H), tryptophane (W), and phenylalanine (F). These amino acids were selected for their reactive groups and positions in the non-helical region of the collagen molecule, which is more accessible for crosslinking reactions and crucial for enhancing mechanical properties. (Figure 1) By exposing these peptides and native collagen to varied UVA energy and riboflavin ratios, we dissected the crosslinking process using liquid chromatography-mass spectrometry (LC-MS). We also compared UVA/R crosslinking with chemical crosslinkers, utilizing Raman microspectroscopy to discern distinct molecular alterations post-crosslinking. We evaluated mechanical strength, thermal stability, degradation resistance, and cytotoxicity, culminating in in vivo implantation trials to assess biocompatibility and tissue regeneration potential. By dissecting the crosslinking process at a molecular level, our study reveals critical insights into the roles and interactions of specific amino acids, shedding light on the intricate dynamics of UVA/R crosslinking. These discoveries hold

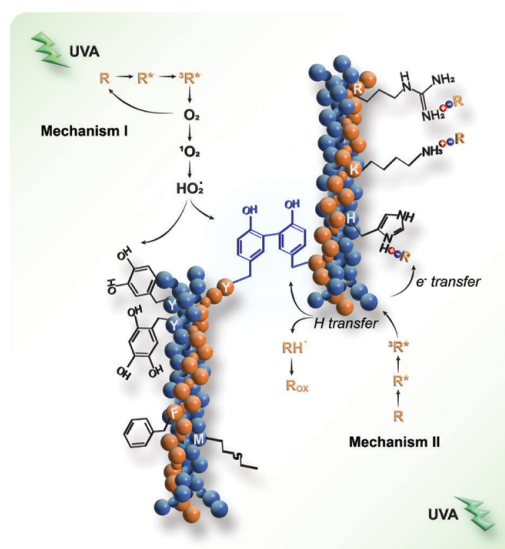


Figure 1. Schematic of UVA/riboflavin collagen crosslinking. UVA: Ultraviolet A light, the source of photoactivation. R: ground state riboflavin. R*: excited state of riboflavin upon initial UVA exposure. ³R*: Triplet state riboflavin after intersystem crossing, a higher energy state capable of engaging in crosslinking reactions. O₂: molecular oxygen. ¹O₂: singlet oxygen, a reactive oxygen species generated by energy transfer from photoactivated riboflavin to molecular oxygen. HO₂*: hydroperoxyl radical. RH: general structure representing a hydrogen donor. R_{ox}: oxidized form of the hydrogen donor following hydrogen transfer. Amino acids: Y (tyrosine), K (lysine), R (arginine), M (methionine), H (histidine), W (tryptophan, not present in porcine collagen type I), F (phenylalanine).

substantial implications for advancing biomaterial science, offering a foundation for developing advanced, biocompatible, and mechanically robust biomaterials, thus paving the way for more effective and safer biomedical applications.

2. Results and Discussion

2.1. Preparation and Characterizations of the Collagen Matrix

Type I collagen, sourced from porcine skin due to its close resemblance to human tissue, offers a robust framework for tissue engineering.^[42,43] This form of collagen is ideal for biomedical applications because of its abundance in the skin and its well-defined triple-helical structure comprising two α 1 chains and one α 2 chain (Figure 2A).^[44,45] SDS-PAGE indicated the integrity and purity of our porcine-derived collagen after a series of mechanical homogenization processions, using rat tail collagen as a control. Figure 2B showcases distinct bands in the SDS-PAGE gel for both porcine skin-derived collagen (P-col) and rat tail-derived collagen (R-col), highlighting the α 1 and α 2 bands at \approx 150 and 140 kDa, respectively. No further bands below the 100 kDa were observed. Higher molecular weight bands, corresponding to dimers (β) and trimers (γ), were also discernible, indicating the collagen matrix's high purity and maintained integrity following mechanical processing.^[46] Circular dichroism (CD) spectroscopy

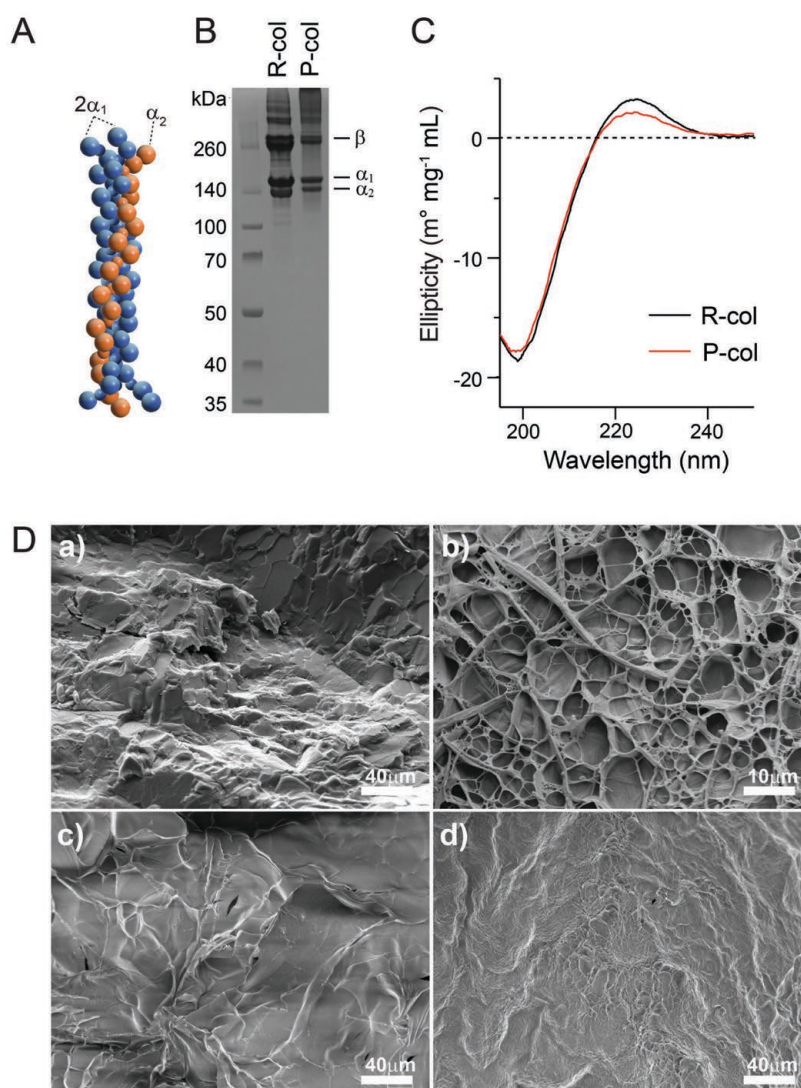


Figure 2. Structural and mechanical characterization of collagen pre- and post-UVA/riboflavin treatment. A) Molecular model of the collagen type I triple helix structure, the fundamental building block of collagen matrices. B) SDS-PAGE analysis depicting the characterization of collagen type I extracted from rat tail (R-col) and porcine skin (P-col). C) Circular dichroism (CD) spectra of R-col and P-col, with ellipticity indicating preservation of the collagen secondary structure. D) Scanning electron microscopy images presenting the morphological examination of non-crosslinked collagen and UVA/R crosslinked collagen in their hydrated-frozen state (a,b), as well as in their lyophilized state (c,d).

provided further confirmation, exhibiting characteristic negative and positive peaks that signify the presence of the collagen's well-maintained triple-helical conformation (Figure 2C).^[47] Such high purity and structural integrity are crucial for the effective interaction with crosslinking agents and precise mechanical property analysis.

Scanning electron microscopy (SEM) was employed to evaluate morphological changes in the collagen matrices before

and after UVA/R crosslinking. (Figure 2D) Initially, the non-crosslinked collagen displayed a unique crystal-like surface texture in its hydrated-frozen state, deviating from the conventional fibrillar structure due to the homogenization and stirring/foaming processes implemented during its preparation (Figure 2Da). This intentional disruption was necessary for further matrix design. Following crosslinking, a noteworthy transformation was observed in the UVA/R crosslinked collagen

matrix. It exhibited an intricate, porous architecture with interconnected voids and pores, ranging from 1 to 20 μm in size, contributing to its three-dimensional complexity. (Figure 2Db) The heterogeneity in pore size may foster a more natural and dynamic environment for cells, allowing for varied cell adhesion, migration, and nutrient diffusion, which are crucial for tissue regeneration and repair.^[48,49] Moreover, the restructured collagen fibers may enhance mechanical cues that can guide cellular alignment and differentiation, thus contributing to the formation of a more functional and organized tissue structure in biomedical applications.^[50,51] Furthermore, the densification and increased stiffness resulting from lyophilization suggest enhanced resistance to mechanical deformation, an essential characteristic for biomaterials exposed to physiological stresses (Figure 2Dc,d). This enhanced mechanical robustness not only ensures the structural integrity of the collagen matrix under varying physical conditions but also potentially extends its functional lifespan, making it more suitable for long-term biomedical applications such as implantable devices or tissue scaffolds.^[52]

2.2. Exploration of the UVA/R Crosslinking Mechanism

Having established the fundamental aspects of the collagen matrix preparation and analyzed its initial characteristics, we then delved into the exploration of the mechanism of UVA/R crosslinking, a pivotal process that significantly alters and enhances the matrix's properties. This section investigates where crosslinks form on the collagen molecule, the role of riboflavin as a catalyst or participator, and further postulates the necessity for adjustments of the collagen UVA/R crosslinking in the various applications.

2.2.1. Where do Crosslinks Form on the Collagen Molecule?

In our study, we probed the crosslinking mechanism of type I collagen at the molecular level, focusing on non-helical regions that enhance mechanical properties post-crosslinking. Employing seven synthetic peptides representing crucial amino acids—tyrosine (Y), lysine (K), arginine (R), methionine (M), histidine (H), tryptophane (W), and phenylalanine (F)—we aimed to identify specific sites of crosslinking. These amino acids were selected for their distinct reactive functionalities and strategic positions within collagen the molecule (Figure S1, Supporting Information). Specifically, tyrosine (Y) possesses a reactive phenol group capable of engaging in covalent bonding.^[53] Lysine (K) and arginine (R) are equipped with amino groups that are candidates for chemical bond formation.^[54–56] Histidine (H) is characterized by an imidazole ring, and phenylalanine (F) by an aromatic ring, both offering potential sites for reactivity.^[57] Our LC-MS analyses delineated a distinct pattern: modifications post-UVA/R treatment occurred exclusively in tyrosine-bearing peptides, likely due to the generation of covalent di-tyrosine linkages (Figure 3A,B). This specificity was further accentuated by the absence of covalent bonding products in the other six amino acids including peptides, underscoring the preferential role of tyrosine in the crosslinking mechanism (Figures S2 and S3, Supporting Information). The propensity for di-tyrosine formation,

initially posited from our synthetic peptide studies, was conclusively corroborated by the LC-MS analysis of hydrolysates of UVA/R crosslinked collagen (Figure 3C,D). During the examination of UVA/R crosslinked collagen, di-tyrosine was reliably identified by using multiple reaction monitoring (MRM) mode in mass spectrometry and authenticated through comparisons with a di-tyrosine standard.^[58] Notably, our LC-MS scrutiny of collagen hydrolysates disclosed a peak highly akin to, yet distinguishable from, the di-tyrosine standard. Acknowledging the likelihood of isomeric or spatial variations within the collagen molecules, we cautiously infer, predicated on mass considerations, that the coinciding peaks could represent di-tyrosine forms (Figure S4, Supporting Information).^[59,60] Given the protein sequence of porcine type I collagen (Access numbers A0A1S7J210 for COL1A1 and A0A1S7J1Y9 for COL1A2), the complete mature collagen molecule should exhibit a molecular weight of 282.85 kDa, encompassing 3152 amino acid residues, inclusive of 13 tyrosine residues. If we assume all these tyrosine residues are equally reactive and available for crosslinking, our LC-MS results intimate that a conservative estimate of crosslinked tyrosine within the collagen matrix is at least 14.3% (Figure S5, Supporting Information). This deduction is instrumental in appraising the extent of collagen crosslinking affected by UVA/R conditions and enriches our comprehension of its mechanisms.

The substantiation of di-tyrosine in hydrolyzed UVA/R crosslinked collagen is a pivotal affirmation of tyrosine's exclusivity in the crosslinking schema. Such evidence not only echoes the synthetic peptide experimental results but also exemplifies the practical relevance of tyrosine crosslinking in collagen matrices. The presence of di-tyrosine serves as a molecular hallmark of successful crosslinking, offering an imperative insight that is anticipated to be crucial for refining UVA/R crosslinking techniques in collagen tailored for biomedical utilizations.

2.2.2. Riboflavin: Crosslinking Catalyst or Participator?

In exploring the role of riboflavin in collagen crosslinking, our study uncovers its dual function as both a catalyst and a participator. By examining the relationship between tyrosine and riboflavin ratios in both the peptide and collagen systems, we observed similar notable trends: a positive correlation between crosslinking efficacy and riboflavin at lower ratios, which reverses at higher concentrations (Figure 3E). For example, in collagen, at lower riboflavin concentrations (tyrosine/riboflavin ratios of 1/0.0625 to 1/0.25), there was a significant increase in the storage modulus compared to the non-crosslinked collagen. However, at higher concentrations, the storage modulus sharply declined (Figure 3F).

The noticeable reduction in the mechanical strength of collagen matrices at elevated riboflavin concentrations prompted an exploration of the underlying mechanisms. Our investigation was guided by a theoretical kinetic model, indicating a critical dependence of the two pathways of riboflavin-mediated photocrosslinking on ambient oxygen levels.^[61] This model inspired our discovery: the crosslinking efficiency is markedly sensitive to riboflavin concentration, particularly in environments with consistent oxygen availability. This nuanced photochemical behavior of riboflavin suggests two primary reaction pathways upon

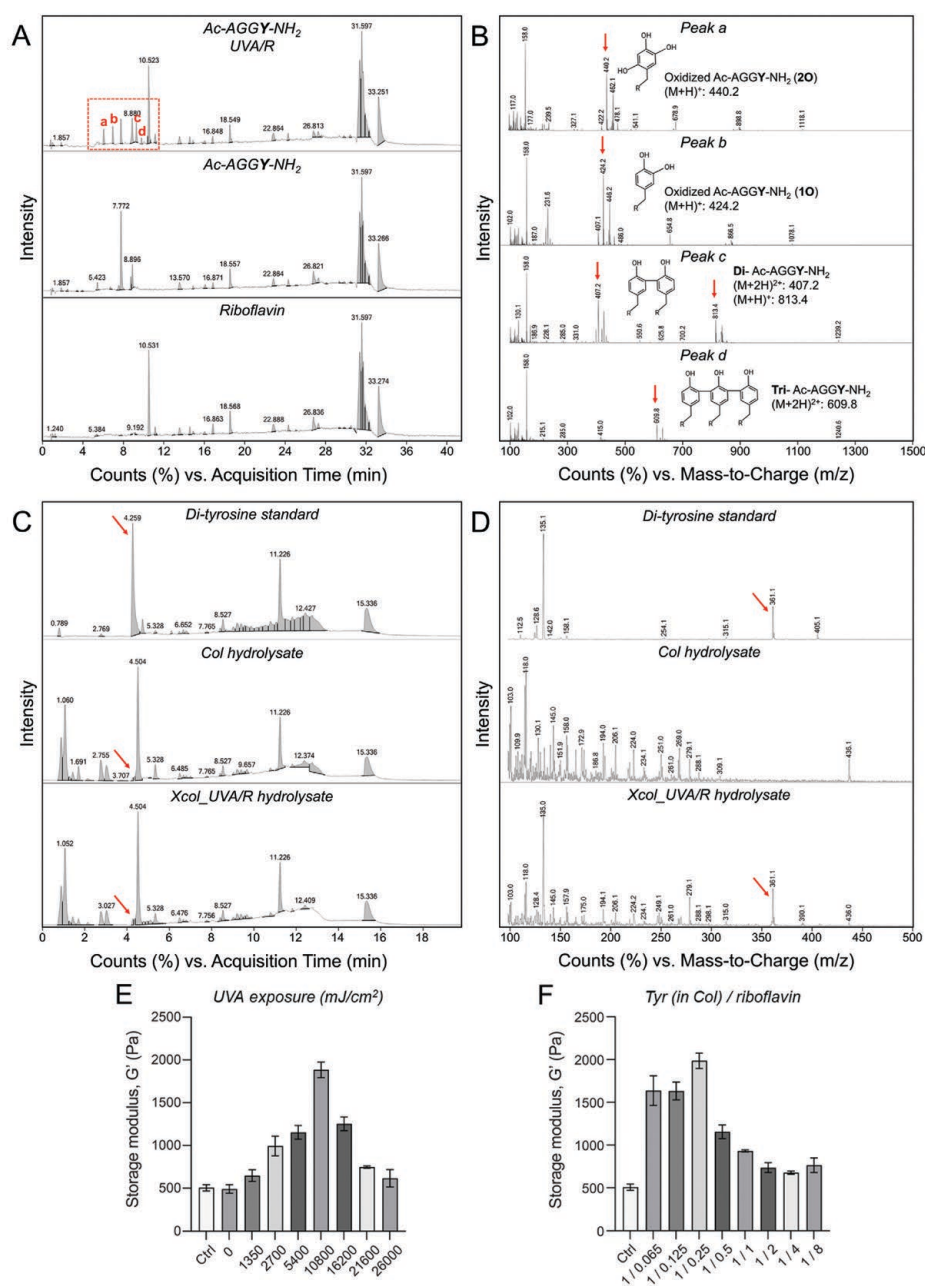


Figure 3. Dissecting the UVA/R crosslinking mechanism in collagen. A) LC-MS chromatograms post UVA/R treatment of Ac-AGGY-NH₂ peptide with control samples of Ac-AGGY-NH₂ and riboflavin. B) Mass spectra correlating with newly emerged peaks (a–d) in chromatograms of UVA/R treated Ac-AGGY-NH₂. C) LC-MS chromatograms of di-tyrosine standard and hydrolysates of non-crosslinked collagen and UVA/R crosslinked collagen, D) with corresponding mass spectra. E) Storage modulus (G') of collagen as a function of UVA exposure (mJ cm^{-2}), showcasing the dose-dependent increase in mechanical properties. F) Storage modulus (G') in relation to the Tyr (in collagen)/riboflavin ratio, illustrating the impact of varying riboflavin concentrations on the mechanical strength of the collagen matrices.

UVA excitation, as illustrated in Figure 1. Initially, riboflavin acts as a photocatalyst, generating ROS that facilitate intermolecular crosslinking, predominantly at tyrosine residues located in the non-helical regions of collagen. This process enhances the mechanical properties of the matrix. However, an alternative pathway becomes predominant at higher riboflavin concentrations, where riboflavin actively engages in the crosslinking reaction, depleting ROS and subsequently diminishing crosslinking efficiency. Furthermore, electron transfer processes may induce interactions between positively charged amino acid residues like lysine, histidine, and arginine, and negatively charged riboflavin, potentially influencing the mechanical properties of the collagen matrix. This aspect merits further experimental validation.

Additionally, UVA exposure for crosslinking the collagen matrix was also optimized in our study. Our findings as illustrated in Figure 3E indicate that the optimal UVA exposure for collagen matrix crosslinking was 10800 mJ cm^{-2} . Beyond this UVA dosage, the storage modulus of the collagen matrices noticeably decreased, suggesting potential degradation of the collagen scaffold due to overexposure. Interestingly, for peptide crosslinking, the optimal UVA dosage was markedly lower, at 600 mJ cm^{-2} (Figure S6, Supporting Information); and in another work, Uemura et al. identified that the optimal UVA exposure for human dentin collagen crosslinking was 1600 mJ cm^{-2} .^[19]

Overall, these insights uncover an additional layer of the UVA/R crosslinking mechanism, highlighting the crucial need to fine-tune riboflavin concentration and UVA exposure for practical applications. The notable disparity between in vivo tissue environments and in vitro collagen crosslinking systems is substantial. Variations in collagen sources (tyrosine residue content), concentration, density, and differing buffer conditions necessitate tailored approaches for adjusting riboflavin concentration and UVA exposure to achieve optimal crosslinking outcomes.^[62]

2.3. Comparative Investigation of the Impact of UVA/R and Chemical Crosslinking on Collagen Matrices

After elucidation of the complexity of the UVA/R crosslinking mechanism, we turned our attention to the comparative investigation aimed at comprehensively evaluating the effects of different chemical crosslinking techniques on collagen matrices. Each analysis contributes to a holistic understanding of the structural and functional alterations induced by UVA/R and other chemical crosslinking methods.

2.3.1. Raman microspectroscopy

Raman microspectroscopy has offered a profound insight into the molecular integrity of collagen matrices subjected to different crosslinking techniques.^[63,64] Detailed peak assignments along with their corresponding references are compiled in Table S3 (Supporting Information). In our study, Col UVA/R crosslinked collagen (Xco_UVA/R) and EDC/NHS crosslinked collagen (Xco_EDC/NHS) retained their quintessential secondary structures post-crosslinking when compared with non-crosslinked collagen (Col), as evidenced by the consistent amide bands across all samples: Amide III (1260 cm^{-1}), Amide II (1452 cm^{-1}), and

Amide I (1664 cm^{-1}) (Figure 4A). The spectra revealed that while the characteristic triple-helix structure of collagen was maintained, there were notable reductions in the intensity of peaks ($815, 936, 971, \text{ and } 1080 \text{ cm}^{-1}$) associated with the side-chain vibrations of amino acids involved in both UVA/R and EDC/NHS crosslinking reactions.^[65–67] Such findings suggest subtle yet definitive molecular rearrangements within the collagen's architecture, particularly affecting vibrational modes, such as C–C stretching, C–C stretching wagging, and CH_3 rocking within lysine, hydroxylysine, and tyrosine residues, which are crucial for the crosslinking process. Notably, the extent of intensity reduction was more pronounced in EDC/NHS crosslinked collagen, indicating a higher abundance of lysine and hydroxylysine-mediated crosslinks compared to the tyrosine-mediated ones in UVA/R crosslinking. An intriguing shift from 936 to 927 cm^{-1} after EDC/NHS crosslinking possibly alludes to heightened tension arising from proline residue packing post-crosslinking.

Further scrutiny via multivariate principal component analysis (PCA) corroborated these structural nuances, discriminating between the untreated and crosslinked samples (Figure 4B–D). The distinct clustering of PC-3 and PC-4 scores elucidated the molecular underpinnings unique to each treatment, with the UVA/R crosslinking manifesting a distinct molecular fingerprint when compared to its chemical counterpart. The PC-3 scores offered positive scores evident for Xco_UVA/R spectra and negative scores for Col and Xco_EDC/NHS. This trend was mirrored in the PC-3 loading plot, featuring prominent peaks at 936 cm^{-1} (proline) and 1688 cm^{-1} (Amide I). In tandem, the PC-4 scores revealed positive ranges for both Xco_UVA/R and Xco_EDC/NHS, whereas Col spectra clustered in the negative range. The corresponding PC-4 loadings plot pinpointed crosslinking-associated peaks at $896, 980, 1099, 1309, 1439, \text{ and } 1655 \text{ cm}^{-1}$, signifying the vibrational modes of ν (C–C), ν (C–N), as well as CH_3/CH_2 twisting, bending, or wagging mode deformation among others, reinforcing the crosslinking-driven molecular distinctions observed.^[65,68–70]

Raman microspectroscopy provided molecular fingerprinting patterns that elucidate the changes occurring at the molecular level in collagen post-crosslinking, as well as the different characteristics between collagen crosslinked by UVA/R and EDC/NHS methods. These spectroscopic findings are pivotal in guiding the functionalization of collagen for advanced biomedical applications.

2.3.2. Size-Exclusion Chromatography of Digested Collagen Matrix

Size-exclusion chromatography (SEC) of collagenase-digested samples revealed marked differences in the molecular profile of collagen matrices post-crosslinking (Figure 4E–G). Given that collagenase primarily cleaves the peptide bonds within collagen molecules at the characteristic Gly-X-Y triplets, where X and Y are often proline or hydroxyproline residues, the enzymatic digestion process yields smaller peptide fragments. The presence of larger peptide fragments in crosslinked samples, especially noticeable in the region of peak 1, is indicative of the effectiveness of crosslinking in impeding enzymatic cleavage. This finding was particularly pronounced in the UVA/R crosslinked sample, where the sizeable peptide entities were retained to a degree

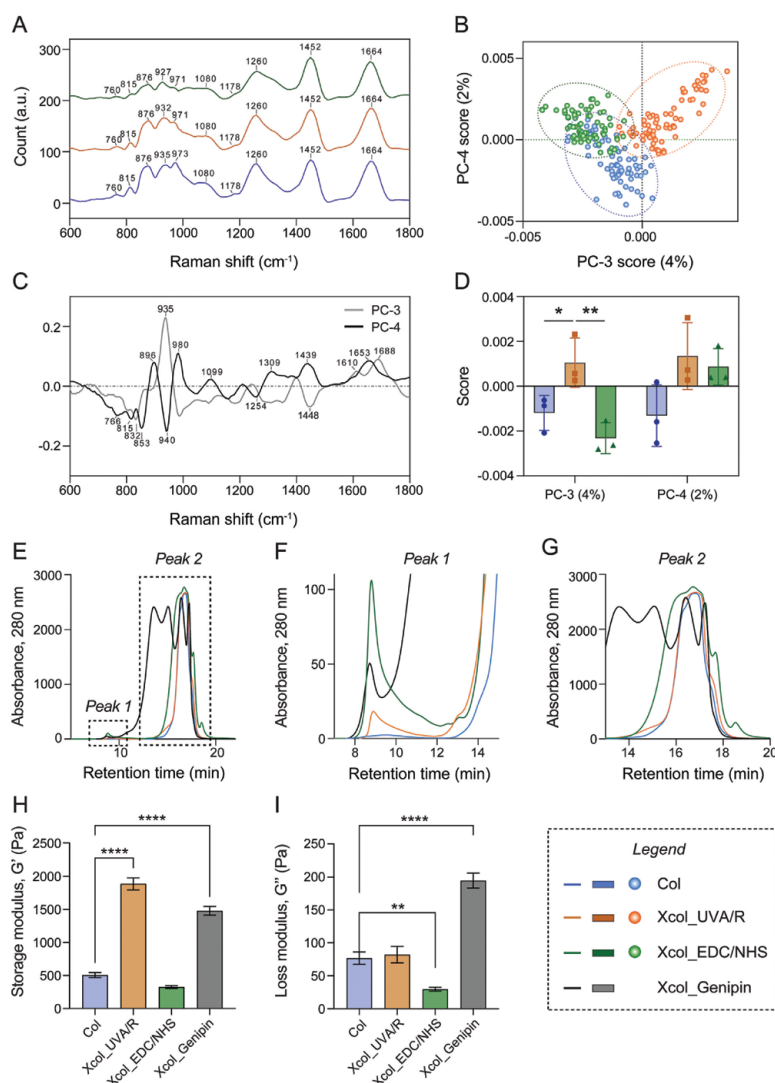


Figure 4. Comprehensive characterization of non-crosslinked collagen (Col), UVA/R crosslinked collagen (Xcol_UVA/R), EDC/NHS crosslinked collagen (Xcol_EDC/NHS), and genipin crosslinked collagen (Xcol_Genipin) matrices. A–D) Raman microspectroscopic analysis: (A) Average Raman spectra highlighting distinct peaks and patterns. Each condition was replicated at least thrice ($n \geq 3$), with multiple spectra acquired for each replicate ($n \geq 25$). Multivariate data analysis outcomes include principal component analysis (PCA) results featuring PCA spectral loadings of PC-3 and PC-4 (C), scores plot of PC-4 versus PC-3 (B), and statistical representation of PC-3 and PC-4 scores as mean values \pm SD (D). Confidence ellipses in (B) signify 95% confidence intervals. E–G) Size-exclusion chromatography analysis: traces depicting the behavior of collagen matrices, as detected using a UV detector. Close-up views of Peak 1 and Peak 2 are detailed in (F) and (G). Dynamic H) storage modulus (G') and I) loss modulus (G'') extracted from the plateau LVE region during frequency sweeps.

similar to that of chemically crosslinked samples. Such an observation highlights the comparable efficacy of UVA/R crosslinking to traditional chemical methods like EDC/NHS and genipin in protecting collagen matrices from enzymatic digestion. Moreover, the UVA/R crosslinking demonstrated an advantageous profile with fewer smaller by-products relative to chem-

ical crosslinking. The chromatograms for the EDC/NHS and genipin-treated samples showed additional peaks, suggesting the presence of by-products, which could potentially lead to cytotoxic effects or provoke immune responses when used in biomedical applications.^[71] In contrast, the UVA/R crosslinking process appears to have resulted in a cleaner profile with less

fragmentation, which may translate to a more favorable safety profile for in vivo applications. The molecular integrity maintained by UVA/R crosslinking, coupled with its reduced by-product profile, positions it as a potent method for preparing collagen-based biomaterials for regenerative medicine.^[38]

2.3.3. Rheological Properties

The rheological properties of crosslinked collagen matrices, as analyzed by dynamic shear-stress amplitude and frequency sweeps, provided insights into the mechanical implications of each crosslinking strategy at physiological temperatures. (Figure 4H,I) Xcol_UVA/R demonstrated an enhanced elastic profile as evidenced by its storage modulus, without a corresponding loss in material resilience. This balance of elasticity and durability underscores the potential of UVA/R crosslinking to fortify the mechanical integrity of collagen scaffolds without sacrificing the material's ability to absorb and dissipate energy, which is an essential characteristic for biomaterials that must endure dynamic physiological environments. On the other hand, Xcol_EDC/NHS presented an unexpectedly lower storage modulus (Figure 4I), suggesting that while chemical crosslinking with EDC/NHS does modify the material, it may not uniformly enhance the elastic properties of the collagen matrix. This finding could have implications for the application of EDC/NHS crosslinked materials in scenarios where mechanical stiffness is a prerequisite. In contrast, Xcol_Genipin showed a marked increase in stiffness, as indicated by its higher storage modulus. However, the increased rigidity may impose limitations on the material's functional compatibility, particularly concerning cellular activities.^[72] Materials that are excessively stiff could potentially hinder cell migration and proliferation, both of which are critical for tissue regeneration and integration.^[73,74]

Taken together, these results suggest that UVA/R crosslinking achieves an optimal balance of stiffness and flexibility, which may be conducive to cellular functions, thus presenting a promising avenue for further development of collagen-based scaffolds for regenerative medicine.

2.3.4. Thermal Stability

Differential scanning calorimetry (DSC) measurements, depicted in Figure 5A,B, provided essential insights into the thermal stability of the collagen matrices. The denaturation temperature (T_m), observed as a peak on the DSC curves, marks the transition point where the collagen triple helix begins to unwind due to the breakdown of stabilizing hydrogen bonds.^[29] This thermal event is accompanied by the absorption of heat, which is quantitatively measured as the change in enthalpy (ΔH).^[29] In our study, a noticeable elevation in T_m was recorded for the crosslinked collagen samples. Specifically, Xcol_UVA/R and Xcol_EDC/NHS show T_m values at 75 and 76.0 °C respectively, indicating enhanced thermal stability potentially conducive to maintaining structural integrity at physiological temperatures. Xcol_Genipin, while displaying a lower T_m at 60.1 °C, still shows increased thermal resistance relative to non-crosslinked collagen. The enthalpy changes (ΔH) associated with the denaturation process,

as depicted in Figure 5B, further support these findings, with Xcol_UVA/R and Xcol_EDC/NHS demonstrating a substantial absorption of heat, reflective of the energy required to disrupt the strengthened collagen structure due to crosslinking. These thermodynamic characteristics imply that the crosslinking confers additional stability to the collagen matrices, which is crucial for their performance under thermal stress in vivo.

2.3.5. Degradation Resistance

Our study extended to a comparative degradation analysis of crosslinked collagen matrices in physiologically relevant conditions using phosphate-buffered saline (PBS) and collagenase solutions (Figure 5C,D). The degradation profile of Xcol_UVA/R was particularly compelling, exhibiting resistance on par with chemically crosslinked matrices, thereby marking a significant improvement over the non-crosslinked collagen. This observation is pivotal, as it is the first to directly compare the degradation resistance of UVA/R crosslinked collagen with chemically crosslinked variants. Xcol_EDC/NHS displayed exceptional durability in PBS, maintaining over 60% of its mass after 30 days, indicative of its potential for applications where extended stability is paramount. Genipin-crosslinked collagen also showed remarkable resistance in collagenase solutions, suggesting its suitability for environments with active enzymatic degradation.

However, the robustness of these chemically crosslinked matrices raises concerns in the tissue engineering context, where scaffold degradation kinetics must be synchronized with tissue regeneration.^[75] Biomaterials that degrade too slowly may disrupt the delicate process of new tissue formation, potentially interfering with cell migration, vascularization, and the natural tissue remodeling process.^[30] Moreover, the persistent presence of non-degraded materials can provoke a sustained inflammatory response, which may adversely affect healing outcomes.^[31] In tissue engineering, the ideal biomaterial should provide initial mechanical support but gradually cede its place to newly formed tissue. Therefore, optimizing the degradation rate to ensure a seamless transition from scaffold to native tissue is critical. Our findings highlight the need for a nuanced approach to the design of collagen-based scaffolds, aiming for a delicate equilibrium that supports initial tissue repair and subsequently allows for natural tissue integration without eliciting chronic inflammation or other negative responses.

2.3.6. In Vitro Cytotoxicity Test

The biocompatibility of our collagen matrices was evaluated through the CCK-8 assay utilizing L929 fibroblasts, following DIN EN ISO 10993-5: 2009 and DIN EN 10993-12: 2021 guidelines. The standard posits that biomaterials should not reduce cell viability below 70% of the control to be considered biocompatible. As shown in Figure 5E, the crosslinked collagen matrices, particularly Xcol_EDC/NHS, exhibited reduced cell viability, suggesting potential cytotoxicity from residual crosslinking agents or by-products. Contrastingly, Xcol_UVA/R surpassed the biocompatibility threshold with viability above 80%, indicating its suitability for tissue engineering applications due to its favorable balance of stability and degradation.

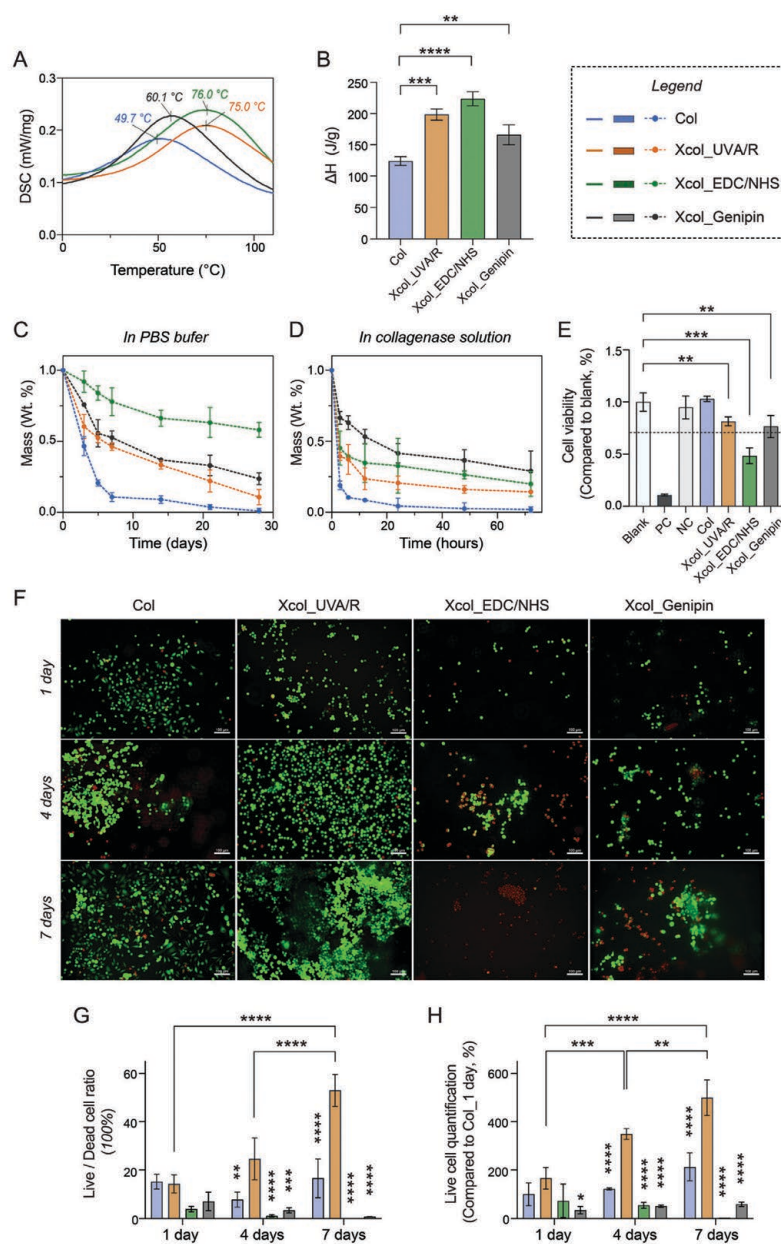


Figure 5. Characterization of collagen matrices and in vitro biological evaluation. A) Differential scanning calorimetry (DSC) curves illustrating the thermal transitions of collagen matrices, marked with peak temperatures (T_m). B) Enthalpy changes (ΔH) during denaturation of collagen matrices. Mass loss during in vitro degradation in C) phosphate-buffered saline (PBS) solution and D) collagenase solution. E) In vitro cytotoxicity test using L929 fibroblasts via CCK-8 assay, following the ISO 10993-5 standard. F) Representative confocal laser scanning microscopy (CLSM) images of live/dead (Calcein-PI) staining of L929 cells cultured on collagen scaffolds at 1-, 4-, and 7-days post-seeding. G) Quantitative analysis of live/dead cell ratio, derived from the CLSM images, using ImageJ software for cell quantification. H) Quantification of live cells, highlighting the cell viability and proliferation across the study period. Statistical evaluation for parts (G) and (H) was performed using ANOVA for multiple comparisons at different time points, with specific comparisons made between the Xcol_UVA/R group and other groups. (Scale bars in the live-dead staining images correspond to 100 μ m. Calcein in green, PI in red.)

Live-dead staining (Figure 5F) with its subsequent quantitative analysis (Figure 5G,H) further highlighted the superior performance of Xcol_UVA/R, which supported cell survival and proliferation. Initially, at day 1, the live/dead ratios for Col and Xcol_UVA/R groups were comparable, corroborating the results of the extraction cytotoxicity test depicted in Figure 5E. However, as the culture progressed to days 4 and 7, the Xcol_UVA/R scaffold demonstrated its superiority with significantly enhanced cell viability and proliferation, likely attributable to its biomechanical attributes. While the non-crosslinked collagen scaffold, despite being biocompatible, did not exhibit the structural integrity necessary for optimal cell-material interactions, as evidenced by its performance at 4 and 7 days. In contrast, the collagen matrices crosslinked with EDC/NHS and genipin displayed diminished live cell ratios throughout the duration of the study, which could raise concerns regarding their cytotoxicity profiles.

Our comprehensive analyses encompassing enzymatic digestion profiles, mechanical strength, thermal stability, and degradation resistance, when juxtaposed with *in vitro* cytotoxicity assessments, reveal a multifaceted evaluation of crosslinked collagen matrices for biomedical applications. Xcol_UVA/R stands out with its balanced profile; it exhibits comparable thermal stability and degradation resistance to chemically crosslinked counterparts, maintaining structural integrity under physiological conditions while supporting robust cell viability and favorable cell-material interactions. The enzymatic digestion results, indicating reduced degradation in crosslinked samples, align with the observed enhancement in mechanical and thermal properties, corroborating the crosslinking's effectiveness in bolstering matrix resilience. However, the mechanical robustness and reduced degradability, as seen in Xcol_EDC/NHS and Xcol_Genipin, may be a detriment to the delicate equilibrium required for tissue regeneration. These matrices show limited enzymatic breakdown and increased thermal resistance, yet this durability could potentially impede natural tissue remodeling, as indicated by their lower cell viability. In the realm of tissue engineering, where scaffold degradation is expected to pave the way for new tissue formation, materials like Xcol_UVA/R that strike an optimal balance between stability and degradability are preferred.^[76,77] They facilitate cellular functions without invoking a prolonged inflammatory response, thereby enhancing the healing outcomes.^[76] In summary, the choice of crosslinking method profoundly impacts the scaffold's performance, with UVA/R crosslinking emerging as a promising approach to creating biocompatible, stable, yet degradable scaffolds conducive to successful tissue engineering applications.

2.4. Histological Assessment of Subcutaneous Implants

The exceptional biocompatibility and osteoconductivity of collagen make it a cornerstone for bone grafting applications. However, its utility has historically been limited by biomechanical stability. Through the application of an innovative UVA/R crosslinking process, we have successfully addressed this limitation, significantly enhancing the mechanical stability of our collagen scaffolds. The integration of inorganic bone substitutes (BS), such as hydroxyapatite and β -TCP, provides the necessary mechanical support for long-term bone remodeling, while lacking the

ECM components crucial for early cell interactions and scaffold degradability. Our innovative injectable composite scaffold with UVA/R crosslinked collagen matrix and BS, therefore, is designed to optimize both initial cell engagement and enduring bone remodeling. Through subcutaneous evaluations and detailed histological assessments of the implanted scaffolds, we've achieved a nuanced understanding of material integrity and tissue response dynamics. This includes an in-depth analysis of tissue reactions, notably immune responses, to ascertain biocompatibility and derive critical insights for future applications. This methodical approach underscores our commitment to thoroughly exploring the interaction between our engineered matrices and biological systems.

2.4.1. Tissue Reaction Analysis

Movat's Pentachrome staining is a multipurpose histological technique that distinctly marks various components of connective tissue, facilitating their differentiation in histological sections.^[78] In this study, Movat's pentachrome staining was utilized to visually distinguish and semi-quantitatively analyze GAG and collagen distribution within the tissue sections, revealing the distinct behaviors of the implanted non-crosslinked collagen and UVA/R crosslinked collagen-based scaffolds (BS-Col and BS-Xcol_UVA/R) within the tissue environment (Figure 6A–C). By day 10 post-implantation, both groups showed collagen matrices within the implantation beds (Figure 6B). Notably, the BS-Xcol_UVA/R group demonstrated a remarkable adherence to the bone substitute surface in contrast to the loosely associated matrix observed in the BS-Col group, suggesting enhanced matrix stability potentially conferred by the UVA/R crosslinking process. The quantitative analysis further corroborated these findings, indicating a higher collagen content within the BS-Xcol_UVA/R implantation sites compared to BS-Col (Figure 6C), which may prove the profound effect of crosslinking on matrix integrity. As the tissue formation progressed, the initially similar glycosaminoglycan (GAG) levels took a consequential turn, showing a decrease over time, suggesting an ongoing tissue response, cellular activity, and a dynamic matrix remodeling process over time.^[79]

By day 30, the BS-Xcol_UVA/R group exhibited a striking retention of collagen content, with the matrix persisting around the bone substitute surfaces. This sustained presence, validated by quantitative analysis, highlighted the enduring effects of UVA/R crosslinking on matrix stability. (Figure 6C) The tissue within the scaffolds had matured, as evidenced by the increased vascularization in both groups.^[80] However, a distinct immune profile was observed; the BS-Col group showed a higher prevalence of macrophages and multinucleated giant cells, suggesting an ongoing response to the scaffold degradation.^[81,82]

2.4.2. Immune Response Evaluation

Our histological exploration into the immune responses at the subcutaneous implantation sites revealed nuanced interactions between the host's defenses and the implanted collagen matrix-based composites. Initially, at day 10, pro-inflammatory CD11c-positive macrophages were prominent around the implants

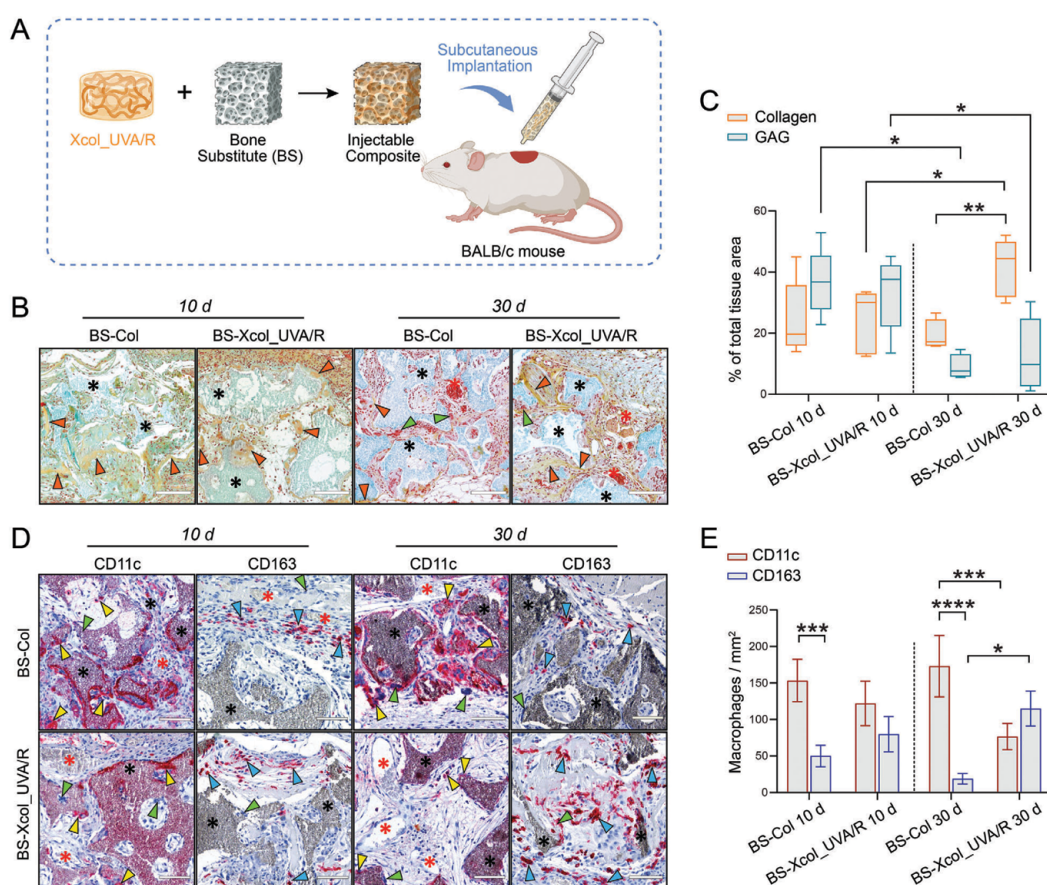


Figure 6. In vivo tissue reaction and immune response to collagen matrix-based materials: BS-Col and BS-Xcol_UVA/R. A) Schematic illustration depicting the injectable composite material composed of collagen matrix and bone substitute (BS), subcutaneously implanted into BALB/c mouse. B) Representative histological images of the implantation areas of BS-Col and BS-Xcol_UVA/R at day 10 and 30 post-implantation using Movat's Pentachrome staining. C) Quantification of Movat's Pentachrome via color deconvolution analysis using ImageJ. Yellow-green = collagen, green-blue = glycosaminoglycan (GAG). Presented as a percentage of the total stained area. D) Representative immunohistochemical images of pro-inflammatory (CD11c) and anti-inflammatory (CD163) macrophage subtypes in the implantation areas of the respective groups. E) Histogrammometric (quantitative) analysis of CD11c-positive and CD163-positive macrophage subtypes in the implantation areas of the respective groups using ImageJ. Black stars = bone substitute (BS), red stars = newly formed vessels, orange triangle = collagen, green triangle = multinuclear giant cells, yellow triangle = CD11c-positive cells, blue triangle = CD163-positive cells. Scale bar = 100 μm .

in both groups, with fewer CD163-positive anti-inflammatory macrophages present in the periphery (Figure 6D). Quantitative assessments (Figure 6E) further delineated the immune landscape, showing a predominance of M1 macrophages (CD11c-positive) over M2 macrophages (CD163-positive) in the BS-Col group, with cell counts of 153.3 ± 29.0 cells/cm² and 50.0 ± 14.7 cells/cm², respectively. In contrast, the BS-Xcol_UVA/R group exhibited fewer M1 macrophages (122.0 ± 30.5 cells/cm²) and a higher incidence of M2 macrophages (79.9 ± 24.2 cells/cm²), suggesting a moderated pro-inflammatory response.^[81]

By day 30, a discernible shift in macrophage polarization was observed. The BS-Col group maintained to show strong CD11c expression (173.0 ± 42.1 cells/cm²) within the implant vicinity,

with scant CD163 expression. In contrast, the BS-Xcol_UVA/R group demonstrated a remarkable increase in anti-inflammatory CD163-positive macrophages (115.0 ± 23.9 cells/cm²) and a reduction in CD11c expression (76.5 ± 17.9 cells/cm²), as quantified in Figure 6E. This shift signifies a significant tilt toward an anti-inflammatory phenotype in the BS-Xcol_UVA/R group, with a striking departure from the persistent pro-inflammatory milieu in the BS-Col group.

The histological assessment of subcutaneous implants provides compelling evidence of the UVA/R crosslinking process's efficacy in enhancing the biostability and integration of collagen matrices within a biological milieu. Early-stage pro-inflammatory macrophage presence, transitioning to an

anti-inflammatory profile in the BS-Xcol_UVA/R group, indicates a typical acute immune response, essential for wound healing and implant integration.^[83] The reduced degradation products and the presence of oxidized tyrosine (DOPA) crosslinked collagen post UVA/R treatment likely contribute synergistically to anti-inflammatory effects. DOPA, which was also one of the products in tyrosine-contained peptides post UVA/R treatment (Figure 3B), plays a significant role in mitigating inflammation, potentially enhancing the biocompatibility of the collagen scaffolds.^[84] This opens up avenues for further research into photochemically crosslinked biomaterials in tissue engineering and regenerative medicine, particularly in understanding and harnessing these mechanisms for controlled immune responses in clinical implant integration and functionality. While our study provides comprehensive insights into biocompatibility and mechanical properties, future research incorporating second harmonic generation (SHG) analysis could offer additional understanding of the ultrastructural changes in collagen fibrillarity,^[78,85–88] enriching our exploration of photochemically crosslinked collagen for tissue engineering and regenerative medicine.

The optimized UVA/R crosslinking process enhances our collagen scaffolds' integration with BS materials, creating a highly effective solution for bone grafting. This innovative approach not only strengthens biomechanical stability but also maximizes the biocompatibility of the composite material, making it well-suited for clinical applications. By incorporating inorganic materials into the collagen matrix, we address the essential need for durable mechanical support, pivotal for successful bone regeneration and remodeling. Crucially, our method boosts initial cell-scaffold interactions, a key element in tissue engineering, while providing the mechanical support vital for bone regeneration.

Beyond bone regeneration, the versatility of UVA/R crosslinked collagen extends to a broad range of applications. It serves as a foundational material for cartilage repair, where its ability to support chondrocyte adhesion and proliferation can be critical. In wound healing, its excellent biocompatibility and conducive environment for cell migration accelerate tissue repair. For vascular tissue engineering, the scaffold supports endothelial and smooth muscle cell growth, essential for forming functional blood vessels. In nerve regeneration, the scaffold can guide neurite outgrowth, offering a promising avenue for repairing nerve injuries. Additionally, the material's tailored degradation rates and compatibility with various bioactive agents make it an excellent candidate for targeted drug delivery and controlled release systems. To unlock the full potential of these materials in clinical settings, a deeper understanding of the underlying mechanisms is essential. Advanced imaging and spectroscopy technologies will play a crucial role in this exploration, offering insights into the scaffold's interaction with biological tissues and its impact on cell behavior. This deepened understanding is critical for tailoring the materials to meet the specific demands of various regenerative medicine applications, ensuring optimized outcomes for tissue repair and regeneration.

3. Conclusion and Outlook

The intricate interplay between the complexity of the collagen molecule and the mysterious UVA/riboflavin (UVA/R) photo-

chemical cross-linking process is a fascinating puzzle that our study has skillfully unraveled. Our comprehensive investigation into the crosslinking mechanism of collagen using six strategically selected synthetic peptides has yielded remarkable insights. HPLC, LC-MS consistently unveil a preference for tyrosine among the amino acids, a revelation that significantly advances our comprehension of the widely employed UVA/R crosslinking technique, particularly in ophthalmology. The preferential targeting of tyrosine sheds light on the specific molecular pathways involved in UV-induced collagen stabilization. Our findings underscore the role of tyrosine in UV-induced crosslinking and the phenol group in tyrosine is also known to be susceptible to photoactivation offering potential engineering strategies for artificial or functionalized biomaterials. Beyond elucidating the mechanisms of UVA/R crosslinking, the results suggest a crucial role of tyrosine in the design and assessment of collagen-based biomaterials and further prompt a reevaluation of existing materials, particularly those chemically modified due to tyrosine-dominated crosslinking, raising pertinent questions for applicants and regulatory agencies alike. The approach presented in this study advocates also the necessity in reevaluation and optimization of UVA crosslinking technique with a focus on maximizing the controllability of the reaction, such as the involvement of defined tyrosine residues into the process by controlled reaction conditions. Through the development of synthetic peptides mirroring potential crosslinking sites, we have uncovered the critical influence of tyrosine residues on the crosslinking mechanism, especially those residing in non-helical regions vital for augmenting mechanical properties. Our *in vivo* studies in BALB/c mice have substantiated the biocompatibility and functional efficacy of UVA/R crosslinked collagen, endorsing its superior potential as a biomaterial for therapeutic use.

Looking ahead, the exploration of UVA/R crosslinking enables transformative implications for a broad spectrum of collagen-based materials, reshaping collagen engineering in part of tissue engineering. The proven biocompatibility and mechanical strength of UVA/R crosslinked collagen beckon additional research into its long-term stability and performance across various biological settings.^[89,90] The potential incorporation of this material into advanced medical devices and implants, such as bioglass, bioactive ions, and gene therapy, stands as a promising development for enhancing patient outcomes.^[91,92] Moreover, the integration of UVA/R crosslinking techniques with burgeoning areas such as biofabrication and 3D bioprinting heralds a new era of innovation. Furthermore, when combined with bioreactor systems or organ-on-a-chip technologies, this technique harbors the potential to advance the development of *in vitro* models that simulate aging and disease-specific extracellular matrix environments. These sophisticated models offer dynamic platforms for exploring disease progression and the mechanisms of aging, thereby promoting the advancement of 3R principles by reducing the reliance on animal testing.^[93,94] Such insights gleaned from these studies could pave the way for innovative treatment and prevention strategies.

In summation, the knowledge gained from our investigations provides a solid foundation for the novel design and utilization of biomaterials, propelling forward the frontiers of biomedical technology and opening new avenues for scientific discovery with far-reaching implications.

4. Animal Trials

Experiments were authorized by the Local Ethical Committee of the Faculty of Medicine at the University of Niš, Serbia, based on the approval of the Veterinary Directorate of the Ministry of Agriculture, Forestry and Water Management of the Republic of Serbia (approval number 323-07-01762/2019-05/9; date of approval: 01 March 2019).

Supporting Information

Supporting Information is available from the Wiley Online Library or from the author.

Acknowledgements

This work was supported by the Federal Ministry of Education and Research (BMBF, Germany, FKZ: 13GW0400A, C and 13GW0430B); and the State Ministry of Baden-Württemberg for Economic Affairs, Labor, and Tourism (FKZ: 35-4223.10/22). L.F. acknowledges the support of the China Scholarship Council (CSC, No. 202008500143). The authors thank the colleagues: Anastasia Binder for the technical support and Claus Burkhardt for insightful discussions and technical support in SEM characterizations (both NMI Reutlingen); as well as Daniel A. Carvajal Berrio (University Tübingen) for the technical support with Raman microspectroscopy. Schematic figures were created with Adobe Illustrator. The statistical analysis of data was performed with GraphPad 9.

Open access funding enabled and organized by Projekt DEAL.

Conflict of Interest

The authors declare no conflict of interest.

Author Contributions

X.X., K.S.-L., and M.B. contributed equally to this work. L.F., K.S.-L., M.B., and X.X. conceptualized the idea for the study; L.F., M.B., K.S.-L., and X.X. designed methodology; X.X., L.F., and M.B. performed validation; L.F. and X.X. performed formal analysis; L.F., O.J., M.H., M.S., S. S., and S. N. performed investigation; O. J., M.B., and X.X. acquired resources for the study; L.F. and X.X. performed data curation; L.F. wrote the original draft; L.F., M.B., X.X., and K.S.-L. wrote, reviewed, and edited the final manuscript; L.F. performed visualization; X.X. and K.S.-L. performed supervision; M.B. and X.X. performed project administration; M.B. and X.X. performed funding acquisition. All authors have read and agreed to the published version of the manuscript.

Data Availability Statement

The data that support the findings of this study are available from the corresponding author upon reasonable request.

Keywords

biomaterial engineering, collagen matrix, photocrosslinking, tissue regeneration, UVA-activated riboflavin

Received: January 29, 2024

Revised: March 14, 2024

Published online:

- [1] L. Fan, Y. Ren, S. Emmert, I. Vučković, S. Stojanovic, S. Najman, R. Schnettler, M. Barbeck, K. Schenke-Layland, X. Xiong, *Int. J. Mol. Sci.* **2023**, *24*, 3744.
- [2] M. Filippi, G. Born, M. Chaaban, A. Scherberich, *Front. Biotechnol.* **2020**, *8*, 474.
- [3] K. Lin, D. Zhang, M. H. Macedo, W. Cui, B. Sarmiento, G. Shen, *Adv. Funct. Mater.* **2019**, *29*, 1804943.
- [4] M. M. Islam, D. B. AbuSamra, A. Chivu, P. Argüeso, C. H. Dohlman, H. K. Patra, J. Chodosh, M. González-Andrades, *Pharmaceutics* **2021**, *13*, 832.
- [5] M. Filippi, B. Dasen, J. Guerrero, F. Garello, G. Isu, G. Born, M. Ehrbar, I. Martin, A. Scherberich, *Biomaterials* **2019**, *223*, 119468.
- [6] D. Dippold, A. Cai, M. Hardt, A. R. Boccaccini, R. E. Horch, J. P. Beier, D. W. Schubert, *Mater. Sci. Eng., C* **2019**, *95*, 217.
- [7] E. Spoerl, M. Huhle, T. Seiler, *Exp. Eye Res.* **1998**, *66*, 97.
- [8] M. Ahearne, Y. Yang, K. Y. Then, K.-K. Liu, *Brit. J. Ophthalmol.* **2007**, *92*, 268.
- [9] R. Uemura, J. Miura, T. Ishimoto, K. Yagi, Y. Matsuda, M. Shimizu, T. Nakano, M. Hayashi, *Sci. Rep.* **2019**, *9*, 1252.
- [10] G. M. Fernandes-Cunha, L. G. Brunel, A. Arboleda, A. Manche, Y. A. Seo, C. Logan, F. Chen, S. C. Heilshorn, D. Myung, *ACS Appl. Bio Mater.* **2023**, *6*, 1787.
- [11] X. Wu, W. Guo, L. Wang, Y. Xu, Z. Wang, Y. Yang, L. Yu, J. Huang, Y. Li, H. Zhang, *Adv. Funct. Mater.* **2022**, *32*, 2110066.
- [12] Q. Li, H. Zhao, H. Wang, G. Zhao, *Biomater. Adv.* **2022**, *137*, 212822.
- [13] K. Wand, R. Neuhann, A. Ullmann, K. Plank, M. Baumann, R. Ritter, M. Griffith, C. P. Lohmann, K. Kobuch, *Cornea* **2015**, *34*, 544.
- [14] C. Dittfeld, C. Welzel, U. König, A. Jannasch, K. Alexiou, E. Blum, S. Bronder, C. Sperling, M. F. Maitz, S.-M. Tugtekin, *Biomater. Adv.* **2023**, *147*, 213328.
- [15] J. Heo, R. H. Koh, W. Shim, H. D. Kim, H.-G. Yim, N. S. Hwang, *Drug Deliv. Trans. Res.* **2016**, *6*, 148.
- [16] P. Urbánek, P. Šuly, J. Ševčík, B. Hanulíková, I. Kuřitka, T. Šopík, P. Stodůlka, *Pharmaceutics* **2023**, *16*, 505.
- [17] N. Diamantides, L. Wang, T. Pruiksma, J. Siemiatkoski, C. Dugopolski, S. Shortkroff, S. Kennedy, L. J. Bonassar, *Biofabrication* **2017**, *9*, 034102.
- [18] J. A. Serna, S. L. Florez, V. A. Talero, J. C. Briceño, C. Muñoz-Camargo, J. C. Cruz, *Polymers* **2019**, *11*, 569.
- [19] Y. W. Lin, K. L. Tsou, C. D. Fay, X. Liu, J. H. Y. Chung, D. Sharma, A. Jeiranikhahmeh, P. H. Kuo, C. K. Tzeng, G. G. Wallace, C. Y. Wu, M. D. Ker, J. I. Chao, Y. T. Cheng, *Bioprinting* **2020**, *20*, e00097.
- [20] T. Zandrini, S. Florczak, R. Levato, A. Ovsianikov, *Trends Biotechnol.* **2022**.
- [21] Q. Zhang, H.-P. Bei, M. Zhao, Z. Dong, X. Zhao, *Biomaterials* **2022**, *286*, 121566.
- [22] A. N. Strat, A. Kirschner, H. Yoo, A. Singh, T. Bagué, H. Li, S. Herberg, P. S. Ganapathy, *Exp. Eye Res.* **2022**, *220*, 109102.
- [23] N. Kopsachilis, K. T. Tsaousis, I. T. Tsinopoulos, F. E. Kruse, U. Welge-Luessen, *Cornea* **2013**, *32*, 1034.
- [24] F. Raiskup, E. Spoerl, *Ocul. Surf.* **2013**, *11*, 65.
- [25] A. S. McCall, S. Kraft, H. F. Edelhauser, G. W. Kidder, R. R. Lundquist, H. E. Bradshaw, Z. Dedeic, M. J. C. Dionne, E. M. Clement, G. W. Conrad, *Investig. Ophthalmol. Vis. Sci.* **2010**, *51*, 129.
- [26] S. Sel, N. Nass, S. Pöttsch, S. Trau, A. Simm, T. Kalinski, G. I. W. Duncker, F. E. Kruse, G. U. Auffarth, H.-J. Brömme, *Redox Rep.* **2014**, *19*, 72.
- [27] Y. Zhang, A. H. Conrad, G. W. Conrad, *J. Biol. Chem.* **2011**, *286*, 13011.
- [28] M. Yamauchi, M. Shiiba, in *Post-Translational Modifications of Proteins, Methods in Molecular Biology*, Humana Press, Totowa, NJ **2008**, pp. 95–108.
- [29] R. Sharif, J. Hjortdal, H. Sejersen, G. Frank, D. Karamichos, *Sci. Rep.* **2017**, *7*, 12517.

- [30] I. Gabriela, M. Iulia, (Ed.: A. A. K. Mohammed), *Biophysical Chemistry - Advance Applications*, IntechOpen, Rijeka **2019**, p. Ch2, <https://doi.org/10.5772/intechopen.88855>.
- [31] E. Fuentes-Lemus, E. Silva, F. Leinisch, E. Dorta, L. G. Lorentzen, M. J. Davies, C. López-Alarcón, *Food Chem.* **2018**, *256*, 119.
- [32] G. Wollensak, E. Spoerl, T. Seiler, *Am. J. Ophthalmol.* **2003**, *135*, 620.
- [33] E. Spoerl, M. Mrochen, D. Sliney, S. Trokel, T. Seiler, *Cornea* **2007**, *26*, 385.
- [34] K. Adamiak, A. Sionkowska, *Int. J. Biol. Macromol.* **2020**, *161*, 550.
- [35] J.-T. Lin, *J. Ophthalmol. Vis. Neurosci.* **2018**, *3*, 17.
- [36] S. K. Subasinghe, K. C. Ogbuehi, G. J. Dias, *Clin. Exp. Ophthalmol.* **2018**, *256*, 1363.
- [37] M. Pehrsson, J. H. Mortensen, T. Manon-Jensen, A.-C. Bay-Jensen, M. A. Karsdal, M. J. Davies, *Expert Rev. Mol. Diagn.* **2021**, *21*, 1049.
- [38] L. Gu, T. Shan, Y.-x. Ma, F. R. Tay, L. Niu, *Trends Biotechnol.* **2019**, *37*, 464.
- [39] J. M. Patel, R. C. Jackson, G. L. Schneider, S. A. Ghodbane, M. G. Dunn, *J. Mater. Sci.: Mater. Med.* **2018**, *29*, 1.
- [40] B. J. Bielajew, J. C. Hu, K. A. Athanasiou, *Nat. Rev. Mater.* **2020**, *5*, 730.
- [41] S. M. Ali, N. Y. Patrawalla, N. S. Kajave, A. B. Brown, V. Kishore, *Biomacromolecules* **2022**, *23*, 5137.
- [42] L. Ge, S. Zheng, H. Wei, *Burns* **2009**, *35*, 46.
- [43] N. Gallo, M. L. Natali, A. Sannino, L. Salvatore, *J. Funct. Biomater.* **2020**, *11*, 79.
- [44] W.-H. Huang, S.-L. Ding, X.-Y. Zhao, K. Li, H.-T. Guo, M.-Z. Zhang, Q. Gu, *Mater. Today Bio.* **2023**, *20*, 100639.
- [45] R. D. B. Fraser, T. P. MacRae, A. Miller, *J. Mol. Biol.* **1987**, *193*, 115.
- [46] C. Meyer, L. Notari, S. P. Becerra, *J. Biol. Chem.* **2002**, *277*, 45400.
- [47] Y. Hashimoto, S. Hattori, S. Sasaki, T. Honda, T. Kimura, S. Funamoto, H. Kobayashi, A. Kishida, *Sci. Rep.* **2016**, *6*, 27734.
- [48] F. J. O'Brien, B. A. Harley, I. V. Yannas, L. J. Gibson, *Biomaterials* **2005**, *26*, 433.
- [49] Z. Yazdanpanah, F. Ketabat, P. Gomez-Picos, A. Raquin, A. Fazel Anvari-Yazdi, B. F. Eames, J. D. Johnston, D. M. L. Cooper, X. Chen, *Nano Select* **2023**, *4*, 537.
- [50] B. Sun, *Cell Rep. Phys. Sci.* **2021**, *2*, 100515.
- [51] C. M. Murphy, F. J. O'Brien, *Cell Adhes. Migr.* **2010**, *4*, 377.
- [52] C. J. Lowe, I. M. Reucroft, M. C. Grota, D. I. Shreiber, *ACS Biomater. Sci. Eng.* **2016**, *2*, 643.
- [53] D. Eyre, *Methods in Enzymology*, Elsevier, New York **1987**, pp. 115–139.
- [54] M. Yamauchi, M. Sricholpech, *Essays Biochem.* **2012**, *52*, 113.
- [55] G. L. Mechanic, E. P. Katz, M. Henmi, C. Noyes, M. Yamauchi, *Biochemistry* **1987**, *26*, 3500.
- [56] S. Udhayakumar, K. G. Shankar, S. Sowndarya, S. Venkatesh, C. Muralidharan, C. Rose, *RSC Adv.* **2017**, *7*, 25070.
- [57] N. Davidenko, D. V. Bax, C. F. Schuster, R. W. Farndale, S. W. Hamaia, S. M. Best, R. E. Cameron, *J. Mater. Sci.: Mater. Med.* **2016**, *27*, 1.
- [58] D. D. Nguyen, S. K. Johnson, M. W. Clarke, *Food Anal. Methods* **2017**, *10*, 3321.
- [59] O. Skaff, K. A. Jolliffe, C. A. Hutton, *J. Org. Chem.* **2005**, *70*, 7353.
- [60] S. J. Nicholls, S. L. Hazen, *Arterioscler., Thromb., Vasc. Biol.* **2005**, *25*, 1102.
- [61] P. Kamaev, M. D. Friedman, E. Sherr, D. Muller, *Investig. Ophthalmol. Vis. Sci.* **2012**, *53*, 2360.
- [62] D. Dippold, A. Cai, M. Hardt, A. R. Boccaccini, R. Horsch, J. P. Beier, D. W. Schubert, *Mater. Sci. Eng., C* **2017**, *72*, 278.
- [63] E. Brauchle, K. Schenke-Layland, *Biotechnol. J.* **2013**, *8*, 288.
- [64] L. Becker, C.-E. Lu, I. A. Montes-Mojarro, S. L. Layland, S. Khalil, A. Nsair, G. P. Duffy, F. Fend, J. Marzi, K. Schenke-Layland, *Acta Biomater.* **2023**, *162*, 278.
- [65] W. T. Cheng, M. T. Liu, H. N. Liu, S. Y. Lin, *Microscopy Res. Tech.* **2005**, *68*, 75.
- [66] E. Katainen, M. Elomaa, U. M. Laakkonen, E. Sippola, P. Niemelä, J. Suhonen, K. Järvinen, *J. Forensic Sci.* **2007**, *52*, 88.
- [67] F. Liao, Q. Ruan, J. Lin, J. Lin, Y. Zeng, L. Li, Z. Huang, N. Liu, R. Chen, in *Based on Surface-Enhanced Raman Spectroscopy Analysis of Serum Albumin in Different Stages of Liver Disease for Early Screening Primary Liver Cancer*, SPIE, Bellingham, WA, pp. 243–248.
- [68] I. Notingher, C. Green, C. Dyer, E. Perkins, N. Hopkins, C. Lindsay, L. L. Hench, *J. R. Soc., Interface* **2004**, *1*, 79.
- [69] G. Shetty, C. Kendall, N. Shepherd, N. Stone, H. Barr, *Br. J. Cancer* **2006**, *94*, 1460.
- [70] C. Y. Huang, G. Balakrishnan, T. G. Spiro, *J. Raman Spectrosc.* **2006**, *37*, 277.
- [71] M. Nair, R. K. Johal, S. W. Hamaia, S. M. Best, R. E. Cameron, *Biomaterials* **2020**, *254*, 120109.
- [72] G. Yang, Z. Xiao, H. Long, K. Ma, J. Zhang, X. Ren, J. Zhang, *Sci. Rep.* **2018**, *8*, 1616.
- [73] W. Kong, C. Lyu, H. Liao, Y. Du, *Biomedical Mater.* **2021**, *16*, 062005.
- [74] Y. Zhang, J. Li, V. H. M. Mouser, N. Roumans, L. Moroni, P. Habibovic, *ACS Nano* **2021**, *15*, 17480.
- [75] G. Montalbano, C. Tomasina, S. Fiorilli, S. Camarero-Espinosa, C. Vitale-Brovarone, L. Moroni, *Materials* **2021**, *14*, 4360.
- [76] L. Wang, C. Wang, S. Wu, Y. Fan, X. Li, *Biomater. Sci.* **2020**, *8*, 2714.
- [77] J. M. Aamodt, D. W. Grainger, *Biomaterials* **2016**, *86*, 68.
- [78] K. Schenke-Layland, U. A. Stock, A. Nsair, J. Xie, E. Angelis, C. G. Fonseca, R. Larbig, A. Mahajan, K. Shivkumar, M. C. Fishbein, *Eur. Heart J.* **2009**, *30*, 2254.
- [79] S. Ghatak, E. V. Maytin, J. A. Mack, V. C. Hascall, I. Atanelishvili, R. M. Rodriguez, R. R. Markwald, S. Misra, *Int. J. Cell Biol.* **2015**, *2015*, 834893.
- [80] M. E. H. Wagner, A. Kampmann, K. Schumann-Moor, N.-C. Gellrich, F. Tavassol, F. Schmeltekop, M. Rücker, M. Lanzer, T. Gander, H. Essig, P. Schumann, *Hypertension Res.* **2021**, *44*, 23.
- [81] A. K. McNally, J. M. Anderson, *Cell fusion in health and disease*, Springer, New York **2011**, pp. 97–111.
- [82] K. Ahmadzadeh, M. Vanoppen, C. D. Rose, P. Matthys, C. H. Wouters, *Front. Cell Dev. Biol.* **2022**, *10*, 873226.
- [83] Y. Oishi, I. Manabe, *Int. Immunol.* **2018**, *30*, 511.
- [84] J. R. N. Recky, M. P. Serrano, M. L. Dántola, C. Lorente, *Free Radical Biol. Med.* **2021**, *165*, 360.
- [85] K. Schenke-Layland, *J. Biophotonics* **2008**, *1*, 451.
- [86] K. Schenke-Layland, I. Riemann, O. Damour, U. A. Stock, K. König, *Adv. Drug Delivery Rev.* **2006**, *58*, 878.
- [87] K. G. M. Brockbank, W. R. MacLellan, J. Xie, S. F. Hamm-Alvarez, Z. Z. Chen, K. Schenke-Layland, *Cell Tissue Banking* **2008**, *9*, 299.
- [88] K. Schenke-Layland, J. Xie, E. Angelis, B. Starcher, K. Wu, I. Riemann, W. R. MacLellan, S. F. Hamm-Alvarez, *Matrix Biol.* **2008**, *27*, 53.
- [89] R. H. M. van der Meijden, D. Daviran, L. Rutten, X. F. Walboomers, E. Macías-Sánchez, N. Sommerdijk, A. Akiva, *Adv. Funct. Mater.* **2023**, *33*, 2212339.
- [90] I. M. Joshi, M. Mansouri, A. Ahmed, D. De Silva, R. A. Simon, P. Esmaili, D. E. Desa, T. M. Elias, E. B. Brown Iii, V. V. Abhyankar, *Adv. Funct. Mater.* **2023**, <https://doi.org/10.1002/adfm.202308071>.
- [91] E. R. Balmayor, *Curr. Opin. Biotechnol.* **2022**, *74*, 8.
- [92] E. R. Balmayor, M. Van Griensven, G. engineering, *Front. Bioeng. Biotechnol.* **2015**, *3*, 9.
- [93] A. Mansoorifar, R. Gordon, R. C. Bergan, L. E. Bertassoni, *Adv. Funct. Mater.* **2021**, *31*, 2006796.
- [94] J. J. Kim, J. Y. Park, V. V.-T. Nguyen, M. Bae, M. Kim, J. Jang, J. Y. Won, D.-W. Cho, *Adv. Funct. Mater.* **2023**, *33*, 2213649.

2.3 Encapsulated Vaterite-Calcite CaCO₃ Particles Loaded with Mg²⁺ and Cu²⁺ Ions with Sustained Release Promoting Osteogenesis and Angiogenesis

Fan, L., Körte, F., Rudt, A., Jung, O., Burkhardt, C., Barbeck, M., & Xiong, X. (2022). *Frontiers in Bioengineering and Biotechnology*, 10, 983988.

2.3.1 Summary and Major Findings

Although collagen serves as an ideal osteoconductive matrix for new bone cell adhesion and proliferation, especially with enhanced mechanical properties and stability by UVA/R crosslinking process, it may be insufficient for inducing bone formation in larger or more complex defects. The role of bioactive ions like calcium (Ca²⁺), copper (Cu²⁺), and magnesium (Mg²⁺) emerges as an economical substitute for protein-based bone healing treatments, effective even in sparse amounts and augmenting bone grafts with essential functionalities. Nevertheless, fine-tuning their release and comprehending the collective influence on bone repair remains an area for continued research.

In this work, the CaCO₃ vaterite-calcite, incorporated with Cu²⁺ and Mg²⁺, were coated with a polyelectrolyte multilayer (PEM) through a sequential application process. This enhancement bolstered the particles' stability and compatibility with biological tissues, while also moderating the metal ion release. The final layer of collagen on the polymeric shell further fostered an optimal osteoconductive setting for bone tissue repair.

To ensure stable encapsulation and controllable release, various microcapsule formulations with four different ratios of Ca²⁺, Cu²⁺, and Mg²⁺ were prepared by coprecipitation. In the coprecipitation system, the morphology of the resulting particles, which is crucial for their performance, is predominantly influenced by two factors: the amount of calcium salt and the ionic interactions between Ca²⁺ and the added Cu²⁺ and Mg²⁺ ions. These factors determine the crystal varieties formed, thereby affecting the ion release kinetics of the particles, which is essential for their application in bone regeneration. Different crystal forms lead to distinct dissolution behaviors, influencing how ions are released over time. For instance, particles with a 40%:30%:30% ratio,

predominantly in the vaterite-calcite phase, demonstrated a stable Cu^{2+} release over two months without initial burst, and a gradual release of Mg^{2+} in the initial week, as measured by ICP-OES. This highlights the importance of controlling ion release kinetics for long-term bone regeneration.

Cytotoxicity studies using fibroblasts L929 determined a safe dosage range for the CaCuMg-PEM-Col microcapsules. Lower extract concentrations showed decreased cytotoxicity, with cell viability dropping below 70% only above 1% extract concentration. This concentration corresponded to Cu^{2+} and Mg^{2+} levels of approximately 15.63 μM and 4.17 μM , respectively. Various microcapsule extracts, including Ca-PEM, CaCu-PEM, CaMg-PEM, CaCuMg-PEM, and CaCuMg-PEM-Col, indicated favorable biocompatibility. Notably, CaCuMg-PEM-Col extracts demonstrated higher cell viability, potentially due to collagen's desorption and its mitigating effect on ion toxicity.

Cell proliferation and differentiation studies with MG63 osteoblast-like cells showed that CaCuMg-PEM-Col microcapsules effectively promoted cell growth and differentiation. Initially, these microcapsules exhibited higher ALP activity in the early stages of differentiation among other groups, followed by a significant decrease at day 14, indicating the synergistic osteogenic effect of Ca^{2+} , Cu^{2+} , Mg^{2+} , and collagen. Additionally, optimal matrix mineralization was observed at a later stage (Day 21), highlighting the microcapsules' efficacy in enhancing osteogenic processes.

Bone regeneration involves key phases of cell proliferation, ECM maturation, and mineralization marked by distinct gene expression shifts. MG63 cell expression related to osteogenesis and angiogenesis was probed, with CaCuMg-PEM-Col microcapsules bolstering osteogenesis and angiogenesis genes. The observed synergy between copper, magnesium, and collagen type I in promoting angiogenesis underscores these microcapsules' role in bone repair.

In conclusion, the CaCuMg-PEM-Col microcapsules developed in this study facilitated sustained release of Ca^{2+} , Cu^{2+} , and Mg^{2+} , creating an environment conducive to bone regeneration, enhancing osteoblast

proliferation, differentiation, ECM maturation and mineralization. The upregulation of osteogenic and angiogenic genes confirms CaCuMg-PEM-Col microcapsules' efficacy as bioactive systems for bone grafting applications, complementing UVA and riboflavin crosslinked collagen scaffolds.

2.3.2 Personal Contribution

In this segment of the study, involved was mainly responsible for conceptualization of the experiments. I was responsible for conducting most of the experimental work, with the exception of ICP-OES measurements, which were carried out by an analytical service provider. Additionally, I took charge of analyzing the data from all results and was instrumental in preparing the initial draft of the manuscript. Furthermore, I played a key role in critically revising the manuscript, incorporating suggestions from peer reviewers to enhance its quality and relevance.



OPEN ACCESS

 EDITED BY
 Yuangang Liu,
 Huaqiao University, China

 REVIEWED BY
 Meng Qin,
 Beijing University of Chemical
 Technology, China
 Min Jiang,
 Nanjing Tech University, China
 Klemen Bohinc,
 University of Ljubljana, Slovenia

 *CORRESPONDENCE
 Mike Barbeck,
 mike.barbeck@med.uni-rostock.de
 Xin Xiong,
 xin.xiong@nmi.de

 SPECIALTY SECTION
 This article was submitted to
 Biomaterials,
 a section of the journal
 Frontiers in Bioengineering and
 Biotechnology

 RECEIVED 01 July 2022
 ACCEPTED 18 July 2022
 PUBLISHED 11 August 2022

 CITATION
 Fan L, Körte F, Rudt A, Jung O,
 Burkhardt C, Barbeck M and Xiong X
 (2022), Encapsulated vaterite-calcite
 CaCO₃ particles loaded with Mg²⁺ and
 Cu²⁺ ions with sustained release
 promoting osteogenesis
 and angiogenesis.
Front. Bioeng. Biotechnol. 10:983988.
 doi: 10.3389/fbioe.2022.983988

 COPYRIGHT
 © 2022 Fan, Körte, Rudt, Jung,
 Burkhardt, Barbeck and Xiong. This is an
 open-access article distributed under
 the terms of the [Creative Commons
 Attribution License \(CC BY\)](https://creativecommons.org/licenses/by/4.0/). The use,
 distribution or reproduction in other
 forums is permitted, provided the
 original author(s) and the copyright
 owner(s) are credited and that the
 original publication in this journal is
 cited, in accordance with accepted
 academic practice. No use, distribution
 or reproduction is permitted which does
 not comply with these terms.

Encapsulated vaterite-calcite CaCO₃ particles loaded with Mg²⁺ and Cu²⁺ ions with sustained release promoting osteogenesis and angiogenesis

 Lu Fan^{1,2}, Fabian Körte¹, Alexander Rudt³, Ole Jung⁴,
 Claus Burkhardt¹, Mike Barbeck^{4*} and Xin Xiong^{1*}
¹NMI Natural and Medical Sciences Institute at the University of Tübingen, Reutlingen, Germany, ²Experimental Medicine, Faculty of Medicine, University of Tübingen, Tübingen, Germany, ³Faculty of Applied Chemistry, Reutlingen University, Reutlingen, Germany, ⁴Medical Center of Rostock University, Rostock, Germany

Bioactive cations, including calcium, copper and magnesium, have shown the potential to become the alternative to protein growth factor-based therapeutics for bone healing. Ion substitutions are less costly, more stable, and more effective at low concentrations. Although they have been shown to be effective in providing bone grafts with more biological functions, the precise control of ion release kinetics is still a challenge. Moreover, the synergistic effect of three or more metal ions on bone regeneration has rarely been studied. In this study, vaterite-calcite CaCO₃ particles were loaded with copper (Cu²⁺) and magnesium (Mg²⁺). The polyelectrolyte multilayer (PEM) was deposited on CaCuMg-CO₃ particles *via* layer-by-layer technique to further improve the stability and biocompatibility of the particles and to enable controlled release of multiple metal ions. The PEM coated microcapsules were successfully combined with collagen at the outmost layer, providing a further stimulating microenvironment for bone regeneration. The *in vitro* release studies showed remarkably stable release of Cu²⁺ in 2 months without initial burst release. Mg²⁺ was released in relatively low concentration in the first 7 days. Cell culture studies showed that CaCuMg-PEM-Col microcapsules stimulated cell proliferation, extracellular maturation and mineralization more effectively than blank control and other microcapsules without collagen adsorption (Ca-PEM, CaCu-PEM, CaMg-PEM, CaCuMg-PEM). In addition, the CaCuMg-PEM-Col microcapsules showed positive effects on osteogenesis and angiogenesis in gene expression studies. The results indicate that such a functional and controllable delivery system of multiple bioactive ions might be a safer, simpler and more efficient alternative of protein growth factor-based therapeutics for bone regeneration. It also provides an effective method for functionalizing bone grafts for bone tissue engineering.

KEYWORDS

bioactive cations, vaterite-calcite, polyelectrolyte multilayer, collagen, bone regeneration

1 Introduction

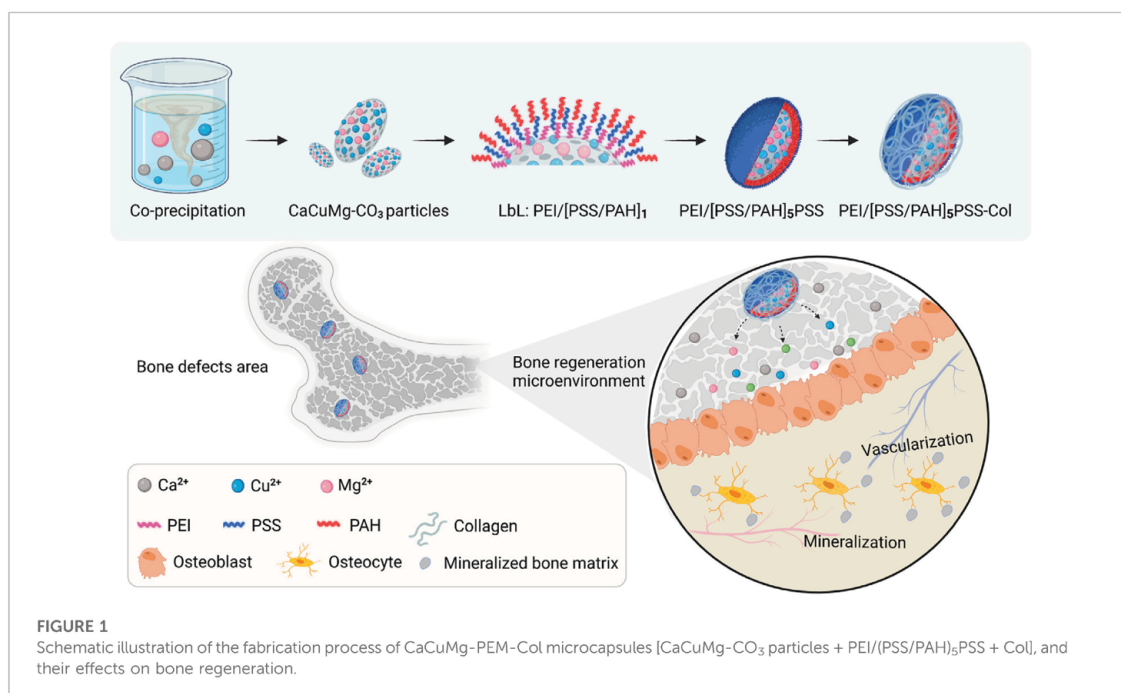
Various materials and functionalization strategies have been developed and extensively investigated in the field of bone regeneration (Lee et al., 2019; O'Neill et al., 2018). Nevertheless, effective vascularization, mineralization and tissue remodeling of regenerating bone tissue remains the main bottleneck for most graft-induced bone healing (Collins et al., 2021; Divband et al., 2021). A major research focus has been the incorporation of protein growth factors into bone implants to improve the efficacy of treatment. Such as the bone morphogenetic protein-2 (BMP-2) has been used clinically to promote bone healing since 2002 due to its diverse functions and osteogenic potential (Halloran et al., 2020; Hettiaratchi et al., 2020). Vascular endothelial growth factor (VEGF) is widely used in bone tissue engineering research for the improvement of tissue vascularization, either alone or in combination with BMP-2 (Liu et al., 2020; Fitzpatrick et al., 2021). However, significant disadvantages are associated with these protein growth factors-based therapeutics, including the severe complications caused by the supraphysiological dose applied, the instability in the fabrication process, and the high cost (Ruehle et al., 2019; Gelebart et al., 2022). Repeated clinical applications of BMP-2 have not been approved as safe and effective by the United States Food and Drug Administration (FDA) (SSED, 2022). Therefore, the alternatives of protein growth factor-based therapeutics are in demand.

Many bioactive metal ions have been shown to modulate osteoblast precursor differentiation *via* growth factor signaling pathways, or other processes to promote bone tissue regeneration (Glenske et al., 2018; O'Neill et al., 2018). Compared to the applications of protein growth factors, the advantages of using metal ions to induce bone tissue repair are manifold, including lower cost, greater simplicity, higher stability, and better efficacy at low concentrations (Glenske et al., 2018; Hurler et al., 2021). One of those efficient bioactive metal ions showed great importance in bone regeneration is calcium ion (Ca^{2+}). The incorporation of Ca^{2+} into bone repair scaffolds has been shown to promote adhesion, proliferation, and differentiation of osteoblasts (Xie et al., 2018; Jeong et al., 2019). Copper ions (Cu^{2+}) show great potential for vascularization, which are critical component of bone formation and tissue engineering (Lin et al., 2020; Kargozar et al., 2021). 50–60% of magnesium ions (Mg^{2+}) are bound in bone and about 40% of Mg^{2+} are sorted in soft tissue (Musso, 2009). Many studies have shown increased bone growth around degradable Mg-alloys (He et al., 2016). Besides, Mg^{2+} showed positive influences to enhance matrix mineralization, osteogenic genes and protein expression of human bone marrow stem cells and osteoblasts (Qiao et al., 2021; Zhao et al., 2021). It should not be underestimated that bioactive cations are able to diffuse through the cellular membrane and regulate the activity of a variety of physiological responses (Mourino et al., 2012; Qiao et al., 2021). Thus, the metal ions induced concentration-dependent

cytotoxicity and nonspecific adverse effects might be observed in neurological, cardiological, hematological, and/or endocrine systems (O'Neill et al., 2018). To reduce or avoid these side effects, a stable delivery system is required that can sustain ion release in the bone defect area both temporally and spatially. On this basis, it is of interest to investigate the synergetic therapy of multiple metal ions for bone regeneration.

Calcium carbonate in its vaterite form is widely used as a sacrificial template for efficient drug delivery. CaCO_3 vaterite based delivery platforms have exhibited numerous advantages, such as the high loading efficiency, beneficial porosity, high mechanical stability, biodegradability preferential safety profile, simple preparation and low cost (Vikulina et al., 2021; Daria et al., 2022; Feng et al., 2022). However, the application as a platform for the delivery of proteins, and their long term and controlled release are limited, because the high ionic strength and pH changes during vaterite formation and sacrifice process would result in a dramatic loss of protein activity and a burst release of the encapsulated drug (Feoktistova et al., 2020). However, they do not impact CaCO_3 being an ideal platform for the delivery of metal ions. Not only as a sacrificial template, CaCO_3 is also one of the cargos, because it contains the important bioactive cations, Ca^{2+} . It was reported that the CaCO_3 particles could be converted into hydroxyapatite crystals in mild acidic environment (Wei et al., 2015). It enables the steady and continuous release of targets as it biodegrades *in vivo*. The CaCO_3 crystals are particularly suitable for loading with multiple active pharmaceutical ingredients by a simple coprecipitation technique. Polyelectrolyte multilayer (PEM) deposited onto the degradable vaterite CaCO_3 crystals *via* a layer-by-layer (LbL) process have served as multifunctional and tailored vehicles for advanced drug delivery (Campbell et al., 2020). Due to their tunable and inherent properties, PEMs can further enhance the biodegradability and bioactivity of CaCO_3 crystals, and efficiently inhibit the initial burst release of cargos caused by the complex microenvironment *in vivo*.

Collagen is the main organic component in the bone matrix. It plays a crucial role in the bone formation and remodeling process (Toosi & Behravan, 2020). It has been widely reported that the incorporation of collagen can significantly improve the mechanical properties, osteoinductivity and osteogenicity of scaffold materials for bone tissue engineering (Zhang et al., 2018; Yu et al., 2020; Zhong et al., 2022). In many cases, due to the formability, homogeneity and reproducibility, coating is a preferable choice to integrate collagen into different bone matrices and scaffolds as well as inorganic bone substitute materials. Brito Barrera et al. fabricated an osteogenic microenvironment relying on PEMs in combination with multilayers of type I collagen and chondroitin sulfate (Brito Barrera et al., 2020). The LbL technique is a method to fabricate coatings by alternate adsorption of polyanions and polycations, which can neatly combine collagen and PEM (Martin et al., 2021). In this study, the CaCO_3 particles were



loaded with Cu²⁺ and Mg²⁺ *via* a co-precipitation process. The co-precipitated particles were further encapsulated with PEMs and collagen, aiming for an elongated and constant release of bioactive cations. Simultaneously, the biofunctionalization of particle surfaces by PEMs and collagen simulated the extracellular microenvironment, together with released bioactive ions promoting bone tissue regeneration. (Figure 1)

2 Materials and methods

2.1 Preparation and characterization of polyelectrolyte multilayers

The polyethyleneimine (PEI, Mw 750 kDa, 50 wt% in water), poly (sodium 4-styrene-sulfonate) (PSS, Mw 70 kDa) were purchased from Sigma-Aldrich, Germany. Poly (allylamine hydrochloride) (PAH, 120–200 kDa) was purchased from Alfa Aesar, Germany. Sodium chloride (NaCl > 99%) was purchased from Sigma-Aldrich, Germany. Collagen from porcine skin (collagen type I content > 90%) was provided by Biotrics bioimplants AG, Germany. Acetic acid (HAc) was purchased from Carl Roth, Germany. All materials were used without further purification. The deionized water (ddH₂O) used in all experiments was prepared in a three stage Milli-Q plus purification system and had a resistivity higher than 18.2 MΩ cm⁻¹.

The polyelectrolytes (PEs) solutions were prepared as follows: PEI was dissolved in ddH₂O at a concentration of 0.01 monomer mol·L⁻¹, pH ~7.0. PSS and PAH were respectively dissolved in 0.5 M of NaCl at a concentration of 2 mg ml⁻¹ and adjusted to pH 7.0. Collagen was dissolved in 0.1 M HAc at a concentration of 2 mg ml⁻¹ at 4°C overnight under continuous agitation at 60 rpm and thereafter the pH was adjusted to pH 5.0 using NaOH.

The deposition was performed manually using the layer-by-layer (LbL) technique as reported previously (Sun et al., 2017). Gold-crystal sensors (QSX 301 Gold, Biolin scientific, Sweden) were used as a model surface. To characterize the buildup process and the properties of the deposited PEMs, quartz-crystal microbalance with dissipation monitoring (QCM-D) measurement using a Q-Sense E4 instrument (Biolin scientific, Sweden) was employed. Firstly, the QCM sensors were treated with Piranha solution (30% (v/v) H₂O₂, 70% (v/v) H₂SO₄) and washed extensively with ddH₂O. PEI was always applied as precursor layer with a positive charge on the substrate followed by repeated rinsing in ddH₂O (three times for 2 min each). After the deposition of PEI, alternate polyanionic PSS and polycationic PAH layers were deposited up to the desired amount of layers [PEI(PSS/PAH)₅ or PEI(PSS/PAH)₅PSS] at pH 7.0 with 10 min incubation for each layer. Each adsorption step was followed by three consecutive rinsing steps with ddH₂O for 2 min each. Prior to the collagen deposition, the PEM layers were equilibrated in pH 5.0 ddH₂O. Collagen was deposited as the last layer by incubating the sensors in collagen solution for another 10 min. The PEM and collagen buildup

process was performed at 22°C. Finally, sensors were immersed in ddH₂O overnight at 37°C for the stability measurements. In brief, the buildup process for the following systems have been monitored on QCM-D: 1) PEI[PSS/PAH]₅ at pH 7.0 switch to pH 5.0 and followed by addition of collagen at pH 5.0; 2) PEI[PSS/PAH]₅PSS at pH 7.0 switch to pH 5.0 and followed by addition of collagen.

The increase in mass adsorbed on the surface of the quartz crystal sensor leads to a decrease in the oscillation frequency (Marx, 2003). The frequency shift ($-\Delta f$) measured after the deposition of each polyelectrolyte provides direct evidence of adsorption of polyelectrolytes (Aggarwal et al., 2013). The mass of adsorbed polyelectrolyte (Δm) can be calculated from the frequency shift using the Sauerbrey equation:

$$\Delta m = -c \frac{\Delta f}{n}$$

where n ($n = 1, 3, \text{ and } 5 \dots 13$) is the overtone number and c is the mass sensitivity constant given by the property of the used quartz crystal (Sauerbrey, 1959). In the present study, f_0 is 5 MHz and c is 17.7 ng Hz⁻¹ cm⁻² as stated by the manufacturer. The adsorbed mass and thickness of the PEMs were calculated using the D-Finder program according to the manufacturer's instruction (Biolin scientific, Sweden). All QCM-D measurements were performed using "open module" system.

2.2 Fabrication of Cu²⁺ and Mg²⁺ loaded vaterite CaCO₃ (CaCuMg-CO₃) particles

Calcium carbonate particles loaded with Cu²⁺ and Mg²⁺ were fabricated on the basis of the previously established co-precipitation approach with some modifications (Sun et al., 2017). Briefly, 0.33 M chloride salt solutions composed of CaCl₂, CuCl₂ and MgCl₂ (Sigma-Aldrich, Germany) at the ratio of 1) 90%: 5%: 5%, 2) 80%: 10%: 10%, 3) 60%: 20%: 20%, 4) 40%: 30%: 30% were prepared and stirred at 500 rpm in 50 ml falcon tubes. 0.33 M Na₂CO₃ (Sigma-Aldrich, Germany) solutions with equal volumes were dropped into the respective chloride salt solutions under continuous stirring at 500 rpm with constant speed (0.6 ml/min) using a syringe pump. Stirring was continued for 1 min after the addition of the Na₂CO₃ solution. The obtained slurries were allowed to stand for 10 min and then centrifuged at 2,719 g for 2 min. The pellets were quickly resuspended in ddH₂O and centrifuged again for the removal of excessive salts from the carbonates. Afterwards the carbonates were washed three times. The full procedure was performed at 22 ± 1°C.

2.3 Encapsulation with polyelectrolyte multilayers and collagen

To enable the desired sustained release and to improve the biocompatibility, the above-described PEM system with collagen

as the most-outer layer was applied for the encapsulation of CaCuMg-CO₃ particles. The freshly prepared CaCuMg-CO₃ particles were encapsulated with PEI[PSS/PAH]₅/PSS-Col in the same manner as described in 2.1 and 2.2. After each deposition and washing step, the particles were quickly but fully resuspended. The incubation with the respective PEs or collagen were carried out using a tube roller at room temperature. Similarly, each deposition step was followed by centrifugation (2,719 g, 2 min) and repeated washing with ddH₂O for three times. The obtained CaCuMg-PEM-Col capsules were lyophilized using a Christ-ε 1-4 LSC plus device (Martin Christ, Osterode am Harz, Germany) and stored at room temperature for subsequent analysis.

For the further investigation of synergistic effects of Cu²⁺, Mg²⁺ and collagen, 1) Ca-PEM, 2) CaCu-PEM, 3) CaMg-PEM; 4) CaCuMg-PEM; 5) CaCuMg-PEM-Col capsules were prepared according to the previously described methods. The ratio of each metal salt was 40%: 30%: 30%.

2.4 Characterization of CaCuMg-PEM-Col capsules

2.4.1 ζ-potential measurements

The charge and compensation of the charge by alternating adsorption of the polyelectrolytes and collagen are closely related to the properties of the PEM, collagen and the capsules. To monitor the charge compensation and characterize the surface, the ζ-potentials of the surface during the LbL-encapsulation was tracked. The electrophoretic mobility of the microcapsules was measured by photon correlation spectroscopy using a Zetasizer NanoZS (Malvern, Herrenberg, Germany). All measurements were performed at 25°C. The mobility was converted into a ζ-potential using the Smoluchowski relation and the system algorithm provided by Malvern (Salmivirta et al., 1996). Immediately after each layering-washing-resuspension process, surface charge was characterized by the ζ-potential ($n = 3$). Samples were always fully resuspended in ddH₂O prior to the measurements. The measurements were performed in triplicate at each adsorption step. Samples were always fully dispersed in distilled water in equilibrium with the room atmosphere. 1 mmol L⁻¹ KCl solution was applied as the model electrolyte, and 0.1 mol L⁻¹ NaOH was used for pH titration from pH 3.0 to 10.0.

2.4.2 Scanning electron microscopy and energy dispersive X-Ray analysis

Scanning electron microscopy (SEM) images and energy dispersive X-Ray analysis (EDS) of capsules were performed with a FIB/SEM microscope (Zeiss crossbeam 550) equipped with an EDS detector (Oxford X-Max). With this set-up we characterized the shape, size, surface morphology and element composition of CaCuMg-PEM-Col capsules. For this observation

the lyophilized samples were attached firmly to carbon tape on a SEM stub without sputter coating. SEM images were then taken at accelerating voltages between 1.5 and 3 kV. The EDS analysis was performed with SEM at an acceleration voltage of 8 kV. The EDS analysis clearly show the distribution of Magnesium, Copper and Calcium in the samples.

2.4.3 Fluorescence microscopy

For the visualization of assembled PEM and adsorbed collagen, fluorescence microscopy (Keyence BZ-X800, KEYENCE Deutschland GmbH, Neu-Isenburg, Germany) was applied. FITC-labeled PAH and type I collagen (Biomol GmbH, Germany) were added to the respective unlabeled PAH and type I collagen solutions at a ratio of 4%. The coating procedure was the same as described above under exclusion of light. Two FITC labeled samples were prepared as 1) CaCuMg-PEM_FITC-Col (FITC labeled PAH at 3rd bilayer) and 2) CaCuMg-PEM-Col_FITC (FITC labeled collagen at the last layer). The samples were resuspended with ddH₂O in a 96-well plate and observed directly under the fluorescence microscope.

2.5 Release kinetics of Ca²⁺, Cu²⁺ and Mg²⁺

The Ca²⁺, Cu²⁺ and Mg²⁺ release profiles were analyzed with a SPECTROBLUE ICP-OES (Inductive coupled plasma-optical emission spectroscopy) analyzer (SPECTRO/AMETEK, Kleve, Germany). Briefly, 0.11 g of each lyophilized sample was immersed in 11 ml Eagle's minimal essential medium (MEM, Gibco) and incubated at 37°C under continuous agitation at 60 rpm. 10 ml supernatant was collected by centrifugation (2,719 g, 2 min) at the specified time points (10 min, 1, 3, 7, 14, 21, 28 and 60 days). After sampling, 10 ml of fresh MEM was added to the residual suspension to continue the release kinetics. For measuring the total ion content, the powder was immersed in 11 ml 5% HAc for 24 h (37°C, 60 rpm), then analyzed using ICP-OES. All solutions used were sterile filtrated using a 0.45 µm membrane filter and the samples were handled and kept sterile. After processing of the measurement signals by the instrument, the measured intensities of the elements were evaluated *via* the Smart Analyzer software.

2.6 Cell culture

In this study, the murine fibroblast cell line L929 (ATCC, CCL1) and human derived osteoblast-like MG63 (ATCC, CRL 142) osteosarcoma cells were purchased from ATCC (VA, United States). L929 cells were grown in RPMI medium 1,640 GlutaMAX supplemented with 10% (v/v) fetal bovine serum (FBS) and 1% penicillin/streptomycin (P/S). MG63 cells were cultivated with MEM plus supplemented with 10% FBS, 1% P/S, and 1% sodium pyruvate, 1% nonessential amino acids

(NEAA) and 1% L-glutamine. All these materials were purchased from Gibco (Carlsbad, CA, United States). Both cells were grown in a humidified 5% CO₂/95% atmosphere and passaged when cell confluence rate was over 80%.

2.7 Cell viability test by cell count kit-8

The cytotoxicity of the CaCuMg-PEM-Col capsules was evaluated by an extraction test and CCK-8 assay of L929 cells according to ISO 10993 part 5 (ISO 10993-5:2009, confirmed in 2017) (ISO, 2009). 10 mg ml⁻¹ of CaCuMg-PEM-Col capsules, positive control (PC, polyurethane film containing 0.1% zinc diethyldithiocarbamate (ZDEC), RM-A, HatanoResearch Institute, Japan), negative control (high density polyethylene film, RM-C, HatanoResearch Institute, Japan) in L929 cell culture medium and blank (only cell culture medium) were incubated at 37°C with gentle shaking at 60 rpm for 24 h. The cells were seeded in 96-well plates (10⁴ cells/well) and cultured at 37°C for 24 h with 5% CO₂. Then, the medium was replaced with the extracts. After culturing for further 24 h, the cell viability of L929 was determined by CCK-8 assay (Sigma-Aldrich, Germany). Briefly, the medium was thoroughly removed, and the cells were then incubated with fresh medium supplemented with 10% CCK-8 reagent. After incubation at 37°C for 2 h, the color change was determined by measuring the absorbance at 450 nm using a microplate reader (TECAN RAINBOW, Germany).

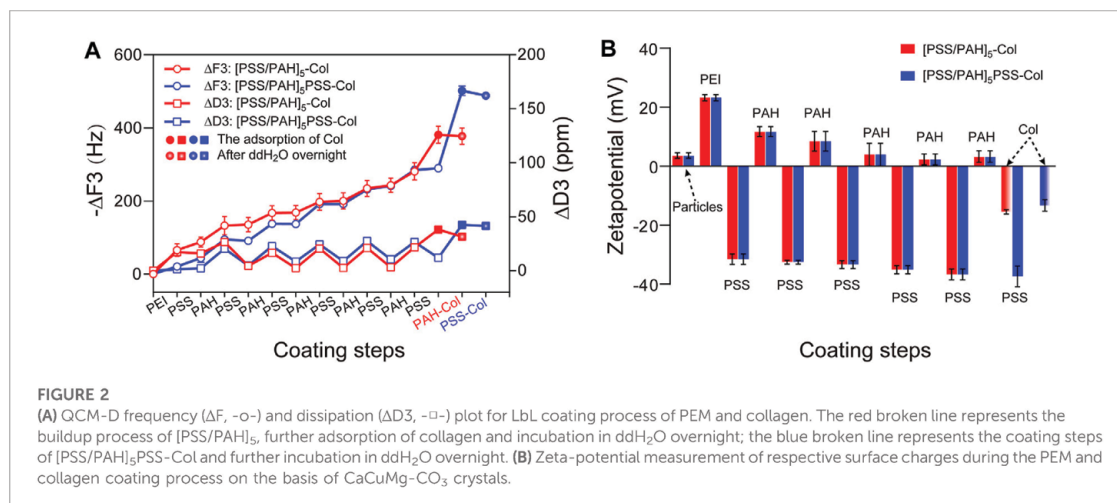
The MG63 cell viability was also evaluated using CCK-8 method. Cells were seeded in 96-well plates (10⁴ cells/well) cultured with complete medium for 24 h. Then, the medium was thoroughly aspirated and replaced by fresh culture medium supplemented with the extracts of capsules. After incubation for the designated times, the cell viability was measured using the CCK-8-assay. The medium was replaced every 3 days.

2.8 Alkaline phosphatase activity measurements

As a key osteogenic maker of osteoblastic differentiation, alkaline phosphatase (ALP) activity was determined by conversion of *p*-nitrophenyl phosphate (pNPP) into *p*-nitrophenol (pNP). Incubating MG63 cells with substrate solution (1 mg ml⁻¹ pNPP, 50 mM glycine, 1 mM MgCl₂, 100 mM TRIS, pH 10.5) at 37°C for 30 min, and then measuring the absorbance at 405 nm using a microplate reader (TECAN RAINBOW, Germany).

2.9 Relative gene expressions

Total RNA extraction, reverse-transcription and real-time PCR were performed by using the Cells-to-CT™ 1-Step TaqMan™ Kit (Thermo Fisher Scientific, Rockford, IL, United States), conducted on



a one-step PCR instrument (Applied Biosystems, Foster City, CA, United States) according to the manufacturer's instruction. For analysis of osteogenic-related genes (COL1A1, MMP1, ALPL, BGLAP, RUNX2) and angiogenic-related genes (VEGFA and HIF1A), the relative expression of mRNAs was calculated using glyceraldehyde-3-phosphate dehydrogenase (GAPDH) as an internal reference standard gene by the $2^{-\Delta\Delta Ct}$ method. All primers were purchased from Thermo Fisher Scientific, and more details are listed in [Supplementary Table S1](#), Supporting information.

2.10 Alizarin red staining

The formation of mineralized matrix nodules after 14 days was determined by Alizarin Red staining. Briefly, MG63 cells were fixed with 99% ethanol at -20°C for 2 h, then washed with tap water for three times. After incubating with 0.5% Alizarin Red solution (pH 4.0, Carl Roth) for 30 min at room temperature and another three washing steps, the resulting staining was assessed with optical microscopy. The bound Alizarin Red was resolved with 10% Cetylpyridium chloride solution (Carl Roth) for photometric quantification at the absorbance of 562 nm using a microplate reader (TECAN RAINBOW, Germany).

3 Results and discussion

3.1 Optimization and characterization of PEM and collagen coating

The buildup process of the PEM-systems was monitored by measurements using QCM-D ([Figure 2A](#)). The regular frequency shifts confirmed the effective adsorption of each deposited

polyelectrolyte-layers and the assembly of the multilayer systems. The collagen was adsorbed on both basic layer-systems $[\text{PSS}/\text{PAH}]_5$ and $[\text{PSS}/\text{PAH}]_5\text{PSS}$ with an average frequency shift of $-380.75 \pm 23.45 \text{ Hz}$ and $-501.77 \pm 13.33 \text{ Hz}$. After overnight incubation in ddH₂O only a slight increase of the frequency could be observed indicating a stable adsorption as reported previously. ([Sun et al., 2017](#)) More (113.23%) collagen could be adsorbed on top of the PSS ($212.06 \pm 33.06 \text{ Hz}$) than PAH ($99.45 \pm 13.47 \text{ Hz}$). At a pH range from 4 to 10, collagen has both positive and negative charges throughout the molecules ([Morozova and Muthukumar, 2018](#)). The higher the pH value, the higher the negative charge measured. At a pH of 5, the collagen was predominantly present as positively charged molecules, resulting in greater adsorption on the negatively charged PSS surface compared to the positively charged PAH surface. After overnight incubation in ddH₂O, the Δf was 3.48 Hz (3.5% frequency increase) and 13.66 Hz (6.4% frequency increase) for PAH-Col and PSS-Col respectively. Energy dissipation was also monitored and plotted in [Figure 2A](#). ΔD indicated primarily the change of the stiffness of the layers. Both PAH-Col and PSS-Col have reduction of dissipation and the ΔD was $-6.6 \pm 4.17 \text{ ppm}$ and $-1.14 \pm 2.45 \text{ ppm}$ respectively. Taking the results of Δf and ΔD together, it might be concluded that the PAH-Col and PSS-Col coatings retained their integrity after deposition because the negligible changes in frequency and mass. The increase in frequency is most likely due to the rearrangement of the PEM and collagen on the surfaces during the long time incubation in ddH₂O. Also, the evaporation of the ddH₂O in the used open cells could result in the slight fluctuation of the measurement. In addition, the fitting of the thickness using the QSense_Dfinder software showed a slight reduction of the thickness of the coatings indicating the tightening of the film-structure ([Supplementary](#)

Table S1). After deposition and during equilibrium in water, PE molecules could complete the arrangement such as interpenetration due to compensation and stabilization of weak interactions, especially hydrogen-bonding and hydrophobicity-interactions between molecules (Wang et al., 2014). The small ΔD suggested a stable system has been formed and kept the stability during further incubation. The slight negative ΔD also indicates the increased stiffness and rigidity of the surface. As described in the literature, the lower overtone represents the adsorption and change at the interface between liquid and thin film, and the comparison of other signals recorded for higher overtones indicates the depth integrity of the system. The signals of overtones 3, 5 and 9 did not differ significantly from each other confirming the linearity, rigidity and rather stiffer property of the systems (Wang et al., 2014). As reported previously, molecular water can be pushed out while the structure of the film was rearranged to a much thinner and stable form. This process will also result in a slight frequency increase due to loss of water molecules from the film (Delajon et al., 2009; Kohler et al., 2009).

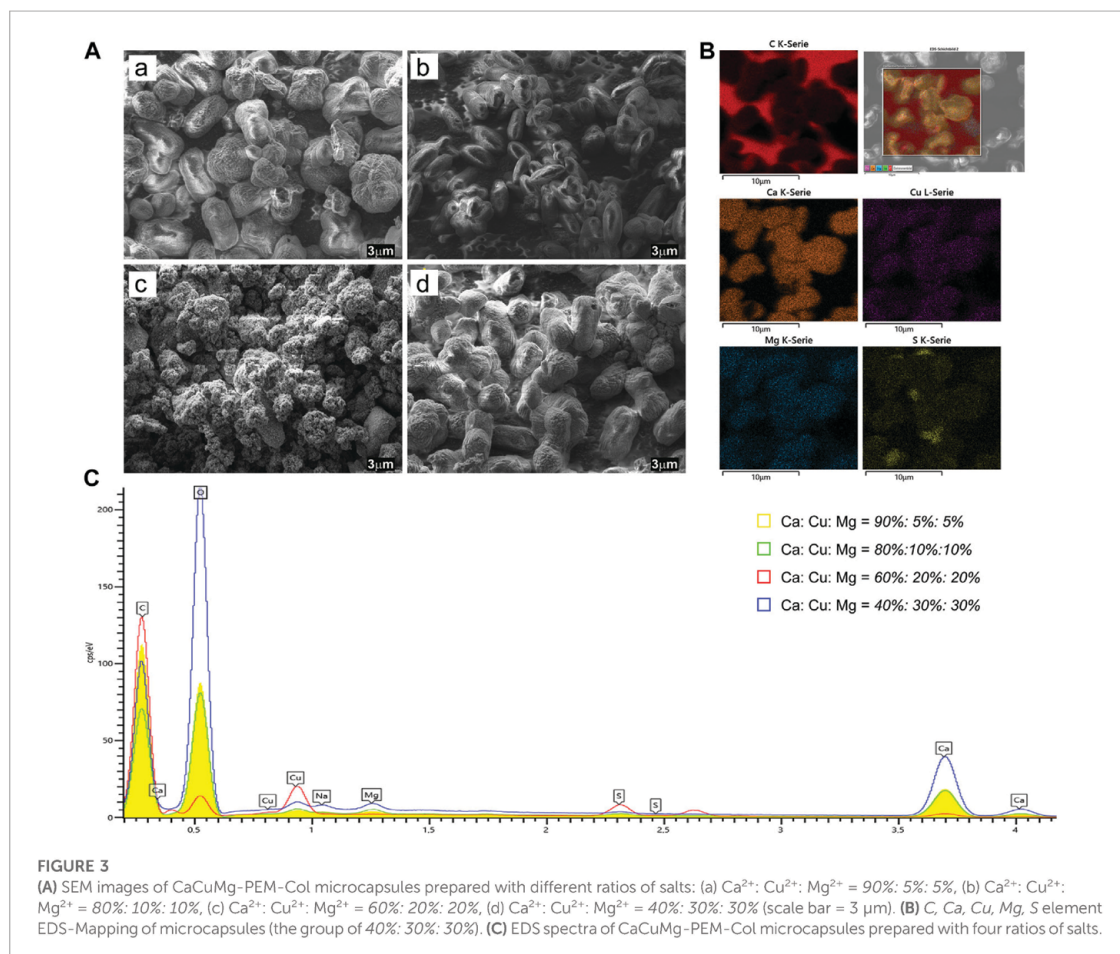
As mentioned above, collagen has both positively and negatively charged moieties, which allows adsorption to differently charged surfaces. The adsorption determined by QCM might be resulted from the adhesive property of collagen. ζ -Potential confirmed the buildup process according to the charge-compensation theory of the PEM-LbL technique (Figure 2B). Moreover, the initial positive charge of the PAH outer layer was reduced to a negative charge (-18.67 mV) after adsorption of collagen, while the strong negative charge of PSS was strongly neutralized to (-24.10 mV) by collagen. This observation was in accordance with the expectation that collagen can be stably adsorbed both on positively and negatively charged surfaces at proper pH value. In one word, the buildup of the designed PEM systems was successfully performed and confirmed by QCM-D analysis. The stability of both systems was proven to be sufficient for further applications. The -PSS showed overall a better adsorption capacity of collagen and stability in comparison to -PAH.

3.2 Characterization of CaCuMg-PEM-Col microcapsules

As mentioned above, the vaterite formation process of CaCO_3 is easily influenced by the experimental conditions and the substances introduced during co-precipitation. In order to guarantee stable encapsulation and sustainable release with the desired controllability, different microcapsule formulations were prepared by co-precipitation. The morphology and elemental composition of CaCuMg-PEM-Col particles were investigated *via* SEM combined with EDS-analysis. When the ratio of Ca^{2+} , Cu^{2+} and Mg^{2+} was 90%: 5%: 5%, the formed particles presented three kinds of morphologies: bigger

spherical particles (41.38% of total) with an average size around 5.0 ± 0.5 μm (diameter), smaller spherical particles (20.69%) in the size of 2.6 ± 0.3 μm , and oval particles (37.93%, 5.6 ± 0.3 $\mu\text{m} \times 2.9 \pm 0.3$ μm) (Figure 3Aa [if subparts are of A]). The SEM image of the 80%: 10%: 10% group showed that most of the particles have an oval shape with relatively uniform size (Length 3.9 ± 0.4 μm Width 1.9 ± 0.3 μm) (Figure 3Ab [if subparts are of A]). Interestingly, in the group of 60%: 20%: 20%, there were no regular shaped vaterite or calcite particles observed. SEM images revealed irregular and porous structures (Figure 3Ac [if subparts are of A]). The particles obtained from the group of 40%: 30%: 30% showed a similar morphology as the 90%: 5%: 5% group. The bigger spherical particles in this sample were around 5.5 ± 0.4 μm and account for 12.90%; the smaller ones were in the size of 2.5 ± 0.4 μm (48.39%) and the oval particles were about L 5.474 ± 0.5 μm W 3.0 ± 0.4 μm (29.27%) (Figure 3Ad [if subparts are of A]).

As one of the most effective platforms for drug encapsulation and delivery, the key parameters for size- and shape-controlled synthesis of CaCO_3 particles have been well studied. The fast mixing of aqueous calcium chloride and sodium carbonate can immediately result in amorphous calcium carbonate (ACC). Under vigorous stirring, the formed ACC in the precipitation system will dissolve first, and then transform within minutes to produce crystalline forms of vaterite and calcite (Shen et al., 2006). However, when the system is introduced with other divalent cations, the co-precipitation reaction and co-crystallization process will be more complicated, thus rarely being reported. In the co-precipitation system of Ca^{2+} , Cu^{2+} , and Mg^{2+} presented in this work, there are two main factors affecting the morphology of obtained particles: the concentration of Ca^{2+} , and the ionic interactions with Cu^{2+} and Mg^{2+} . It is known that the higher content of Ca^{2+} within a certain range would lead to high yield of vaterite; trace amounts of Cu^{2+} , and Mg^{2+} , which have a smaller ion size than Ca^{2+} could enter and distort the lattice of just formed CaCO_3 -crystals, and thus influence the size and morphology of the final particles, as shown in Figure 3Aa [if subparts are of A]) (Svenskaya et al., 2018). A certain proportion of Mg^{2+} was reported to promote the formation of vaterite CaCO_3 crystals (Kulp and Switzer, 2007). Among the four ratios in this study, 10% of Mg^{2+} might play the optimal role in vaterite formation. Particles obtained at the ratio of 80%: 10%: 10% showed the most regular oval vaterite morphology (Figure 3Ab [if subparts are of A]). With the increase of Cu^{2+} and Mg^{2+} content, the crystals gradually transformed from vaterite to calcite leading to a reduced uniformity in the particles. The particles from the ratio of 60%: 20%: 20% appeared to stay at the transformation phase of ACC-vaterite, and particles of 40%: 30%: 30% were at vaterite-calcite stage or mixture of different crystallization products (Figures 3Ac,d [if subparts are of A]). Most likely the ions find an equilibrium among vaterite and calcite during particle formation depending on the ratios and precipitation conditions.



This could be due to the excessive electronegativity of Cu^{2+} and Mg^{2+} , which led to a distortion of the crystal plane structure; furthermore, the increasing cocrystallization with CuCO_3 ($\text{Cu}_2\text{CO}_3(\text{OH})_2$) and MgCO_3 suppressed the formation and stability of CaCO_3 vaterite. Additional influence from the PEM coating should also be considered as a morphology-stabilizing factor. The particles were encapsulated in their precipitated shapes without further modifications as a substrate for coating deposition. CaCO_3 has a water solubility of 15 mg L^{-1} and MgCO_3 0.14 g L^{-1} . More complicated, the Cu^{2+} will form so called basic copper carbonate consisting of $\text{Cu}_2\text{CO}_3(\text{OH})_2$ which has a negligible solubility in water. The basic copper carbonate has a typical monoclinic crystal and spertiniite morphology. Also the formation of dolomite, $\text{CaMg}(\text{CO}_3)_2$ would further enhance the alternating morphology due to the structural arrangement of the Ca^{2+} and Mg^{2+} ions. These properties derived from basic copper carbonate and dolomite could explain the morphological

changes from ACC, to vaterite and calcite in this complex mixture system as shown in Figure 3A. These mixtures of dolomite and basic copper carbonate will also further affect the release kinetics by means of dissolution and degradation.

X-ray energy dispersive spectroscopic (EDS)-mapping images and spectra further revealed the element composition of CaCuMg-PEM-Col capsules. The SEM EDS-mapping images showed that the elements including C, Ca, Cu, Mg, S were uniformly distributed on particles prepared with these four ratios (Figure 3B and Supplementary Figure S1). The EDS spectra exhibited the characteristic peaks for C, Ca, Cu, Mg, and S (Figure 3C) present in the surfaces of the microcapsules. The obtained element composition ratio is shown in Supplementary Table S2. No significant difference in the element composition ratio of the group of 95%: 5%: 5% and 80%: 10%: 10% was observed. The high ratio of Cu and low ratio of Ca in the group of 60%: 20%: 20% suggested a high amount of $\text{CuCO}_3/\text{Cu}_2\text{CO}_3(\text{OH})_2$ in the surfaces of microcapsules. The

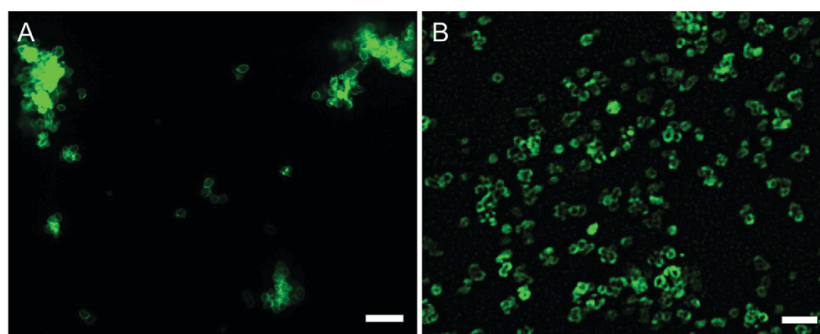


FIGURE 4
Micrographs of (A) FITC-labeled PAH coated at 3rd bilayer of CaCuMg-PEM-Col and (B) FITC-labeled collagen coated at the outmost layer (scale bar = 50 μm).

group of 40%: 30%: 30% exhibited a relatively more uniform distribution of elements.

Fluorescence microscope imaging was applied to further visualize the adsorbed PEM and collagen on CaCuMg- CO_3 crystals. As shown in Figure 4A, FITC-PAH was uniformly coated on the particles, forming a thin green layer along the particle surfaces. Similarly, the deposition of the FITC-collagen layer was also successfully observed on the surface of the encapsulated particles (Figure 4B). Interestingly, it was found that the CaCuMg-PEM-Col particles exhibited better dispersion than the CaCuMg-PEM particles after further adsorption of collagen. This is consistent with the measurement of the zeta potential. Since the adsorption of collagen leads to a higher negative charge distribution on the surface of the particles, the repulsion between the negatively charged particles is enhanced.

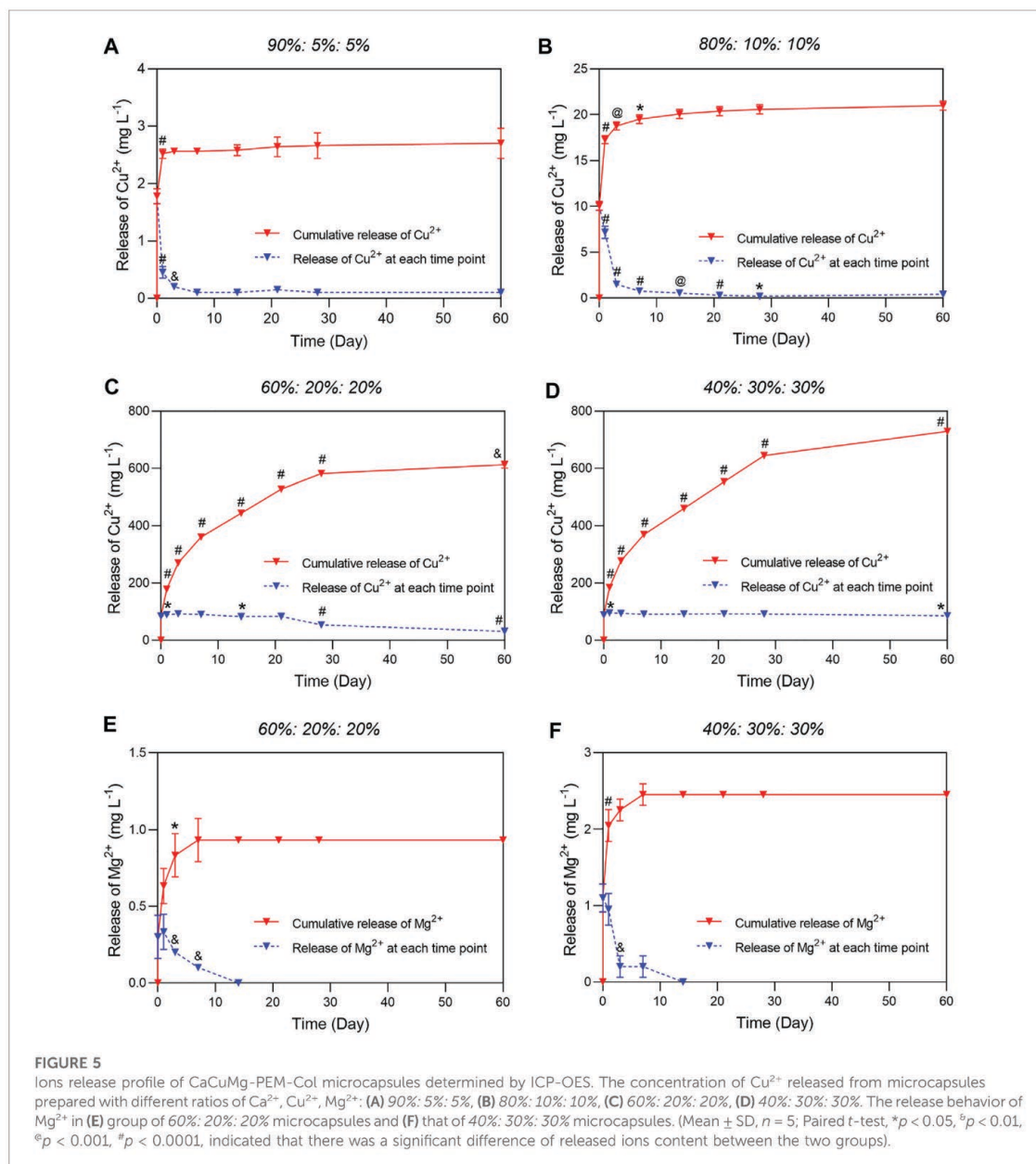
3.3 Ion release behavior of CaCuMg-PEM-Col microcapsules

The release kinetics of the target bioactive cations Cu^{2+} and Mg^{2+} are of particular importance as a sudden increase in concentration due to excessive release of these cations will result in bone loss, irregular crosslinking or excessive cytotoxicity (Wong et al., 2014; Wang et al., 2016). Therefore, the stability and controllability of ion release kinetics during the long-term bone regeneration process is crucial. In this study, we investigated and compared the ion release behavior of the microcapsules prepared with different salt ratios *via* ICP-OES measurements. The two groups with higher Ca^{2+} -content showed a burst release of Cu^{2+} in the first hours and 3 days, then followed by a very slow and incomplete release until day 60 (Figures 5A,B). While the two groups with increased Cu^{2+} and Mg^{2+} content showed stable release throughout the analyzed period without initial burst release (Figures 5C,D). Notably, the Mg^{2+} in the first two groups

were below the detection limits of the ICP-OES. But in the groups of 60%: 20%: 20% and 40%: 30%: 30%, trace Mg^{2+} was slowly released in the first 7 days (Figures 5E,F). The amount of target bioactive ions Cu^{2+} and Mg^{2+} released from the capsules differed dramatically between the high and low Ca^{2+} -content groups. The cumulative release profile of Ca^{2+} also showed an initial burst release in groups of 95%: 5%: 5% and 80%: 10%: 10% (Supplementary Figure S2). Interestingly, the concentration of Ca^{2+} decreased as the release process prolonged, whereas the Ca^{2+} release of the other two groups was stable and slow. When the Ca^{2+} content was replaced by increased Cu and Mg content, CaMg CO_3 crystallizes in the nucleation region was surrounded by relatively unstable basic Cu and Mg(OH) $_2$ /Mg CO_3 . In particular, the Mg CO_3 is destabilized by hydration to Mg(OH) $_2$. This reaction cascade dynamically determines the surface morphology of the particles and the release behavior. The higher the Cu content the easier the Cu^{2+} can be released (Figures 5C,D). The unstable surface portion of the Cu/Mg was easily released within the first 7 days. As the dissolution front approaches the calcite core, the release was more limited by the dissolution of the calcite, especially for the Mg. This could explain the relatively short continuous release of Mg measured by ICP (Figures 5E,F). The release curve of Ca^{2+} also confirms the above mentioned mechanisms. After the release of unstable vaterite from the surface, the release rate decreased significantly for a short time, and then rose slowly because of the slow dissolution of calcite core (Supplementary Figure S2). The large amount of Mg^{2+} was increasingly co-crystallized in nucleation region of calcite or dolomite crystals which limited the dissolution process.

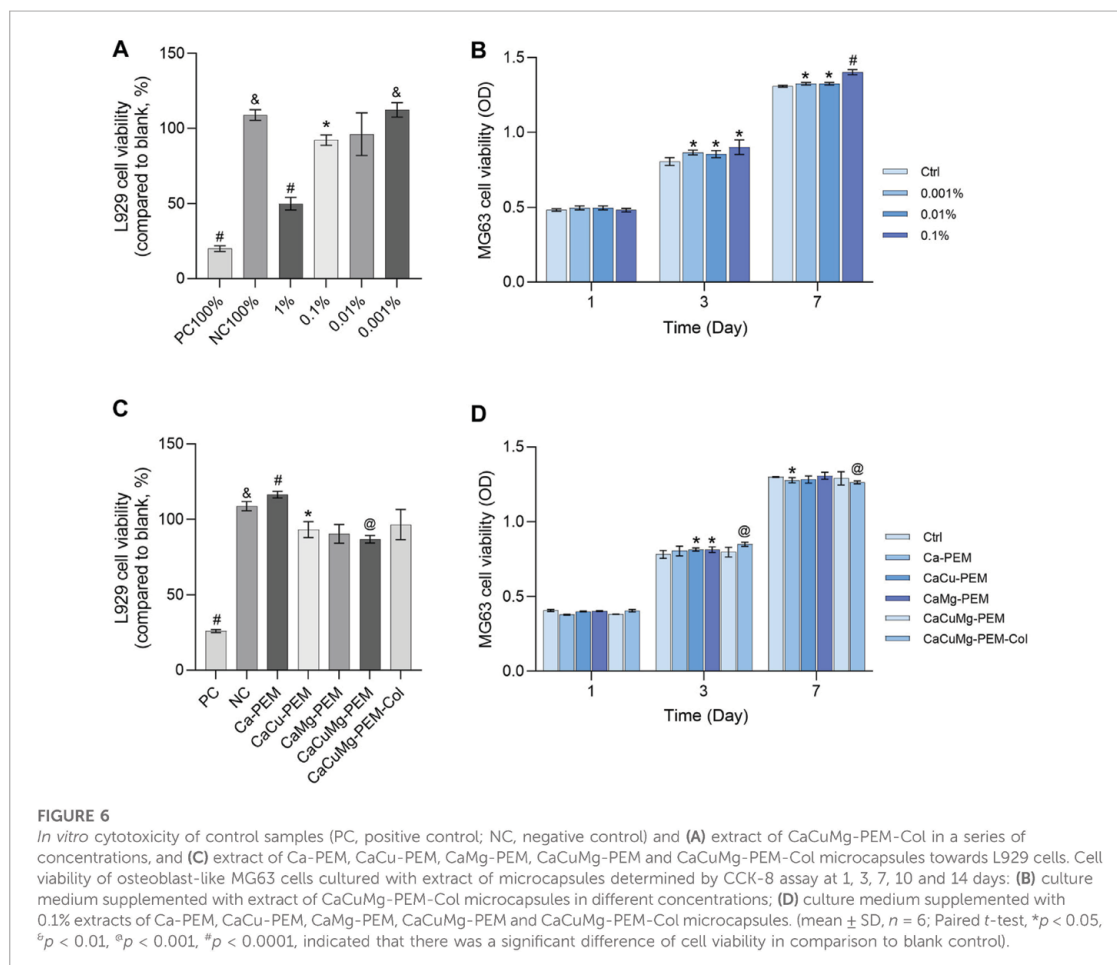
3.4 *In vitro* cytotoxicity

In addition to achieve the sustained release function as an encapsulation system, PEM and collagen were also used to mimic



bone tissue ECM to promote osteogenic differentiation *via* modifying different surface properties which in turn stimulating numerous interfacial interactions with the cells adsorbed to the coated surfaces (Brito Barrera et al., 2020; Sankar et al., 2021). Collagen is an indispensable matrix protein that stimulates various signaling pathways such as cell adhesion, mobility, wound healing, proliferation, and an

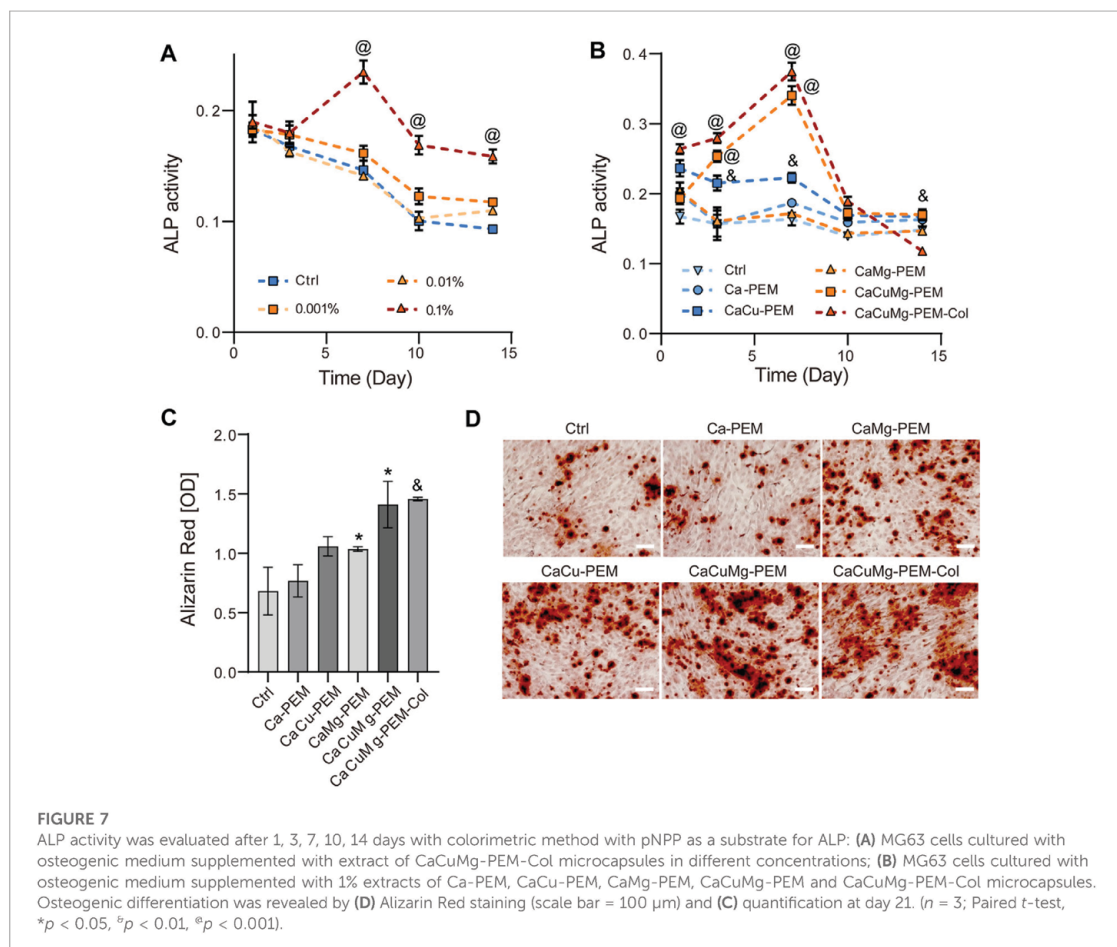
important process to complete bone regeneration, named ECM remodeling (Zhang et al., 2018). Other physicochemical properties of the surface are also decisive for proper bone regeneration, such as surface roughness, hardness, electrical charge and charge density (Bharadwaz and Jayasuriya, 2020). The PEM provides a highly tunable surface fulfilling these demands. The negative charge of the coated surface attracts



cells and makes them easy to adhere; in addition, cell adhesion and the necessary cell motility are more active on harder surfaces than on softer ones (Sahebalzamani et al., 2022). Therefore, a PEM-Col surface has been chosen for proof of this strategy. In this study, mouse derived L929 fibroblasts were used to evaluate the cytotoxicity of CaCuMg-PEM-Col microcapsules. The cell viability assay has been performed *via* an extraction test on L929 and evaluated by CCK-8 assay. According to the ISO standard, metabolic activity below 70% is considered to be cytotoxic. As shown in Figure 6A, the microcapsules showed a decrease in cytotoxicity with decreasing extract concentration, while the viability of fibroblasts was below 70% only when the extract concentration was higher than 1%. According to the results of ICP measurements as shown in Figure 5, the concentration of Cu^{2+} in 1% extract was 15.63 μM and the concentration of Mg^{2+} is 4.17 μM . These measurements formed the basis for determining a suitable dosage range of

the microcapsules. To exclude the bias due to PEM, collagen and their probable degradation products, the extracts of five types of microcapsules have been applied for the cytotoxic evaluation, including Ca-PEM, CaCu-PEM, CaMg-PEM, CaCuMg-PEM and CaCuMg-PEM-Col. All the extracts did not exhibit any significant cytotoxicity on L929 cells (Figure 6C), suggesting good biocompatibility of the microcapsules. It was found that the cells treated with CaCuMg-PEM-Col extract showed higher viability compared to CaCuMg-PEM without a collagen layer, which might be a result of slight desorption of collagen from the surface of the microcapsules. The beneficial effects from the collagen layer might also reduce the toxicity resulting from Mg^{2+} and Cu^{2+} ions within certain concentration threshold (Cu^{2+} : 15.63 μM ; Mg^{2+} : 4.17 μM).

Main task of this trimetal microcapsules is to stimulate the bone regeneration *via* controlled release of these bioactive cations. Therefore, cell proliferation of osteoblast-like

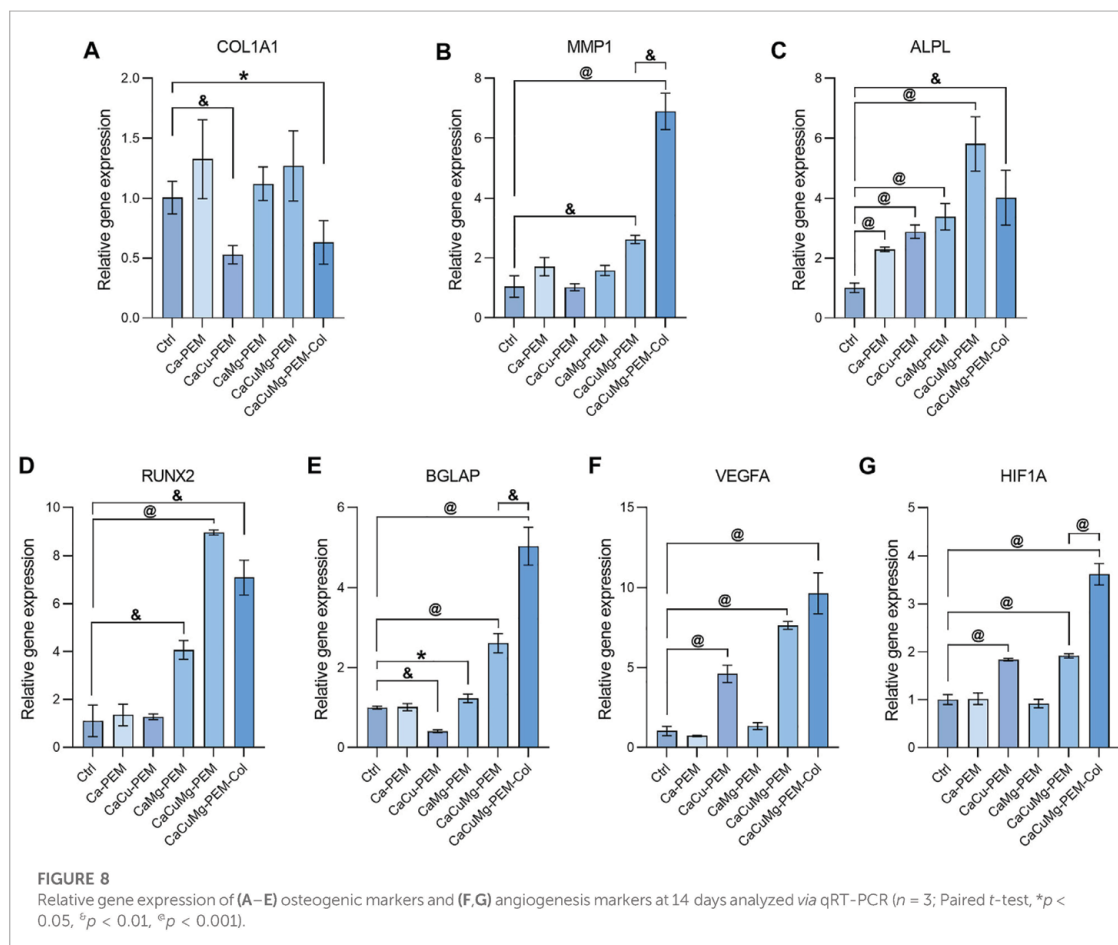


MG63 cells was also carried out by using CCK-8 assay on the cell cultures at 1st, 3rd, and 7th days. Results in Figure 6B showed that cell viability on the 1st day was not markedly affected in any condition of microcapsules extracts (0.001%, 0.01%, and 0.1%) because the cells need sufficient time to recover after the passaging and transfer into the test-cultures. On the 3rd day, cells viability higher than 70% was observed for the groups treated with ionic extracts, all of which were higher than those of the blank controls. The cell viability of the group of 0.1% of microcapsule extract was obviously higher than other groups on the 7th day. A similar trend was observed with cell viability measured by addition of Ca-PEM, CaCu-PEM, CaMg-PEM, CaCuMg-PEM and CaCuMg-PEM-Col capsules (Figure 6D). Results revealed that the cell proliferation ability of the microcapsule groups was similar to or higher than that of blank control. And the cells in the CaCuMg-PEM-Col group showed the highest viability on the 3rd and 7th day. These results indicate that metal ions and CaCuMg-PEM-Col microcapsules

did not induce any cytotoxic effect but promoted osteoblast proliferation in conjunction with type I collagen.

3.5 Osteogenic differentiation of osteoblast-like MG63 cells *in vitro*

Bone regeneration mainly includes proliferation and differentiation of osteoblasts. The previous viability measurements confirmed the positive effects of CaCuMg-PEM-Col microcapsules on cell proliferation. Therefore, the impacts on osteogenic differentiation were further investigated. ALP is an early marker of osteoblast differentiation which is an important indicator for bone formation and mineralization as well as for the bone regeneration progress (Hu & Olsen, 2016). The cellular ALP activity of MG63 cells treated with different microcapsule extracts were monitored on the 1st, 3rd, 7th,



10th and 14th days. As shown in Figure 7A, on the 1st and 3rd day, ALP activity of cells treated with the extract of CaCuMg-PEM-Col microcapsules (0.001%, 0.01%, and 0.1%) were at a similar level as the blank control. Cellular ALP activity of the group of 0.1% reached peak on the 7th day, which was significantly higher than groups of 0.001%, 0.01% and ctrl. From day 7 onwards, decrease in ALP activity was observed under all conditions. Nevertheless, ALP activity of cells treated with 0.1% of microcapsule extracts was still significantly higher than other treated groups and control group. Therefore, 0.1% was adopted as the concentration used for the subsequent investigation (Figure 7B). On the 1st day, cells treated with osteogenic medium supplemented with sample extracts including Ca-PEM, CaCu-PEM, CaMg-PEM, CaCuMg-PEM and CaCuMg-PEM-Col showed higher ALP activity than control group which was only treated with osteogenic medium. On days 3 and 7, the levels and trends of ALP activity in the Ca-PEM and

CaMg-PEM groups were the same as those in the blank control group, first increasing and then slowly decreasing. However, there was no significant difference in the expression levels between groups. The group of CaCu-PEM showed a similar trend but significantly higher ALP activity at these time points. Notably, the levels of ALP activity in the CaCuMg-PEM and CaCuMg-PEM-Col groups continued to increase over time, reaching a peak on day 7, in which the ALP activity in these two groups was significantly higher than other groups, and gradually decreased thereafter to levels close to those of the other groups. This indicates the significant synergistic regulation of Cu^{2+} and Mg^{2+} and collagen in osteoblasts differentiation. Interestingly, the ALP activity of the CaCuMg-PEM-Col group also showed the largest decrease among all groups after exhibiting the highest levels on days 1, 3, 7, and 10. It is suggested that CaCuMg-PEM microcapsules further functionalized with collagen could better mimic ECM, thus providing a more suitable microenvironment for bone

regeneration and promoting the proliferation and differentiation of osteoblasts. ALP activity downregulated by CaCuMg-PEM-Col at day 14 indicated that the initiation of ECM mineralization completed earlier than other groups.

The effect of CaCuMg-PEM-Col on late differentiation (matrix mineralization) was investigated after 21 days of culture *via* Alizarin Red staining and quantification. As shown in Figure 7D, stronger Alizarin Red staining was observed on CaCuMg-PEM and CaCuMg-PEM-Col as compared to CaCu-PEM, CaMg-PEM, and blank control. Similarly, the result of quantification shows that mineralization on CaCu-PEM ($p < 0.05$), CaCuMg-PEM ($p < 0.05$) and CaCuMg-PEM-Col ($p < 0.01$) were significantly higher than the control group, suggesting that the microcapsules have a positive influence on osteoblast mineralization (Figure 7C).

3.6 Expression of osteogenesis and angiogenesis-related genes

As discussed previously, the bone regeneration process can be briefly divided into three periods: proliferation, ECM maturation and mineralization. Two transition points of gene expression of certain marker genes controlling cell proliferation and differentiation have been reported (Stein et al., 1990). The first transition occurs after completion of proliferation and initiation of ECM, when ALP and collagen are upregulated. The second transition takes place at the initiating of ECM mineralization. In this study, we investigated the gene expression related to osteogenesis and angiogenesis of MG63 at day 14 *via* real-time PCR (Lynch et al., 1995). As shown in Figure 8A, the COL1A1 expression of CaCu-PEM and CaCuMg-PEM-Col were significantly lower than blank control (osteogenic medium). This might result by the ECM-mimicking effect from the PEM and PEM-Col capsules. Reasonably, when compared to the blank control the matrix metalloproteinase-1 (MMP1) gene expression was markedly higher in the CaCuMg-PEM group ($p < 0.01$) and CaCuMg-PEM-Col group ($p < 0.001$) due to the presence of collagen (Figure 8B). All groups of microcapsules (Ca-PEM, CaCu-PEM, CaMg-PEM, CaCuMg-PEM, and CaCuMg-PEM-Col) showed significantly higher expression of ALPL in comparison to the blank control (osteogenic medium), among which the expression in the CaCuMg-PEM group was the highest, followed by the CaCuMg-PEM-Col (Figure 8C). The expression of RUNX2 in groups of CaMg-PEM, CaCuMg-PEM, and CaCuMg-PEM-Col were significantly higher than other groups (Figure 8D). The expression pattern of osteocalcin (BGLAP) was roughly similar to that of MMP1, showed the highest level in the CaCuMg-PEM-Col group, followed by the CaCuMg-PEM group (Figure 8E).

During osteogenic differentiation, (pre-) osteoblasts play a central role in communication with endothelial cells to ensure the temporal and spatial coupling of osteogenesis and angiogenesis *via* the regulation of gene expressions involved in angiogenesis. Interestingly, high expression of VEGFA and HIF1A were found in osteoblasts conditioned with CaCu-PEM, CaCuMg-PEM, and CaCuMg-PEM-Col extracts as shown in Figures 8F,G, suggesting that copper plays a more important role in the promotion of angiogenesis. Notably, we found significant synergistic effects of copper and magnesium, as well as the addition of type I collagen, on angiogenesis.

4 Conclusion

Bioactive metal ions including Ca^{2+} , Cu^{2+} and Mg^{2+} play a predominant role in the process of bone regeneration, which are recognized as an alternative for bone growth factor-based therapeutics. However, a delivery system with high stability and loading capacity of multiple metal ions, and controlled release kinetics is currently highly required. In this study, the vaterite-calcite CaCO_3 particles were effectively loaded with Cu^{2+} and Mg^{2+} , then coated with PEM to improve the crystal stability for better sustained release behavior, and further successfully functionalized with collagen to mimic bone tissue ECM. Ca^{2+} , Cu^{2+} and Mg^{2+} could sustainably release from the microcapsules and induce a proper bone regeneration microenvironment, regulating the osteoblasts proliferation and differentiation, promoting the ECM maturation and mineralization. It was shown that both osteogenesis and angiogenesis-related gene expressions were upregulated. Therefore, CaCuMg-PEM-Col microcapsules present a type of bioactive metal ion encapsulation and delivery system for the functionalization of bone graft materials. The presented strategy of combining multi metal ions with biocompatible PEM and collagen provides new inspiration and important prospects for bone tissue engineering.

Data availability statement

The original contributions presented in the study are included in the article/Supplementary Materials, further inquiries can be directed to the corresponding authors.

Author contributions

LF contributed to methodology, investigation, writing the original article, data curation. FK contributed to methodology and validation. AR and OJ contributed to investigation. CB

contributed to methodology. MB contributed to methodology, reviewed and edited the manuscript, and funding acquisition. XX contributed to conceptualization, reviewing and editing the article, funding acquisition, investigation, and supervision.

Funding

This work was supported by the Federal Ministry of Education and Research (BMBF, Germany, FKZ: 13GW0400C); and the State Ministry of Baden-Württemberg for Economic Affairs, Labour and Tourism.

Acknowledgments

LF acknowledges the support by the China Scholarship Council (CSC, No. 202008500143). We thank our colleagues Clarissa Geiger, Anastasia Binder for their technique assistance, and Birgit Schröppel for insightful discussions and technique support in SEM and EDX mapping. Schematic figure was created with *BioRender*. The statistical analysis of data was performed with *GraphPad 9*.

References

- Aggarwal, N., Altgarde, N., Svedhem, S., Zhang, K., Fischer, S., and Groth, T. (2013). Effect of molecular composition of heparin and cellulose sulfate on multilayer formation and cell response. *Langmuir* 29 (45), 13853–13864. doi:10.1021/la4028157
- Bharadwaz, A., and Jayasuriya, A. C. (2020). Recent trends in the application of widely used natural and synthetic polymer nanocomposites in bone tissue regeneration. *Mater. Sci. Eng. C* 110, 110698. doi:10.1016/j.msec.2020.110698
- Brito Barrera, Y. A., Hause, G., Menzel, M., Schmelzer, C. E. H., Lehner, E., Mader, K., et al. (2020). Engineering osteogenic microenvironments by combination of multilayers from collagen type I and chondroitin sulfate with novel cationic liposomes. *Mat. Today Bio* 7, 100071. doi:10.1016/j.mtbio.2020.100071
- Campbell, J., Kastania, G., and Volodkin, D. (2020). Encapsulation of low-molecular-weight drugs into polymer multilayer capsules templated on vaterite CaCO₃ crystals. *Micromachines (Basel)* 11 (8), 717. doi:10.3390/mi11080717
- Collins, M. N., Ren, G., Young, K., Pina, S., Reis, R. L., and Oliveira, J. M. (2021). Scaffold fabrication technologies and structure/function properties in bone tissue engineering. *Adv. Funct. Mat.* 31, 2010609. doi:10.1002/adfm.202010609
- Daria, B., Trushina, T. N. B., Belyakov, Sergei, and Antipina, Maria N. (2022). Calcium carbonate vaterite particles for drug delivery: Advances and challenges. *Mater. Today Adv.* 14 (2590-0498), 100214. doi:10.1016/j.mtadv.2022.100214
- Delajon, C., Gutberlet, T., Mohwald, H., and Krastev, R. (2009). Absorption of light and heavy water vapours in polyelectrolyte multilayer films. *Colloids Surfaces B Biointerfaces* 74 (2), 462–467. doi:10.1016/j.colsurfb.2009.08.051
- Divband, B., Aghazadeh, M., Al-Qaim, Z. H., Samiei, M., Hussein, F. H., Shaabani, A., et al. (2021). Bioactive chitosan biguanidine-based injectable hydrogels as a novel BMP-2 and VEGF carrier for osteogenesis of dental pulp stem cells. *Carbohydr. Polym.* 273, 118589. doi:10.1016/j.carbpol.2021.118589
- Feng, Z., Yang, T., Dong, S., Wu, T., Jin, W., Wu, Z., et al. (2022). Industrially synthesized biosafe vaterite hollow CaCO₃ for controllable delivery of anticancer drugs. *Mater. Today Chem.* 24, 100917. doi:10.1016/j.mtchem.2022.100917
- Feoktistova, N. A., Vikulina, A. S., Balabushevich, N. G., Skirtach, A. G., and Volodkin, D. (2020). Bioactivity of catalase loaded into vaterite CaCO₃ crystals via adsorption and co-synthesis. *Mater. Des.* 185, 108223. doi:10.1016/j.matdes.2019.108223
- Fitzpatrick, V., Martin-Moldes, Z., Deck, A., Torres-Sanchez, R., Valat, A., Cairns, D., et al. (2021). Functionalized 3D-printed silk-hydroxyapatite scaffolds for

Conflict of interest

The authors declare that the research was conducted in the absence of any commercial or financial relationships that could be construed as a potential conflict of interest.

Publisher's note

All claims expressed in this article are solely those of the authors and do not necessarily represent those of their affiliated organizations, or those of the publisher, the editors and the reviewers. Any product that may be evaluated in this article, or claim that may be made by its manufacturer, is not guaranteed or endorsed by the publisher.

Supplementary material

The Supplementary Material for this article can be found online at: <https://www.frontiersin.org/articles/10.3389/fbioe.2022.983988/full#supplementary-material>

enhanced bone regeneration with innervation and vascularization. *Biomaterials* 276, 120995. doi:10.1016/j.biomaterials.2021.120995

Gelebart, P., Cuenot, S., Sinquin, C., Halgand, B., Sourice, S., Le Visage, C., et al. (2022). Microgels based on Infernan, a glycosaminoglycan-mimetic bacterial exopolysaccharide, as BMP-2 delivery systems. *Carbohydr. Polym.* 284, 119191. doi:10.1016/j.carbpol.2022.119191

Glenske, K., Donkiewicz, P., Kowitsch, A., Milosevic-Oljaca, N., Rider, P., Rofall, S., et al. (2018). Applications of metals for bone regeneration. *Int. J. Mol. Sci.* 19 (3), 826. doi:10.3390/ijms19030826

Halloran, D., Vratshasha, V., Durbano, H. W., and Nohe, A. (2020). Bone morphogenetic protein-2 conjugated to quantum Dot[®]s is biologically functional. *Nanomater. (Basel)* 10 (6), 1208. doi:10.3390/nano10061208

He, L. Y., Zhang, X. M., Liu, B., Tian, Y., and Ma, W. H. (2016). Effect of magnesium ion on human osteoblast activity. *Braz. J. Med. Biol. Res.* 49 (7), 1. doi:10.1590/1414-431X2016257

Hettiaratchi, M. H., Krishnan, L., Rouse, T., Chou, C., McDevitt, T. C., and Gulberg, R. E. (2020). Heparin-mediated delivery of bone morphogenetic protein-2 improves spatial localization of bone regeneration. *Sci. Adv.* 6 (1), eaay1240. doi:10.1126/sciadv.aay1240

Hu, K., and Olsen, B. R. (2016). Osteoblast-derived VEGF regulates osteoblast differentiation and bone formation during bone repair. *J. Clin. Invest.* 126 (2), 509–526. doi:10.1172/JCI82585

Hurler, K., Oliveira, J. M., Reis, R. L., Pina, S., and Goetz-Neunhoffer, F. (2021). Ion-doped brushite cements for bone regeneration. *Acta Biomater.* 123, 51–71. doi:10.1016/j.actbio.2021.01.004

ISO (2009). *Biological evaluation of medical devices — Part 5: Tests for in vitro cytotoxicity*. Geneva, Switzerland: ISO, 10993–10995. Available at: <https://www.iso.org/standard/36406.html>.

Jeong, J., Kim, J. H., Shim, J. H., Hwang, N. S., and Heo, C. Y. (2019). Bioactive calcium phosphate materials and applications in bone regeneration. *Biomater. Res.* 23, 4. doi:10.1186/s40824-018-0149-3

Kargozar, S., Mozafari, M., Ghodrati, S., Fiume, E., and Baino, F. (2021). Copper-containing bioactive glasses and glass-ceramics: From tissue regeneration to cancer therapeutic strategies. *Mater. Sci. Eng. C* 121, 111741. doi:10.1016/j.msec.2020.111741

- Kohler, R., Donch, I., Ott, P., Laschewsky, A., Fery, A., and Krastev, R. (2009). Neutron reflectometry study of swelling of polyelectrolyte multilayers in water vapors: Influence of charge density of the polycation. *Langmuir* 25 (19), 11576–11585. doi:10.1021/la901508w
- Kulp, E. A., and Switzer, J. A. (2007). Electrochemical biomineralization: The deposition of calcite with chiral morphologies. *J. Am. Chem. Soc.* 129 (49), 15120–15121. doi:10.1021/ja076303b
- Lee, J., Byun, H., Madhurakatt Perikamana, S. K., Lee, S., and Shin, H. (2019). Current advances in immunomodulatory biomaterials for bone regeneration. *Adv. Healthc. Mat.* 8 (4), e1801106. doi:10.1002/adhm.201801106
- Lin, Z., Cao, Y., Zou, J., Zhu, F., Gao, Y., Zheng, X., et al. (2020). Improved osteogenesis and angiogenesis of a novel copper ions doped calcium phosphate cement. *Mater. Sci. Eng. C* 114, 111032. doi:10.1016/j.msec.2020.111032
- Liu, H., Du, Y., Yang, G., Hu, X., Wang, L., Liu, B., et al. (2020). Delivering proangiogenic factors from 3D-printed polycaprolactone scaffolds for vascularized bone regeneration. *Adv. Healthc. Mat.* 9, e2000727. doi:10.1002/adhm.202000727
- Lynch, M. P., Stein, J. L., Stein, G. S., and Lian, J. B. (1995). The influence of type I collagen on the development and maintenance of the osteoblast phenotype in primary and passaged rat calvarial osteoblasts: Modification of expression of genes supporting cell growth, adhesion, and extracellular matrix mineralization. *Exp. Cell Res.* 216 (1), 35–45. doi:10.1006/excr.1995.1005
- Martin, J. R., Howard, M. T., Wang, S., Berger, A. G., and Hammond, P. T. (2021). Oxidation-Responsive, tunable growth factor delivery from polyelectrolyte-coated implants. *Adv. Healthc. Mat.* 10 (9), e2001941. doi:10.1002/adhm.202001941
- Marx, K. A. (2003). Quartz crystal microbalance: A useful tool for studying thin polymer films and complex biomolecular systems at the solution-surface interface. *Biomacromolecules* 4 (5), 1099–1120. doi:10.1021/bm020116i
- Morozova, S., and Muthukumar, M. (2018). Electrostatic effects in collagen fibril formation. *J. Chem. Phys.* 149 (16), 163333. doi:10.1063/1.5036526
- Mourino, V., Cattalini, J. P., and Boccaccini, A. R. (2012). Metallic ions as therapeutic agents in tissue engineering scaffolds: An overview of their biological applications and strategies for new developments. *J. R. Soc. Interface* 9 (68), 401–419. doi:10.1098/rsif.2011.0611
- Musso, C. G. (2009). Magnesium metabolism in health and disease. *Int. Urol. Nephrol.* 41 (2), 357–362. doi:10.1007/s11255-009-9548-7
- O'Neill, E., Awale, G., Daneshmandi, L., Umerah, O., and Lo, K. W. (2018). The roles of ions on bone regeneration. *Drug Discov. Today* 23 (4), 879–890. doi:10.1016/j.drudis.2018.01.049
- Qiao, W., Wong, K. H. M., Shen, J., Wang, W., Wu, J., Li, J., et al. (2021). TRPM7 kinase-mediated immunomodulation in macrophage plays a central role in magnesium ion-induced bone regeneration. *Nat. Commun.* 12 (1), 2885. doi:10.1038/s41467-021-23005-2
- Ruehle, M. A., Krishnan, L., Vantucci, C. E., Wang, Y., Stevens, H. Y., Roy, K., et al. (2019). Effects of BMP-2 dose and delivery of microvascular fragments on healing of bone defects with concomitant volumetric muscle loss. *J. Orthop. Res.* 37 (3), 553–561. doi:10.1002/jor.24225
- Sahebalzamani, M., Ziminska, M., McCarthy, H. O., Levingstone, T. J., Dunne, N. J., and Hamilton, A. R. (2022). Advancing bone tissue engineering one layer at a time: A layer-by-layer assembly approach to 3D bone scaffold materials. *Biomater. Sci.* 10, 2734–2758. doi:10.1039/d1bm01756j
- Salmivirta, M., Lidholt, K., and Lindahl, U. (1996). Heparan sulfate: A piece of information. *FASEB J.* 10 (11), 1270–1279. doi:10.1096/fasebj.10.11.8836040
- Sankar, D., Mony, U., and Rangasamy, J. (2021). Combinatorial effect of plasma treatment, fiber alignment and fiber scale of poly (epsilon-caprolactone)/collagen multiscale fibers in inducing tenogenesis in non-tenogenic media. *Mater. Sci. Eng. C* 127, 112206. doi:10.1016/j.msec.2021.112206
- Sauerbrey, G. (1959). Verwendung von Schwingquarzen zur Waegung duenner Schichten und zur Mikrowaegung. *Z. Phys.* 155 (2), 206–222. doi:10.1007/bf01337937
- Shen, Q., Wei, H., Zhou, Y., Huang, Y., Yang, H., Wang, D., et al. (2006). Properties of amorphous calcium carbonate and the template action of vaterite spheres. *J. Phys. Chem. B* 110 (7), 2994–3000. doi:10.1021/jp055063o
- SSED (2022). *Summary of safety and effectiveness data*. Silver Spring, MD, United States: SSED. Available at: https://www.accessdata.fda.gov/cdrh_docs/pdf/P000058B.pdf.
- Stein, G. S., Lian, J. B., and Owen, T. A. (1990). Relationship of cell growth to the regulation of tissue-specific gene expression during osteoblast differentiation. *FASEB J.* 4 (13), 3111–3123. doi:10.1096/fasebj.4.13.2210157
- Sun, L., Xiong, X., Zou, Q., Ouyang, P., and Krastev, R. (2017). Controlled heparinase-catalyzed degradation of polyelectrolyte multilayer capsules with heparin as responsive layer. *J. Appl. Polym. Sci.* 134 (23), 44916. doi:10.1002/app.44916
- Svenskaya, Y. I., InozemtsevaGorin, O. A., Ivanova, A. G., Shtykov, S. N., Gorin, D. A., Parakhonskiy, B. V., et al. (2018). Key parameters for size- and shape-controlled synthesis of vaterite particles. *Cryst. Growth & Des.* 18 (1), 331–337. doi:10.1021/acs.cgd.7b01328
- Toosi, S., and Behravan, J. (2020). Osteogenesis and bone remodeling: A focus on growth factors and bioactive peptides. *Biofactors* 46 (3), 326–340. doi:10.1002/biof.1598
- Vikulina, A., Webster, J., Voronin, D., Ivanov, E., Fakhru'llin, R., Vinokurov, V., et al. (2021). Mesoporous additive-free vaterite CaCO₃ crystals of untypical sizes: From submicron to Giant. *Mater. Des.* 197, 109220. doi:10.1016/j.matdes.2020.109220
- Wang, H., Zhao, S., Xiao, W., Xue, J., Shen, Y., Zhou, J., et al. (2016). Influence of Cu doping in borosilicate bioactive glass and the properties of its derived scaffolds. *Mater. Sci. Eng. C* 58, 194–203. doi:10.1016/j.msec.2015.08.027
- Wang, K. F., Nagarajan, R., and Camesano, T. A. (2014). Antimicrobial peptide alamethicin insertion into lipid bilayer: A QCM-D exploration. *Colloids Surfaces B Biointerfaces* 116, 472–481. doi:10.1016/j.colsurfb.2014.01.036
- Wei, Q., Lu, J., Wang, Q., Fan, H., and Zhang, X. (2015). Novel synthesis strategy for composite hydrogel of collagen/hydroxyapatite-microsphere originating from conversion of CaCO₃ templates. *Nanotechnology* 26 (11), 115605. doi:10.1088/0957-4844/26/11/115605
- Wong, H. M., Chu, P. K., Frankie, K. L., Leung, F. K. L., Cheung, K. M. C., Luk, K. D. K., et al. (2014). Engineered polycaprolactone-magnesium hybrid biodegradable porous scaffold for bone tissue engineering. *Prog. Nat. Sci. Mater. Int.* 24 (5), 561–567. doi:10.1016/j.pnsc.2014.08.013
- Xie, H., Gu, Z., He, Y., Xu, J., Xu, C., Li, L., et al. (2018). Microenvironment construction of strontium-calcium-based biomaterials for bone tissue regeneration: The equilibrium effect of calcium to strontium. *J. Mat. Chem. B* 6 (15), 2332–2339. doi:10.1039/c8tb00306h
- Yu, L., Rowe, D. W., Perera, I. P., Zhang, J., Suib, S. L., Xin, X., et al. (2020). Intrafibrillar mineralized collagen-hydroxyapatite-based scaffolds for bone regeneration. *ACS Appl. Mat. Interfaces* 12 (16), 18235–18249. doi:10.1021/acsami.0c00275
- Zhang, D., Wu, X., Chen, J., and Lin, K. (2018). The development of collagen based composite scaffolds for bone regeneration. *Bioact. Mat.* 3 (1), 129–138. doi:10.1016/j.bioactmat.2017.08.004
- Zhao, Z., Li, G., Ruan, H., Chen, K., Cai, Z., Lu, G., et al. (2021). Capturing magnesium ions via microfluidic hydrogel microspheres for promoting cancellous bone regeneration. *ACS Nano* 15, 13041–13054. doi:10.1021/acsnano.1c02147
- Zhong, Z., Wu, X., Wang, Y., Li, M., Li, Y., Liu, X., et al. (2022). Zn/Sr dual ions-collagen co-assembly hydroxyapatite enhances bone regeneration through procedural osteo-immunomodulation and osteogenesis. *Bioact. Mat.* 10, 195–206. doi:10.1016/j.bioactmat.2021.09.013

CHAPTER 3

DISCUSSION & OUTLOOK

3. Discussion and Outlook

3.1 Refining UVA/R Crosslinking Process for Specific Collagen Systems

The UVA/R crosslinking technique, initially a groundbreaking advancement in corneal strengthening for keratoconus treatment (Spoerl et al., 1998), has evolved into an effective and biocompatible method for wider applications in collagen crosslinking. For corneal treatment, the UVA/R procedure typically includes steps like corneal epithelium abrasion followed by applying a 0.1% riboflavin solution mixed with 20% dextran every 3 minutes for 30 minutes. This is succeeded by a carefully timed exposure to UVA light, specified at 370 ± 5 nm wavelength and 3 mW/cm^2 irradiance, for 30 minutes (Spoerl et al., 2007). This regimen is designed to achieve deep penetration and thorough saturation within the corneal stroma while protecting the underlying corneal endothelium (Spoerl et al., 2007). However, applying the protocol unmodified to other collagen systems may not yield the desired outcomes due to differing tissue characteristics and material requirements. Hence there is a compelling need for customized optimization of the UVA/R crosslinking process tailored to the specific requirements of various collagen-based systems, ensuring the distinct properties and functional demands of each application.

The efficiency and potential damage of UV light in crosslinking processes are influenced by its wavelength, irradiance, and exposure time (Spoerl et al., 2007). UVA at 370 ± 5 nm are chosen for riboflavin activation, which resonates with its absorption peak. Short exposure time up to 120 minutes (21.6 J/cm^2), can curb photochemical injury through inherent antioxidative defenses of the lens (Andley and Clark, 1989). In our study, the results revealed that the optimal mechanical strength in crosslinked collagen matrices was achieved with UVA at 370 nm and 3 mW/cm^2 , yielding a total dose of 10.8 J/cm^2 per side (Fan et al., 2024). In pursuit of a more efficient and faster UV crosslinking process, there have been explorations into using UVB ray (280-315 nm), which has more energy per photon than UVA (Görlitz et al., 2023). However, UVB's potential for quicker crosslinking is tempered by concerns over possible material and cellular

damage, including DNA damage, making it less appropriate for cell-containing materials or direct application to living tissues (Leung and Murray, 2021). The risk of photokeratitis associated with UVB, particularly at dose between 0.12 and 0.56 J/cm², raises additional concerns (Olsen and Ringvold, 1982). Explorations into application of shorter wavelength UV irradiation ($\lambda = 254$ nm) across a range of intensities (from 0.06 to 0.96 J/cm²) for crosslinking collagen- and gelatin-based scaffolds indicate that, although effective, there is still an increased risk of denaturation or damage to the collagen structure (Davidenko et al., 2015). This risk is particularly pronounced at the highest tested intensity of 0.96 J/cm² (Davidenko et al., 2016). These findings underscore the importance of carefully balancing UV intensity and exposure duration in the cross-linking process to ensure integrity and safety of the scaffolds.

The UV penetration depth in tissues or collagen-based materials is influenced by the UV wavelength, riboflavin amount, tissue or material density, and optical properties. For example, UVB light, with its shorter wavelength and higher energy photons, tends to penetrate less deeply than UVA, making it more effective for surface crosslinking in thinner materials like films or membranes (Sionkowska, 2005). On another hand, its limited penetration depth poses challenges for thicker materials, potentially leading to uneven crosslinking (Grewal et al., 2009). Contrarily, UVA light can penetrate several millimeters into biological tissues or materials like collagen scaffolds, a capability often underappreciated due to the misconception of its limitation to 400 μ m in corneal crosslinking (Ash et al., 2017, Finlayson et al., 2022). Currently, precise measurements and detailed investigations of UVA light penetration in specific types of collagen-based materials are still scarce and necessary. In our research, the preparation of a stable and homogenized collagen foam (Ole et al., 2023), followed by riboflavin incubation, not only established the basic porous structure but also enhanced the optical properties for UVA penetration. This led to a crosslinked collagen matrix with homogenized morphology and mechanical properties extending 3-5 mm into the material. This advancement opens new avenues for the development of robust and functional

scaffolds, extending the applicability of UVA/R crosslinking technology in the field of regenerative medicine.

The riboflavin concentration is another pivotal parameter in the UVA/R crosslinking process (Iseli et al., 2011). The UVA absorption coefficient is proportional to the riboflavin concentration up to a threshold of 0.04% (Spoerl et al., 2007). Beyond this threshold, for example, 0.1% commonly applied in corneal crosslinking, typically aimed at ensuring tissue saturation and safety (Zhang et al., 2016). When applied to different materials and objectives, like dentin strengthening or enhancing the mechanical properties of collagen gels, the concentration of riboflavin and its process conditions vary significantly (Zhang et al., 2016, Mazzotta et al., 2021). For example, Uemura et al. demonstrated that dentin treated with a 0.1% riboflavin solution followed by 1,600 mW/cm² UVA irradiation for 10 minutes yielded the highest flexural strength and contributed to prevent the root caries (Uemura et al., 2019). In contrast, when enhancing collagen gel mechanical properties, as demonstrated by Heo et al., a different approach is taken due to the absence of tissue barriers. Their work with a meniscus scaffold used a lower riboflavin concentration (0.01%), shorter pre-incubation (20 minutes), and UV exposure time (3 minutes) to optimize viability and elasticity (Heo et al., 2016). Interestingly, our research demonstrated that a riboflavin concentration of 0.013%, which was derived from a specific tyrosine residues/riboflavin molar ratio of 1/0.25, yielded the highest elasticity as well as degradation resistance for the collagen matrix (Fan et al., 2024). During the material fabrication process, a notable advantage is the ability to thoroughly mix water-soluble riboflavin directly with collagen, ensuring the uniform penetration and distribution throughout the material. It is important to note that while riboflavin is water-soluble, its solubility is around 0.07 g/L (approximately 186 μM) at 20 °C, and 0.10-0.13 g/L (approximately 265.7-345.4 μM) at 25-27.5°C (1972). This brings up an interesting question: can riboflavin solutions with concentrations exceeding these solubility limits still be uniformly and effectively mixed with collagen materials? This consideration is critical in ensuring the effective and homogeneous integration of riboflavin into the collagen matrix for optimal crosslinking.

Thus, customizing the UVA/R crosslinking parameters is crucial for expanding the technique's utility beyond corneal applications, enabling its successful integration into the wider landscape of regenerative medicine and tissue engineering.

3.2 Unraveling the Mechanisms of UVA/R Collagen Crosslinking

The UVA/R crosslinking process, while initiated by the photoactivation of riboflavin to produce reactive oxygen species, is significantly influenced by collagen's molecular structure and the complex interactions with riboflavin (Hatami-Marbini and Jayaram, 2018, Chen et al., 2024). Contrary to a simplistic perception of riboflavin merely acting as a photosensitizer, leading to non-specific covalent bonding within the collagen structure, our research illuminates the crosslinking sites on collagen, and the nuanced relationship between riboflavin concentration and its efficacy (Fan et al., 2023a, Fan et al., 2024).

When exposed to UVA light, riboflavin indeed initiates the formation of reactive oxygen species, leading to covalent bonding within the collagen structure, thereby enhancing its mechanical properties (Uemura et al., 2019). However, this process is influenced by the intricate molecular structure of collagen and the biochemical interactions of riboflavin (Chen et al., 2024, Hatami-Marbini and Jayaram, 2018). As mentioned above, the absorption coefficient of riboflavin elevates linearly to its concentration threshold of 0.04% (Spoerl et al., 2007, Sel et al., 2014). This plateau, previously noted in our exploration of optimal conditions for UVA/R crosslinking, underscores the nuanced interplay between riboflavin concentration and its efficacy as a photosensitizer in the crosslinking process (Fan et al., 2023a). Nonetheless, our investigation has uncovered that lower concentrations of riboflavin significantly increase the storage modulus of collagen, while higher concentrations result in a decline (Fan et al., 2023a, Fan et al., 2024). These intriguing findings have spurred further exploration into the complexities of UVA/R crosslinking in collagen. Our study delves into the specific sites where crosslinks form within the collagen molecule, scrutinizing the role of riboflavin—whether it acts merely

as a catalyst or as an active participant in the crosslinking process (Fan et al., 2024).

Collagen's triple-helical structure, rich in amino acids such as glycine, proline, and hydroxyproline, contributes to its robust tensile strength. However, it is the presence of amino acids like tyrosine, lysine, and arginine that provides potential sites for crosslink formation, a subject of much debate concerning the selectivity of the UVA/R process. For instance, tyrosine, with its reactive phenol group (Eyre, 1987), and lysine's ϵ -amino group and arginine's guanidinium group, are potential sites for chemical bond formation (Yamauchi and Sricholpech, 2012, Mechanic et al., 1987, Udhayakumar et al., 2017). Histidine's imidazole and phenylalanine's benzyl group also offer potential reactive sites (Davidenko et al., 2016). Some researchers discuss that the process is non-selective (Uemura et al., 2019, Zhang et al., 2011), whereas others point to amino acids—lysine, histidine, arginine, tyrosine, or methionine—as key players in the crosslinking process (Yamauchi and Shiiba, 2008, Sharif et al., 2017, Gabriela and Iulia, 2019, Fuentes-Lemus et al., 2018). Therefore, to pinpoint specific crosslinking sites, our study utilized synthetic peptides representing critical amino acids, including tyrosine, lysine, arginine, methionine, histidine, tryptophan, and phenylalanine (Fan et al., 2024). The results revealed that modifications post-UVA/riboflavin treatment occurred predominantly in tyrosine-containing peptides, forming covalent di-tyrosine linkages that signify a unique pathway of crosslinking within the collagen molecule (Fan et al., 2024). The presence of di-tyrosine in hydrolyzed UVA/R crosslinked collagen further confirmed tyrosine's critical involvement in this process.

Tyrosine's role in UVA/R crosslinking is attributed to its unique aromatic structure, which facilitates photochemical reactions. Studies have shown that the excited states of riboflavin engage in type I photochemistry, leading to electron transfer from tyrosine's phenolic group (Lu and Liu, 2002). This results in the formation of phenoxyl radicals, which are highly reactive and can interact with other tyrosine radicals to form dityrosine links (Dalsgaard et al., 2011). While phenylalanine, also possessing an aromatic structure, was considered a

potential site for crosslinking, our results indicate it does not form crosslinked products post-UVA/R treatment (Fan et al., 2024). This highlights the significance of the hydroxy group in tyrosine for photochemical crosslinking. Additionally, although tryptophan can form reactive radicals under UVA/R, it tends towards different pathways, creating products like kynurenines instead of covalent bonds (Fan et al., 2024).

Further exploring the effects of riboflavin concentration on collagen's mechanical properties revealed a delicate balance where both too low and too high concentrations could detract from the desired outcomes (Fan et al., 2023a, Fan et al., 2024). The noticeable reduction in strength at higher concentrations indicates a complex role of riboflavin beyond being a mere photosensitizer (Fan et al., 2023a, Fan et al., 2024). Guided by a theoretical kinetic model emphasizing the role of oxygen levels in riboflavin-mediated photocrosslinking (Kamaev et al., 2012), we discovered a marked sensitivity of the crosslinking efficiency to riboflavin concentration. This suggests that riboflavin has two primary reaction pathways upon UVA excitation (Kamaev et al., 2012). Initially, riboflavin acts as a photosensitizer, generating ROS that facilitate intermolecular crosslinking, predominantly at tyrosine residues. However, at elevated concentrations, an alternative pathway predominates, where riboflavin participates directly in reactions, leading to ROS depletion and reduced crosslinking efficiency (Kamaev et al., 2012, Fan et al., 2024). Additionally, potential electron transfer processes might influence interactions between positively charged amino acids like lysine, histidine, and arginine, and negatively charged riboflavin, further impacting the collagen matrix's mechanical properties (Fan et al., 2024). This complex behavior of riboflavin necessitates further experimental study to fully understand its role in collagen crosslinking.

Our findings not only deepen the understanding of the UVA/R crosslinking mechanism but also underscore the critical need for precise control over riboflavin concentration and UVA exposure to tailor the process for various collagen-based applications effectively. This tailored approach, considering factors like collagen source, tyrosine content, and environmental conditions, is essential for ensuring the crosslinking process's efficacy and applicability in

clinical and material science contexts (Dippold et al., 2017). This refined understanding enables a more informed regulatory assessment and contributes to advancing the development and application of biomaterials within the field.

3.3 Impact of UVA/R Crosslinking on Collagen Matrix Properties

UVA/R crosslinking, originally conceptualized for keratoconus treatment, has proven its efficacy in not only enhancing corneal mechanics but also in broadening our understanding of its beneficial impacts on collagen matrices (Franke et al., 2021). This technique has been pivotal in augmenting collagen's tensile strength, stiffness, and degradation resistance, alongside altering its surface properties to foster improved cellular interactions (Cheng et al., 2024).

Our investigation has pinpointed tyrosine as a critical site for crosslink formation within collagen, especially in type I collagen's non-helical N- and C-terminal regions (Fan et al., 2024). The formation of crosslinks, such as dityrosine and trityrosine linkages, in those non-helical terminal regions is instrumental in stabilizing the collagen's triple helical structure, facilitating the assembly of fibrils and fibers (Koseki et al., 2021, Edens et al., 2001). This assembly process underpins the enhanced tensile strength and mechanical force resistance of collagen-based materials (Eyre and Wu, 2005). Rheological analysis revealed that UVA/R crosslinked collagen matrices exhibit a significantly higher storage modulus ($G' = 2000$ Pa) compared to their non-crosslinked collagen counterparts ($G' = 500$ Pa), without compromising loss modulus ($G'' \approx 80$ Pa). This indicates that while crosslinking bolsters the matrix's elasticity and structural integrity, it does not markedly affect its viscous behavior or damping capacity under cyclic loading. Such increased stiffness and resilience are crucial for creating a supportive environment for cell adhesion, proliferation, and differentiation, vital for tissue engineering and regenerative medicine (Guimarães et al., 2020, Yi et al., 2022).

Collagen's physiological degradation, whether in PBS buffer due to hydrolytic actions or in collagenase solutions through enzymatic hydrolysis, is mitigated by UVA/R crosslinking. The degradation of collagen in PBS is

fundamentally a result of hydrolysis, where water molecules cleave peptide bonds. The hydrogen atoms from water attack the amide nitrogen atoms, and the hydroxyl groups target the carbonyl carbon atoms, leading to the breakdown of the peptide bond and the eventual dissociation into individual amino acids (Tucker et al., 2018, Vallecillo-Rivas et al., 2021). When exposed to collagenase solutions, the degradation of collagen is primarily driven by enzymatic hydrolysis. Collagenase enzymes specifically target peptide bonds adjacent to glycine residues, which are prevalent in collagen and crucial for maintaining its triple helical structure (Eckhard et al., 2014). Glycine-leucine or glycine-isoleucine bonds are particularly susceptible to enzymatic cleavage (Eckhard et al., 2014). In type I collagen, these enzymes typically initiate the unwinding of the triple helix, allowing for further hydrolysis of peptide bonds within the structure (Chen et al., 2018, Chung et al., 2004). The application of UVA/R crosslinking introduces extra covalent bonds, especially in collagen's more susceptible non-helical regions, thereby boosting the chemical stability and structural integrity of the collagen matrix (Fan et al., 2024). This enhancement significantly extends collagen's durability against hydrolytic and enzymatic degradation in both PBS and collagenase environments, highlighting the protective and stabilizing benefits of UVA/R crosslinking on collagen's structural longevity.

Importantly, UVA/R crosslinking is selective, targeting tyrosine residues for covalent bond formation without adversely affecting other amino acid residues. This selectivity preserves essential binding sites for cellular or molecular interactions, such as RGD sequence, which are integral for cellular signaling and tissue regeneration (Koseki et al., 2021, Fuentes-Lemus et al., 2022).

In vivo, UVA/R crosslinked collagen materials demonstrate reduced inflammatory responses and superior tissue regeneration compared to non-crosslinked alternatives (Fan et al., 2024). The crosslinking-induced structural stability diminishes the release of immunogenic debris by slowing enzymatic degradation (Hebels et al., 2023). Moreover, the maintenance of functional cell-binding sites within the crosslinked collagen scaffolds could also attribute to

facilitate the recruitment and activation of cells crucial for tissue repair, such as fibroblasts and osteoblasts (Hebels et al., 2023, Stumptner et al., 2019).

By enhancing both the mechanical and biological properties of collagen-based materials, UVA/R crosslinking presents a promising platform for tissue engineering and regenerative medicine, promoting cell growth and differentiation while providing essential structural support.

3.4 UVA/R vs. Chemical Crosslinking: A Comparative Analysis

Given the efficiency and well-investigated mechanisms of chemical crosslinking techniques, such as EDC/NHS and genipin, this project undertakes a comparative evaluation between UVA/R crosslinking and chemical crosslinking of collagen. This comparison aims to explore the impact of each method on the properties of collagen matrices, utilizing various analytical techniques. These include molecular fingerprinting through Raman spectroscopy, SEC of collagenase-digested matrices, rheological properties, thermal stability, degradation profiles, cell viability and proliferation (Fan et al., 2024).

EDC/NHS crosslinking, known for promoting amide bonds between collagen's carboxyl and amine groups, contrasts with UVA/R crosslinking's specificity for tyrosine residues (Dasgupta et al., 2021, Wissink et al., 2001). This distinction raises important questions about the precision and outcomes of these crosslinking approaches, warranting detailed molecular and functional bond analyses. Raman spectroscopy, particularly, shines in its ability to detect subtle changes in the collagen structure post-crosslinking, providing invaluable insights into the crosslinking processes' molecular dynamics (Martinez et al., 2019, Becker et al., 2023). In our results, Raman spectroscopy's sensitivity to vibrational modes enabled the detection of alterations in C-C stretching, wagging, and CH₃ rocking motions within lysine, hydroxylysine, and tyrosine residues—key sites of crosslinking-induced modifications (Lu Fan, 2024). The insights gleaned from Raman spectroscopic analysis are invaluable, not only for elucidating the mechanistic underpinnings of crosslinking effects on collagen but also for guiding the functionalization of collagen in the design of biomaterials.

Our findings reveal that UVA/R-crosslinked collagen matrices exhibit a preferable equilibrium between structural resilience and biodegradability, outperforming chemically crosslinked counterparts in mechanical strength and biocompatibility (Lu Fan, 2024). This balance is crucial for the functionalization of collagen in advanced biomedical applications. Conversely, EDC/NHS crosslinking method (Xcol_EDC/NHS) resulted in unexpectedly lower storage modulus, suggesting that this method might compact the collagen structure more than adding to its bulk, thus enhancing thermal stability and hydrolytic resistance without significantly affecting the matrix's elasticity or viscosity (Nair et al., 2020).

In contrast, genipin stands out by directly acting as a crosslinker, engaging primary amino groups in collagen to establish crosslinks (Utami Nike et al., 2022). Each crosslink may involve one or two genipin molecules (Vo et al., 2021), contributing not only to a high storage modulus but also to the highest loss modulus observed in Xcol_Genipin (Lu Fan, 2024). However, this interaction also seems to confer superior enzymatic degradation resistance to genipin-crosslinked matrices, potentially due to genipin's obstructive effect on enzymatic access (Výborný et al., 2019). Despite this, the altered native collagen structure may compromise the thermal stability of genipin-crosslinked matrices compared to those treated with UVA/R or EDC/NHS (Yan et al., 2022).

At the cellular interaction level, EDC/NHS and genipin-crosslinked collagen matrices encountered several obstacles, notably the diminished accessibility of cell-binding sites and potential cytotoxic effects (Lu Fan, 2024). The altered mechanical properties, including reduced elasticity in Xcol_EDC/NHS and significantly increased viscosity in Xcol_Genipin, likely contributed negatively to cellular outcomes (Yi et al., 2022). While the general consensus is that EDC/NHS and genipin are safer alternatives to other chemical crosslinkers like glutaraldehyde, some studies reported potential cytotoxicity at very high concentrations or incomplete removal of residual crosslinkers in thicker collagen matrices like scaffolds (Ahmad et al., 2015, Robinson et al., 2022, Kawamura et al., 2021). Furthermore, the intricate degradation products of genipin-crosslinked collagen, as revealed through SEC

analysis in our studies, indicate that degrades might negatively impact cell viability and functionality (Lu Fan, 2024). The cytotoxic observations led to the decision against pursuing in vivo studies with these chemically crosslinked collagen matrices. Their degradation characteristics suggest that while they offer enhanced long-term stability, this could potentially hinder tissue regenerative processes, making them more suitable for non-regenerative applications. An example includes the development of collagen membranes for guided bone regeneration in dental applications, presenting a viable alternative use (Park et al., 2015, Ren et al., 2022).

This comparative study sheds light on the distinct effects of UVA/R, EDC/NHS, and genipin crosslinking on collagen matrices, underscoring the balance between mechanical robustness, enzymatic degradation resistance, and biocompatibility. UVA/R crosslinking stands out for providing a versatile and balanced solution applicable across a range of biomedical fields. Conversely, EDC/NHS and genipin crosslinking face challenges, especially concerning cytotoxicity and cellular interactions, necessitating a judicious choice of crosslinking method tailored to the specific demands of the application. These insights guide future research aimed at refining collagen-based scaffolds for enhanced application in regenerative medicine and beyond, emphasizing the strategic selection of crosslinking techniques to meet the nuanced needs of tissue engineering.

3.5 Bioactive Ion Encapsulation System for Enhancing Osteogenesis and Angiogenesis

Bioactive ions such as Ca^{2+} , Cu^{2+} , and Mg^{2+} are integral to the processes of osteogenesis and angiogenesis, offering an efficient and stable alternative to traditional bone growth factor-based therapeutics (Table 1) (O'Neill et al., 2018). The integration of these ions into tissue regeneration strategies hinges on the development of sophisticated encapsulation and delivery systems that can precisely control their release (Sun et al., 2021). Achieving an ideal release profile for these ions is essential for maximizing their synergistic potential in promoting tissue repair and regeneration.

Across the broader scope of tissue engineering and regenerative medicine, various strategies have been explored for the encapsulation and delivery of bioactive ions. These strategies include the use of biodegradable polymers such as PLGA, PCL, and PLA (Popok, 2012), as well as hydrogels (Popok, 2012), coated metal implants (Kao et al., 2019), magnesium alloys (Yang et al., 2021), bioactive glasses (BGs) (Schatkoski et al., 2021). Among these, bioactive glasses are emerging as a preferred method for ion release, with studies demonstrating their capability for sustained ion delivery. For instance, research on lithium and cobalt co-doped BG nanoparticles demonstrated a sustained release pattern of Co^{2+} (approximately 15 mg/L) and Li^{2+} (approximately 3 mg/L) over 14 days (Zhang et al., 2024). Similarly, Sutthavas et al. investigated the integration of Zn^{2+} in bioactive glasses and silica nanoparticles in various configurations, revealing how ion release profiles vary with the pH of the surrounding environment and highlighting the challenge of achieving efficient ion release for bone regeneration (Sutthavas et al., 2022). The highest Zn^{2+} release concentration only reached around 0.025 mg/L, which barely reached the efficient concentration range necessary for bone regeneration (Table 1) (Sutthavas et al., 2022). These findings underline the ongoing need for advancements in ion delivery systems to achieve concentrations effective for bone regeneration.

Diverging from broader strategies, our research specifically targets the encapsulation of Cu^{2+} and Mg^{2+} ions within vaterite-calcite CaCO_3 particles via co-precipitation (Fan et al., 2022). To improve these particles' stability and biocompatibility and ensure a gradual ion release, we utilized the LbL strategy for PEM coating on CaCuMg-CO_3 microcapsules (Fan et al., 2022). Incorporating these microcapsules into a collagen matrix fosters a conducive microenvironment for tissue regeneration (Fan et al., 2022). Our in vitro release demonstrated a remarkable consistent stable release of Cu^{2+} (approximately 700 mg/L) over 60 days, with no initial burst release, and a controlled release of Mg^{2+} (approximately 2.5 mg/L) in the first 7 days, attributed to the specific ion co-precipitation and encapsulation techniques employed (Fan et al., 2022).

Our investigation further extends to osteogenesis and angiogenesis related gene expression using the MG63 cell line as a model. These cells, owing to their high similarity to osteoblasts, serve as a valuable tool for understanding the cellular behaviors and gene expression patterns essential for bone formation and healing (Yu et al., 2018). The promising outcomes obtained from alkaline phosphatase (ALP) activity assessments, Alizarin Red staining, and gene expression analyses conducted on MG63 cells treated with Mg^{2+} and Cu^{2+} ion-loaded microcapsules indicate a promising potential for bone regeneration (Dvorakova et al., 2023, Zheng et al., 2017, Fan et al., 2022). These microcapsules not only promote osteoblast differentiation and matrix mineralization but also enhance angiogenesis.

In conclusion, this study presents a novel strategy leveraging PEM coated $CaCO_3$ vaterite-calcites integrated with bioactive ions, particularly in conjunction with collagen matrices, to bolster bone regeneration. This approach, emphasizing controlled bioactive ion release within a biomimetic environment, represents a cutting-edge direction in the development of functional bone graft materials, aiming to improve the outcomes of bone repair and regeneration processes.

Table 1. Frequently applied bioactive ions in bone healing: effective concentrations and material ion release profiles.

Bioactive ions	Effects on bone regeneration	Effective concentrations (mg/L)	Release level from materials (mg/L)
Ca^{2+}	Essential for bone formation and mineralization	90-110 (Hannink and Arts, 2011)	HA/TCP scaffold: 32.8 / day (Seol et al., 2014)

Mg ²⁺	Enhances bone formation and osseointegration	12.15 – 50 (Wong et al., 2013)	PLGA microspheres: 30–50 (Yuan et al., 2019); Mg/PCL composite: 38 – 203 (Wong et al., 2013)
Sr ²⁺	Promotes osteoblast proliferation and inhibits osteoclast activity, enhancing angiogenesis and repressing osteoclastogenesis	Stimulatory effects on osteoblasts: 8.7 – 87.6 ; inhibitory effects on osteoclasts: 8.7 – 2102.8 (Bonnelye et al., 2008, Reginster and Meunier, 2003)	BGs[Ca–Sr–Na–Zn–Si]: 7.5–3500 (Murphy et al., 2009)
Cu ²⁺	Stimulates angiogenesis, has osteoinductive properties, and provides antibacterial activity	0.00635 – 0.635 (Gaetke and Chow, 2003)	0.5Cu-CPC: 0.24–0.74 (Bari et al., 2017)
Zn ²⁺	Supports osteogenesis and cellular bioactivity	2.45 – 6.5 (Yamaguchi et al., 2004, Ito et al., 2002)	BGs[Ca–Sr–Na–Zn–Si]: 3 – 750 (Murphy et al., 2009)
Si ⁴⁺	Stimulates osteoblast proliferation and differentiation and enhances collagen type 1 synthesis.	5 – 20 (Xynos et al., 2001, Shi et al., 2015)	BGs[45S5]: 16.5 ± 3.5 (Shi et al., 2015)
Co ²⁺	Stimulates erythropoietin production, which indirectly affects bone healing through angiogenesis.	0.00589 – 20 (Chen et al., 2020, Perez et al., 2015)	Co-MBG: 0 – 20 (Wu et al., 2012)

3.6 Outlook

The study on ultraviolet A and riboflavin (UVA/R) crosslinked collagen and multiple bioactive ion capsules presents a significant leap forward in BTE, offering promising transformation prospects for future research and clinical applications. The integration of the mechanical strength and biocompatibility of collagen scaffolds with the osteoinductive potential of bioactive ions such as Mg^{2+} and Cu^{2+} not only promises enhanced bone regeneration but also opens up new avenues for personalized and more effective bone defect treatments.

The incorporation of this CaCuMg-PEM-Col capsules within UVA/R crosslinked collagen-based composite scaffolds represents a novel strategy in the field of BTE. Future research will delve into synergistic effects of mechanical support provided by collagen scaffold combined with osteoinductive and angiogenesis potential of bioactive ions. The investigation will be deeper into the ion release kinetics within 3D cell cultures, alongside evaluations of bone repair and vascularization, to validate the scaffold's functionality in fostering bone integration and recovery. Expanding the spectrum of bioactive ions to include elements like zinc, strontium, or silicon could further enhance the scaffold's regenerative potential, each contributing distinct qualities to expedite healing and scaffold-bone tissue integration (Zhong et al., 2022, Hurle et al., 2021).

Advancing to *in vivo* models is a critical next step for assessing bone defect healing using these composite scaffolds, facilitating a direct comparison with existing treatments such as BMP2 therapies. These investigations will illuminate the scaffold's capability to equal or exceed the efficacy of current growth factor-based interventions, setting the stage for extensive pre-clinical and clinical testing. Such trials are instrumental in verifying the material's clinical viability, focusing on its safety, effectiveness, and superiority in bone regeneration contexts.

Furthermore, the UVA/R crosslinking technique offers avenues for refinement, particularly in crafting collagen scaffolds with tailored mechanical attributes. This refinement process will aim not only to bolster the scaffolds'

structural integrity but also to investigate the impact of mechanical stimuli on stem cell behavior and tissue repair (LaGuardia et al., 2023, Zhou et al., 2021). Precisely adjusting mechanical properties could yield groundbreaking insights into the interplay between biomechanical signals and bone tissue regeneration, offering profound implications for the field (Camarero-Espinosa and Moroni, 2021).

By applying these optimized scaffolds in cutting-edge research models, such as organ-on-a-chip systems, there lies an opportunity to dissect tissue regeneration processes, disease modeling, and pharmacological testing with greater accuracy. Such models will enable detailed studies of the intricate relationships between mechanical stimuli and cellular activities in a controlled setting, aligning with the 3Rs principle by minimizing animal model reliance and emphasizing human-centric investigations (Azizipour et al., 2020, Mansoorifar et al., 2021).

In conclusion, the advancement and fine-tuning of UVA/R crosslinked collagen-based scaffolds, enriched with multiple bioactive ions, offer a multifaceted approach to BTE. This future direction not only aims to elucidate the dynamics of ion release and foster bone restoration but also seeks to refine scaffold mechanics for broader scientific applications. As research advances, these innovations are expected not only to deepen our understanding of bone regeneration mechanisms but also to usher in more effective, personalized, and ethically conscious solutions for treating bone defects.

CHAPTER 4

SUMMARY & ZUSSAMMENFASSUNG

4. Summary

This project has embarked on a journey to redefine the landscape of bone tissue engineering (BTE) through the advanced ultraviolet A and riboflavin (UVA/R) crosslinked collagen scaffolds and a bioactive cation encapsulation system, featuring Cu^{2+} and Mg^{2+} within vaterite-calcite CaCO_3 particles. The research meticulously deciphers the complexities of the UVA/R crosslinking mechanism, specifically its interaction with tyrosine residues in collagen, uncovering insights that not only broaden our understanding of collagen stabilization but also herald new advancements in the functional enhancement of collagen-based biomaterials via refined crosslinking methods. The investigation reveals that tyrosine residues serve as critical sites for crosslinking, with riboflavin acting both as a catalyst and a competitive inhibitor. The UVA/R crosslinked collagen matrices distinguished themselves by achieving a balanced interplay between stability and degradability, superior mechanical attributes, and enhanced biocompatibility compared to their chemically crosslinked counterparts. In vivo assessments further underscored the exceptional biocompatibility of the UVA/R crosslinked matrices, showcasing their capability to mitigate tissue inflammation and foster regeneration.

Concurrently, this thesis introduces an innovative encapsulation strategy for the controlled delivery of essential bioactive ions for bone regeneration. The encapsulation system, augmented by polyelectrolyte multilayers and collagen matrix functionalization, closely emulates the bone tissue microenvironment, creating an ideal milieu for bone healing through the sustained release of Ca^{2+} , Cu^{2+} , and Mg^{2+} ions. This approach not only bolsters osteoblast proliferation and differentiation but also significantly upregulates the expressions of genes related to osteogenesis and angiogenesis, illuminating the profound potential of the developed microcapsules in advancing BTE endeavors.

By synergistically bridging the mechanical and biochemical realms of tissue engineering, this dissertation presents a comprehensive strategy that enriches both the physical and biological efficacy of engineered scaffolds for bone regeneration. The in-depth elucidation of the UVA/R crosslinking

dynamics and the introduction of an innovative multi-ion delivery mechanism constitute significant strides in the field, offering novel insights and refined methodologies for the design and crafting of next-generation biomaterials. This work not only enriches the academic discourse in tissue engineering but also sets a new benchmark for the development of functionalized bone graft materials, highlighting a significant stride towards more effective and personalized therapeutic interventions in bone regeneration.

5. Zusammenfassung

In diesem Projekt wurde ein neuer Ansatz für das Knochengewebe-Engineering entwickelt, der auf fortschrittlichen Ultraviolett-A- und Riboflavin (UVA/R)-vernetzten Kollagengerüsten sowie einem bioaktiven Kationen-Einkapselungssystem basiert, das Cu^{2+} und Mg^{2+} in Vaterit-Calcit- CaCO_3 -Partikeln enthält. Die Studie untersucht detailliert die Komplexität des UVA/R-Vernetzungsmechanismus, insbesondere die Interaktion mit Tyrosinresten im Kollagen, und liefert Erkenntnisse, die nicht nur das Verständnis zur Stabilisierung von Kollagen erweitern, sondern auch neue Fortschritte bei der funktionellen Optimierung von kollagenbasierten Biomaterialien durch verfeinerte Vernetzungsmethoden ermöglichen. Die Ergebnisse zeigen, dass Tyrosinreste kritische Stellen für die Vernetzung darstellen, wobei Riboflavin sowohl als Katalysator als auch als kompetitiver Hemmstoff fungiert. Die UVA/R-vernetzten Kollagenmatrizen zeichnen sich durch ein ausgewogenes Verhältnis von Stabilität und Abbaubarkeit, verbesserte mechanische Eigenschaften sowie eine höhere Biokompatibilität im Vergleich zu chemisch vernetzten Alternativen aus. In-vivo-Untersuchungen belegen darüber hinaus die hervorragende Biokompatibilität der UVA/R-vernetzten Matrizen und deren Fähigkeit, Gewebeentzündungen zu reduzieren und die Regeneration zu fördern.

Darüber hinaus stellt diese Dissertation eine innovative Einkapselungsstrategie zur kontrollierten Freisetzung essenzieller bioaktiver Ionen für die Knochenregeneration vor. Das entwickelte System, das durch Polyelektrolytmultischichten und die Funktionalisierung der Kollagenmatrix ergänzt wird, simuliert das Mikroumfeld von Knochengewebe und schafft optimale Bedingungen für die Heilung durch eine kontinuierliche Freisetzung von Ca^{2+} -, Cu^{2+} - und Mg^{2+} -Ionen. Dieser Ansatz fördert sowohl die Proliferation und Differenzierung von Osteoblasten als auch die signifikante Erhöhung der Expression von Genen, die mit der Osteogenese und Angiogenese in Verbindung stehen, und unterstreicht damit das

vielversprechende Potenzial der entwickelten Mikrokapseln für die Weiterentwicklung des Knochengewebe-Engineerings.

Indem mechanische und biochemische Aspekte des Tissue-Engineerings synergetisch verknüpft werden, präsentiert diese Dissertation eine umfassende Strategie, die sowohl die physische als auch biologische Wirksamkeit der entwickelten Gerüste für die Knochenregeneration verbessert. Die detaillierte Analyse der UVA/R-Vernetzungsdynamik sowie die Einführung eines innovativen Mehrionen-Freisetzungsmechanismus markieren bedeutende Fortschritte auf diesem Gebiet und bieten neue Einblicke sowie verfeinerte Methoden für die Gestaltung und Entwicklung von Biomaterialien der nächsten Generation. Diese Arbeit bereichert nicht nur die akademische Diskussion im Bereich des Tissue Engineerings, sondern setzt auch neue Maßstäbe bei der Entwicklung funktionalisierter Knochenersatzmaterialien und stellt einen wichtigen Schritt in Richtung wirksamerer und personalisierter therapeutischer Ansätze für die Knochenregeneration dar.

6. References

1972. CHAPTER 14 - RIBOFLAVIN. In: SEBRELL, W. H. & HARRIS, R. S. (eds.) *The Vitamins (Second Edition)*. Academic Press.
- ADAMCZYK, A., MEULENKAMP, B., WILKEN, G. & PAPP, S. 2020. Managing bone loss in open fractures. *OTA International*, 3, e059.
- ADAMIAK, K. & SIONKOWSKA, A. 2020a. Current methods of collagen cross-linking: Review. *International Journal of Biological Macromolecules*, 161, 550-560.
- ADAMIAK, K. & SIONKOWSKA, A. 2020b. Current methods of collagen cross-linking: Review. *Int J Biol Macromol*, 161, 550-560.
- AHMAD, Z., SHEPHERD, J. H., SHEPHERD, D. V., GHOSE, S., KEW, S. J., CAMERON, R. E., BEST, S. M., BROOKS, R. A., WARDALE, J. & RUSHTON, N. 2015. Effect of 1-ethyl-3-(3-dimethylaminopropyl) carbodiimide and N-hydroxysuccinimide concentrations on the mechanical and biological characteristics of cross-linked collagen fibres for tendon repair. *Regenerative Biomaterials*, 2, 77-85.
- ALBREKTSSON, T. & JOHANSSON, C. 2001. Osteoinduction, osteoconduction and osseointegration. *Eur Spine J*, 10 Suppl 2, S96-101.
- ALI, S. M., PATRAWALLA, N. Y., KAJAVE, N. S., BROWN, A. B. & KISHORE, V. 2022. Species-Based Differences in Mechanical Properties, Cytocompatibility, and Printability of Methacrylated Collagen Hydrogels. *Biomacromolecules*, 23, 5137-5147.
- ALONZO, M., PRIMO, F. A., KUMAR, S. A., MUDLOFF, J. A., DOMINGUEZ, E., FREGOSO, G., ORTIZ, N., WEISS, W. M. & JODDAR, B. 2021. Bone tissue engineering techniques, advances, and scaffolds for treatment of bone defects. *Current opinion in biomedical engineering*, 17, 100248.
- ANDLEY, U. P. & CLARK, B. A. 1989. Generation of oxidants in the near-UV photooxidation of human lens alpha-crystallin. *Investigative Ophthalmology & Visual Science*, 30, 706-713.
- ANDRICH, S., HAASSTERT, B., NEUHAUS, E., FROMMHOLZ, K., AREND, W., OHMANN, C., GREBE, J., VOGT, A., BRUNONI, C., JUNGBLUTH, P., THELEN, S., DINTSIOS, C. M., WINDOLF, J. & ICKS, A. 2021. Health care utilization and excess costs after pelvic fractures among older people in Germany. *Osteoporos Int*, 32, 2061-2072.
- ANSELME, K., PLOUX, L. & PONCHE, A. 2011. Cell/material interfaces: Influence of surface chemistry and surface topography on cell adhesion.
- ASH, C., DUBEC, M., DONNE, K. & BASHFORD, T. 2017. Effect of wavelength and beam width on penetration in light-tissue interaction using computational methods. *Lasers in Medical Science*, 32, 1909-1918.
- AZIZIPOUR, N., AVAZPOUR, R., ROSENZWEIG, D. H., SAWAN, M. & AJJI, A. 2020. Evolution of biochip technology: A review from lab-on-a-chip to organ-on-a-chip. *Micromachines*, 11, 599.
- BARI, A., BLOISE, N., FIORILLI, S., NOVAJRA, G., VALLET-REGÍ, M., BRUNI, G., TORRES-PARDO, A., GONZÁLEZ-CALBET, J. M., VISAI, L. & VITALE-BROVARONE, C. 2017. Copper-containing mesoporous bioactive glass nanoparticles as multifunctional agent for bone regeneration. *Acta Biomaterialia*, 55, 493-504.

- BECKER, L., LU, C.-E., MONTES-MOJARRO, I. A., LAYLAND, S. L., KHALIL, S., NSAIR, A., DUFFY, G. P., FEND, F., MARZI, J. & SCHENKE-LAYLAND, K. 2023. Raman microspectroscopy identifies fibrotic tissues in collagen-related disorders via deconvoluted collagen type I spectra. *Acta Biomaterialia*, 162, 278-291.
- BELLUCCI, D., SOLA, A., ANESI, A., SALVATORI, R., CHIARINI, L. & CANNILLO, V. 2015. Bioactive glass/hydroxyapatite composites: Mechanical properties and biological evaluation. *Materials Science and Engineering: C*, 51, 196-205.
- BHAGWAT, P. K. & DANDGE, P. B. 2018. Collagen and collagenolytic proteases: A review. *Biocatalysis and Agricultural Biotechnology*, 15, 43-55.
- BIELAJEW, B. J., HU, J. C. & ATHANASIOU, K. A. 2020. Collagen: quantification, biomechanics and role of minor subtypes in cartilage. *Nature Reviews Materials*, 5, 730-747.
- BONNELYE, E., CHABADEL, A., SALTEL, F. & JURDIC, P. 2008. Dual effect of strontium ranelate: stimulation of osteoblast differentiation and inhibition of osteoclast formation and resorption in vitro. *Bone*, 42, 129-138.
- BOSCH-RUÉ, È., DÍEZ-TERCERO, L., BUITRAGO, J. O., CASTRO, E. & PÉREZ, R. A. 2023. Angiogenic and immunomodulation role of ions for initial stages of bone tissue regeneration. *Acta Biomaterialia*.
- BUTLER, M. F., NG, Y. F. & PUDNEY, P. D. A. 2003. Mechanism and kinetics of the crosslinking reaction between biopolymers containing primary amine groups and genipin. *Journal of Polymer Science Part A: Polymer Chemistry*, 41, 3941-3953.
- CAMARERO-ESPINOSA, S. & MORONI, L. 2021. Janus 3D printed dynamic scaffolds for nanovibration-driven bone regeneration. *Nature communications*, 12, 1031.
- CHARBONNIER, B., HADIDA, M. & MARCHAT, D. 2021. Additive manufacturing pertaining to bone: Hopes, reality and future challenges for clinical applications. *Acta Biomaterialia*, 121, 1-28.
- CHEN, D., JIANG, D. & KE, Z. 2024. The potential application of formulation with pimelic acid as eye drops for corneal collagen cross-linking. *Medicine in Novel Technology and Devices*, 100296.
- CHEN, J., LI, L., YI, R., GAO, R. & HE, J. 2018. Release kinetics of Tilapia scale collagen I peptides during tryptic hydrolysis. *Food Hydrocolloids*, 77, 931-936.
- CHEN, S., MICHÁLEK, M., GALUSKOVÁ, D., MICHÁLKOVÁ, M., ŠVANČÁREK, P., TALIMIAN, A., KAŇKOVÁ, H., KRAXNER, J., ZHENG, K., LIVERANI, L., GALUSEK, D. & BOCCACCINI, A. R. 2020. Multi-targeted B and Co co-doped 45S5 bioactive glasses with angiogenic potential for bone regeneration. *Materials Science and Engineering: C*, 112, 110909.
- CHENG, J., YANG, L., YE, Y., HE, L., CHEN, S. & WANG, J. 2024. Mendelian Randomisation Analysis of Causal Association between Lifestyle, Health Factors, and Keratoconus. *Bioengineering*, 11, 221.

- CHENG, X., ZHAO, K., ZHA, X., DU, X., LI, Y., CHEN, S., WU, Y., LI, S., LU, Y., ZHANG, Y., XIAO, X., LI, Y., MA, X., GONG, X., CHEN, W., YANG, Y., JIAO, J., CHEN, B., LV, Y., GAO, J., HONG, G., PAN, Y., YAN, Y., QI, H., RAN, L., ZHAI, J., WANG, L., LI, K., FU, H., WU, J., LIU, S., BLAKE, G. M., PICKHARDT, P. J., MA, Y., FU, X., DONG, S., ZENG, Q., GUO, Z., HIND, K., ENGELKE, K., TIAN, W. & CHINA HEALTH BIG DATA PROJECT, I. 2021. Opportunistic Screening Using Low-Dose CT and the Prevalence of Osteoporosis in China: A Nationwide, Multicenter Study. *J Bone Miner Res*, 36, 427-435.
- CHEUNG, D. T., PERELMAN, N., KO, E. C. & NIMNI, M. E. 1985. Mechanism of crosslinking of proteins by glutaraldehyde III. Reaction with collagen in tissues. *Connective Tissue Research*, 13, 109-115.
- CHUNG, L., DINAKARPANDIAN, D., YOSHIDA, N., LAUER-FIELDS, J. L., FIELDS, G. B., VISSE, R. & NAGASE, H. 2004. Collagenase unwinds triple-helical collagen prior to peptide bond hydrolysis. *The EMBO Journal*, 23, 3020-3030-3030.
- CUNNIFFE, G. M. & O'BRIEN, F. J. 2011. Collagen scaffolds for orthopedic regenerative medicine. *Jom*, 63, 66-73.
- DALSGAARD, T. K., NIELSEN, J. H., BROWN, B. E., STADLER, N. & DAVIES, M. J. 2011. Dityrosine, 3,4-Dihydroxyphenylalanine (DOPA), and Radical Formation from Tyrosine Residues on Milk Proteins with Globular and Flexible Structures as a Result of Riboflavin-Mediated Photo-oxidation. *Journal of Agricultural and Food Chemistry*, 59, 7939-7947.
- DASGUPTA, A., SORI, N., PETROVA, S., MAGHDOURI-WHITE, Y., THAYER, N., KEMPER, N., POLK, S., LEATHERS, D., COUGHENOUR, K., DASCOLI, J., PALIKONDA, R., DONAHUE, C., BULYSHEVA, A. A. & FRANCIS, M. P. 2021. Comprehensive collagen crosslinking comparison of microfluidic wet-extruded microfibers for bioactive surgical suture development. *Acta Biomaterialia*, 128, 186-200.
- DAVIDENKO, N., BAX, D. V., SCHUSTER, C. F., FARNDAL, R. W., HAMAIA, S. W., BEST, S. M. & CAMERON, R. E. 2015. Optimisation of UV irradiation as a binding site conserving method for crosslinking collagen-based scaffolds. *Journal of Materials Science: Materials in Medicine*, 27, 14.
- DAVIDENKO, N., BAX, D. V., SCHUSTER, C. F., FARNDAL, R. W., HAMAIA, S. W., BEST, S. M. & CAMERON, R. E. 2016. Optimisation of UV irradiation as a binding site conserving method for crosslinking collagen-based scaffolds. *Journal of Materials Science: Materials in Medicine*, 27, 1-17.
- DESAI, N. P. & HUBBELL, J. A. 1991. Solution technique to incorporate polyethylene oxide and other water-soluble polymers into surfaces of polymeric biomaterials. *Biomaterials*, 12, 144-153.
- DI SILVIO, L. & JAYAKUMAR, P. 2009. 13 - Cellular response to osteoinductive materials in orthopaedic surgery. In: DI SILVIO, L. (ed.) *Cellular Response to Biomaterials*. Woodhead Publishing.
- DILLOW, A. K. & TIRRELL, M. 1998. Targeted cellular adhesion at biomaterial interfaces. *Current Opinion in Solid State and Materials Science*, 3, 252-259.

- DIPPOLD, D., CAI, A., HARDT, M., BOCCACCINI, A. R., HORCH, R., BEIER, J. P. & SCHUBERT, D. W. 2017. Novel approach towards aligned PCL-Collagen nanofibrous constructs from a benign solvent system. *Materials Science and Engineering: C*, 72, 278-283.
- DVORAKOVA, J., WIESNEROVA, L., CHOCHOLATA, P., KULDA, V., LANDSMANN, L., CEDIKOVA, M., KRIPNEROVA, M., EBERLOVA, L. & BABUSKA, V. 2023. Human cells with osteogenic potential in bone tissue research. *BioMedical Engineering OnLine*, 22, 33.
- ECKHARD, U., HUESGEN, P. F., BRANDSTETTER, H. & OVERALL, C. M. 2014. Proteomic protease specificity profiling of clostridial collagenases reveals their intrinsic nature as dedicated degraders of collagen. *Journal of Proteomics*, 100, 102-114.
- EDENS, W. A., SHARLING, L., CHENG, G., SHAPIRA, R., KINKADE, J. M., LEE, T., EDENS, H. A., TANG, X., SULLARDS, C., FLAHERTY, D. B., BENIAN, G. M. & LAMBETH, J. D. 2001. Tyrosine cross-linking of extracellular matrix is catalyzed by Duox, a multidomain oxidase/peroxidase with homology to the phagocyte oxidase subunit gp91phox. *Journal of Cell Biology*, 154, 879-892.
- EDMUNDSON, M., THANH, N. T. K. & SONG, B. 2013. Nanoparticles based stem cell tracking in regenerative medicine. *Theranostics*, 3, 573.
- ELSALANTY, M. E. & GENECOV, D. G. 2009. Bone grafts in craniofacial surgery. *Craniofacial Trauma Reconstr*, 2, 125-34.
- EYRE, D. 1987. [7] Collagen cross-linking amino acids. *Methods in enzymology*. Elsevier.
- EYRE, D. R. & WU, J.-J. 2005. Collagen Cross-Links. In: BRINCKMANN, J., NOTBOHM, H. & MÜLLER, P. K. (eds.) *Collagen: Primer in Structure, Processing and Assembly*. Berlin, Heidelberg: Springer Berlin Heidelberg.
- FAN, L., JUNG, O., HERRMANN, M., SHIROKIKH, M., STOJANOVIC, S., NAJMAN, S., KÖRTE, F., XIONG, X., SCHENKE - LAYLAND, K. & BARBECK, M. 2024. Deciphering UVA/Riboflavin Collagen Crosslinking: A Pathway to Improve Biomedical Materials. *Advanced Functional Materials*, 2401742.
- FAN, L., KÖRTE, F., RUDT, A., JUNG, O., BURKHARDT, C., BARBECK, M. & XIONG, X. 2022. Encapsulated vaterite-calcite CaCO₃ particles loaded with Mg²⁺ and Cu²⁺ ions with sustained release promoting osteogenesis and angiogenesis. *Frontiers in Bioengineering and Biotechnology*, 10, 983988.
- FAN, L., REN, Y., BURKHARDT, C., JUNG, O., SCHNETTLER, R., BARBECK, M. & XIONG, X. 2023a. Evaluation of Injectable Composite Material Comprising Biphasic Bone Substitutes and Crosslinked Collagen. *Advanced Engineering Materials*, 25, 2300508.
- FAN, L., REN, Y., EMMERT, S., VUČKOVIĆ, I., STOJANOVIC, S., NAJMAN, S., SCHNETTLER, R., BARBECK, M., SCHENKE-LAYLAND, K. & XIONG, X. 2023b. The Use of Collagen-Based Materials in Bone Tissue Engineering. *International Journal of Molecular Sciences*, 24, 3744.
- FATHI-ACHACHELOUEI, M., KNOPF-MARQUES, H., RIBEIRO DA SILVA, C. E., BARTHÈS, J., BAT, E., TEZCANER, A. & VRANA, N. E. 2019. Use of

- nanoparticles in tissue engineering and regenerative medicine. *Frontiers in bioengineering and biotechnology*, 7, 113.
- FINLAYSON, L., BARNARD, I. R. M., MCMILLAN, L., IBBOTSON, S. H., BROWN, C. T. A., EADIE, E. & WOOD, K. 2022. Depth Penetration of Light into Skin as a Function of Wavelength from 200 to 1000 nm. *Photochemistry and Photobiology*, 98, 974-981.
- FRANKE, M. A. D., LANDES, T., SEILER, T. G., KHAYYAT, D., JOHANNSMIEIER, S., HEINEMANN, D. & RIPKEN, T. 2021. Corneal riboflavin gradients and UV-absorption characteristics after topical application of riboflavin in concentrations ranging from 0.1 to 0.5%. *Experimental Eye Research*, 213, 108842.
- FUENTES-LEMUS, E., HÄGGLUND, P., LÓPEZ-ALARCÓN, C. & DAVIES, M. J. 2022. Oxidative Crosslinking of Peptides and Proteins: Mechanisms of Formation, Detection, Characterization and Quantification. *Molecules* [Online], 27.
- FUENTES-LEMUS, E., SILVA, E., LEINISCH, F., DORTA, E., LORENTZEN, L. G., DAVIES, M. J. & LÓPEZ-ALARCÓN, C. 2018. α - and β -casein aggregation induced by riboflavin-sensitized photo-oxidation occurs via di-tyrosine cross-links and is oxygen concentration dependent. *Food chemistry*, 256, 119-128.
- GABRIELA, I. & IULIA, M. 2019. Application of Riboflavin Photochemical Properties in Hydrogel Synthesis. In: MOHAMMED, A. A. K. (ed.) *Biophysical Chemistry*. Rijeka: IntechOpen.
- GAETKE, L. M. & CHOW, C. K. 2003. Copper toxicity, oxidative stress, and antioxidant nutrients. *Toxicology*, 189, 147-163.
- GEORGIADIS, M., MÜLLER, R. & SCHNEIDER, P. 2016. Techniques to assess bone ultrastructure organization: orientation and arrangement of mineralized collagen fibrils. *Journal of the Royal Society Interface*, 13, 20160088.
- GILLMAN, C. E. & JAYASURIYA, A. C. 2021. FDA-approved bone grafts and bone graft substitute devices in bone regeneration. *Materials Science and Engineering: C*, 130, 112466.
- GÖRLITZ, M., JUSTEN, L., ROCHETTE, P. J., BUONANNO, M., WELCH, D., KLEIMAN, N. J., EADIE, E., KAIKIDZU, S., BRADSHAW, W. J., JAVORSKY, E., CRIDLAND, N., GALOR, A., GUTTMANN, M., MEINKE, M. C., SCHLEUSENER, J., JENSEN, P., SÖDERBERG, P., YAMANO, N., NISHIGORI, C., O'MAHONEY, P., MANSTEIN, D., CROFT, R., COLE, C., DE GRUIJL, F. R., FORBES, P. D., TROKEL, S., MARSHALL, J., BRENNER, D. J., SLINEY, D. & ESVELT, K. 2023. Assessing the safety of new germicidal far-UVC technologies. *Photochemistry and Photobiology*, n/a.
- GREENBERG, C. S., BIRCKBICHLER, P. J. & RICE, R. H. 1991. Transglutaminases: multifunctional cross-linking enzymes that stabilize tissues. *The FASEB journal*, 5, 3071-3077.
- GREWAL, D. S., BRAR, G. S., JAIN, R., SOOD, V., SINGLA, M. & GREWAL, S. P. S. 2009. Corneal collagen crosslinking using riboflavin and ultraviolet-A light for keratoconus: one-year analysis using Scheimpflug imaging. *Journal of Cataract & Refractive Surgery*, 35, 425-432.

- GU, L., SHAN, T., MA, Y.-X., TAY, F. R. & NIU, L. 2019. Novel biomedical applications of crosslinked collagen. *Trends in biotechnology*, 37, 464-491.
- GUIMARÃES, C. F., GASPERINI, L., MARQUES, A. P. & REIS, R. L. 2020. The stiffness of living tissues and its implications for tissue engineering. *Nature Reviews Materials*, 5, 351-370.
- GUO, S. A. & DIPIETRO, L. A. 2010. Factors affecting wound healing. *Journal of dental research*, 89, 219-229.
- HANNINK, G. & ARTS, J. J. C. 2011. Bioresorbability, porosity and mechanical strength of bone substitutes: what is optimal for bone regeneration? *Injury*, 42, S22-S25.
- HARRIS, E. D., RAYTON, J. K., BALTHROP, J. E., DI SILVESTRO, R. A. & GARCIA-DE-QUEVEDO, M. 1980. Copper and the Synthesis of Elastin and Collagen. *Ciba Foundation Symposium 79 - Biological Roles of Copper*.
- HART, N. H., NEWTON, R. U., TAN, J., RANTALAINEN, T., CHIVERS, P., SIAFARIKAS, A. & NIMPHIUS, S. 2020. Biological basis of bone strength: anatomy, physiology and measurement. *Journal of musculoskeletal & neuronal interactions*, 20, 347.
- HATAMI-MARBINI, H. & JAYARAM, S. M. 2018. Effect of UVA/Riboflavin Collagen Crosslinking on Biomechanics of Artificially Swollen Corneas. *Investigative Ophthalmology & Visual Science*, 59, 764-770.
- HEBELS, E. R., VAN STEENBERGEN, M. J., HAEGEBAERT, R., SEINEN, C. W., MESQUITA, B. S., VAN DEN DIKKENBERG, A., REMAUT, K., RIJCKEN, C. J. F., VAN RAVENSTEIJN, B. G. P., HENNINK, W. E. & VERMONDEN, T. 2023. Mechanistic Study on the Degradation of Hydrolysable Core-Crosslinked Polymeric Micelles. *Langmuir*, 39, 12132-12143.
- HEO, J., KOH, R. H., SHIM, W., KIM, H. D., YIM, H.-G. & HWANG, N. S. 2016. Riboflavin-induced photo-crosslinking of collagen hydrogel and its application in meniscus tissue engineering. *Drug Delivery and Translational Research*, 6, 148-158.
- HOFF, P., GABER, T., STREHL, C., JAKSTADT, M., HOFF, H., SCHMIDT-BLEEK, K., LANG, A., RÖHNER, E., HUSCHER, D. & MATZIOLIS, G. 2017. A pronounced inflammatory activity characterizes the early fracture healing phase in immunologically restricted patients. *International journal of molecular sciences*, 18, 583.
- HOSSEINKHANI, H., DOMB, A. J., SHARIFZADEH, G. & NAHUM, V. 2023. Gene therapy for regenerative medicine. *Pharmaceutics*, 15, 856.
- HOVEIDAEI, A. H., SADAT-SHOJAI, M., MOSALAMIAGHILI, S., SALARIKIA, S. R., ROGHANI-SHAHRAKI, H., GHADERPANAHI, R., ERSI, M. H. & CONWAY, J. D. 2023. Nano-hydroxyapatite structures for bone regenerative medicine: Cell-material interaction. *Bone*, 116956.
- HURLE, K., OLIVEIRA, J. M., REIS, R. L., PINA, S. & GOETZ-NEUNHOEFFER, F. 2021. Ion-doped brushite cements for bone regeneration. *Acta biomaterialia*, 123, 51-71.

- ISELI, H. P., POPP, M., SEILER, T., SPOERL, E. & MROCHEN, M. 2011. Laboratory measurement of the absorption coefficient of riboflavin for ultraviolet light (365 nm). *Journal of Refractive Surgery*, 27, 195-201.
- ISLAM, M. M., ABUSAMRA, D. B., CHIVU, A., ARGÜESO, P., DOHLMAN, C. H., PATRA, H. K., CHODOSH, J. & GONZÁLEZ-ANDRADES, M. 2021. Optimization of collagen chemical crosslinking to restore biocompatibility of tissue-engineered scaffolds. *Pharmaceutics*, 13, 832.
- ITO, A., KAWAMURA, H., OTSUKA, M., IKEUCHI, M., OHGUSHI, H., ISHIKAWA, K., ONUMA, K., KANZAKI, N., SOGO, Y. & ICHINOSE, N. 2002. Zinc-releasing calcium phosphate for stimulating bone formation. *Materials Science and Engineering: C*, 22, 21-25.
- JUS, S., STACHEL, I., SCHLOEGL, W., PRETZLER, M., FRIESS, W., MEYER, M., BIRNER-GRÜNBERGER, R. & GUEBITZ, G. M. 2011. Cross-linking of collagen with laccases and tyrosinases. *Materials Science and Engineering: C*, 31, 1068-1077.
- KAMAEV, P., FRIEDMAN, M. D., SHERR, E. & MULLER, D. 2012. Photochemical Kinetics of Corneal Cross-Linking with Riboflavin. *Investigative Ophthalmology & Visual Science*, 53, 2360-2367.
- KAO, H., CHEN, C.-C., HUANG, Y.-R., CHU, Y.-H., CSIK, A. & DING, S.-J. 2019. Metal ion-dependent tailored antibacterial activity and biological properties of polydopamine-coated titanium implants. *Surface and Coatings Technology*, 378, 124998.
- KAWAMURA, T., YUNOKI, S., OHYABU, Y., URAOKA, T. & MURAMATSU, K. 2021. Crosslinking Efficacy and Cytotoxicity of Genipin and Its Activated Form Prepared by Warming It in a Phosphate Buffer: A Comparative Study. *Materials* [Online], 14.
- KETABAT, F., KARKHANEH, A., MEHDINAVAZ AGHDAM, R. & HOSSEIN AHMADI TAFTI, S. 2017. Injectable conductive collagen/alginate/polypyrrole hydrogels as a biocompatible system for biomedical applications. *Journal of Biomaterials Science, Polymer Edition*, 28, 794-805.
- KOPSACHILIS, N., TSAOUSIS, K. T., TSINOPOULOS, I. T., KRUSE, F. E. & WELGE-LUESSEN, U. 2013. A novel mechanism of UV-A and riboflavin-mediated corneal cross-linking through induction of tissue transglutaminases. *Cornea*, 32, 1034-1039.
- KOSEKI, K., YAMAMOTO, A., TANIMOTO, K., OKAMOTO, N., TENG, F., BITO, T., YABUTA, Y., KAWANO, T. & WATANABE, F. 2021. Dityrosine Crosslinking of Collagen and Amyloid- β Peptides Is Formed by Vitamin B12 Deficiency-Generated Oxidative Stress in *Caenorhabditis elegans*. *International Journal of Molecular Sciences* [Online], 22.
- KRAMER, R. Z., BELLA, J., MAYVILLE, P., BRODSKY, B. & BERMAN, H. M. 1999. Sequence dependent conformational variations of collagen triple-helical structure. *Nature Structural Biology*, 6, 454-457.
- KYRIAKIDES, T. R., KIM, H.-J., ZHENG, C., HARKINS, L., TAO, W. & DESCHENES, E. 2022. Foreign body response to synthetic polymer biomaterials and the role of adaptive immunity. *Biomedical Materials*, 17, 022007.

- LAGUARDIA, J. S., SHARIATI, K., BEDAR, M., REN, X., MOGHADAM, S., HUANG, K. X., CHEN, W., KANG, Y., YAMAGUCHI, D. T. & LEE, J. C. 2023. Convergence of Calcium Channel Regulation and mechanotransduction in skeletal regenerative Biomaterial Design. *Advanced Healthcare Materials*, 12, 2301081.
- LEUNG, W. Y. & MURRAY, V. 2021. The influence of DNA methylation on the sequence specificity of UVB-and UVC-induced DNA damage. *Journal of Photochemistry and Photobiology b: Biology*, 221, 112225.
- LI, Q., XU, S., FENG, Q., DAI, Q., YAO, L., ZHANG, Y., GAO, H., DONG, H., CHEN, D. & CAO, X. 2021a. 3D printed silk-gelatin hydrogel scaffold with different porous structure and cell seeding strategy for cartilage regeneration. *Bioactive materials*, 6, 3396-3410.
- LI, Q., ZHAO, H., WANG, H. & ZHAO, G. 2022. Properties of the acellular porcine cornea crosslinked with UVA/riboflavin as scaffolds for Boston Keratoprosthesis. *Biomaterials Advances*, 137, 212822.
- LI, Y., LIU, Y., LI, R., BAI, H., ZHU, Z., ZHU, L., ZHU, C., CHE, Z., LIU, H. & WANG, J. 2021b. Collagen-based biomaterials for bone tissue engineering. *Materials & Design*, 210, 110049.
- LIN, J.-T. 2018. A critical review on the kinetics, efficacy, safety, nonlinear law and optimal protocols of corneal cross-linking. *of*, 10, 35-38.
- LIN, W., XU, L. & LI, G. 2020a. Molecular Insights Into Lysyl Oxidases in Cartilage Regeneration and Rejuvenation. *Frontiers in Bioengineering and Biotechnology*, 8.
- LIN, X., PATIL, S., GAO, Y.-G. & QIAN, A. 2020b. The bone extracellular matrix in bone formation and regeneration. *Frontiers in pharmacology*, 11, 521497.
- LIN, Y. W., TSOU, K. L., FAY, C. D., LIU, X., CHUNG, J. H. Y., SHARMA, D., JEIRANIKHAMENEH, A., KUO, P. H., TZENG, C. K., WALLACE, G. G., WU, C. Y., KER, M. D., CHAO, J. I. & CHENG, Y. T. 2020c. A microvalve cell printing technique using riboflavin photosensitizer for selective cell patterning onto a retinal chip. *Bioprinting*, 20, e00097.
- LIU, Y., LIU, N., NA, J., LI, C., YUE, G., FAN, Y. & ZHENG, L. 2023. Wnt/ β -catenin plays a dual function in calcium hydroxide induced proliferation, migration, osteogenic differentiation and mineralization in vitro human dental pulp stem cells. *International Endodontic Journal*, 56, 92-102.
- LU, C.-Y. & LIU, Y.-Y. 2002. Electron transfer oxidation of tryptophan and tyrosine by triplet states and oxidized radicals of flavin sensitizers: a laser flash photolysis study. *Biochimica et Biophysica Acta (BBA) - General Subjects*, 1571, 71-76.
- LU FAN, O. J., MARKUS HERRMANN, MARINA SHIROKIKH, SANJA STOJANOVIC, STEVO NAJMAN, FABIAN KÖRTE, XIN XIONG, KATJA SCHENKE-LAYLAND, AND MIKE BARBECK 2024. Deciphering UVA/Riboflavin Collagen Crosslinking: A Pathway to Improved Biomedical Materials. *Advanced Functional Materials*, Under submission.
- LUO, T. & KIICK, K. L. 2017. Collagen-like peptide bioconjugates. *Bioconjugate chemistry*, 28, 816-827.
- LUO, Y., LIU, H., ZHANG, Y., LIU, Y., LIU, S., LIU, X. & LUO, E. 2023. Metal ions: The unfading stars of bone regeneration—From bone metabolism

- regulation to biomaterial applications. *Biomaterials Science*, 11, 7268-7295.
- MAKADIA, H. K. & SIEGEL, S. J. 2011. Poly lactic-co-glycolic acid (PLGA) as biodegradable controlled drug delivery carrier. *Polymers*, 3, 1377-1397.
- MALCOR, J.-D. & MALLEIN-GERIN, F. 2022. Biomaterial functionalization with triple-helical peptides for tissue engineering. *Acta Biomaterialia*, 148, 1-21.
- MANSOORIFAR, A., GORDON, R., BERGAN, R. C. & BERTASSONI, L. E. 2021. Bone-on-a-Chip: Microfluidic Technologies and Microphysiologic Models of Bone Tissue. *Advanced Functional Materials*, 31, 2006796.
- MARTINEZ, M. G., BULLOCK, A. J., MACNEIL, S. & REHMAN, I. U. 2019. Characterisation of structural changes in collagen with Raman spectroscopy. *Applied Spectroscopy Reviews*, 54, 509-542.
- MARUYAMA, M., RHEE, C., YAO, Z. & GOODMAN, S. B. 2020. Modulation of the inflammatory response and bone healing. *Frontiers in endocrinology*, 11, 542565.
- MAZZOTTA, C., FERRISE, M., GABRIELE, G., GENNARO, P. & MEDURI, A. 2021. Chemically-boosted corneal cross-linking for the treatment of keratoconus through a riboflavin 0.25% optimized solution with high superoxide anion release. *Journal of Clinical Medicine*, 10, 1324.
- MCCALL, A. S., KRAFT, S., EDELHAUSER, H. F., KIDDER, G. W., LUNDQUIST, R. R., BRADSHAW, H. E., DEDEIC, Z., DIONNE, M. J. C., CLEMENT, E. M. & CONRAD, G. W. 2010. Mechanisms of corneal tissue cross-linking in response to treatment with topical riboflavin and long-wavelength ultraviolet radiation (UVA). *Investigative ophthalmology & visual science*, 51, 129-138.
- MECHANIC, G. L., KATZ, E. P., HENMI, M., NOYES, C. & YAMAUCHI, M. 1987. Locus of a histidine-based, stable trifunctional, helix to helix collagen cross-link: stereospecific collagen structure of type I skin fibrils. *Biochemistry*, 26, 3500-3509.
- MINOR, A. J. & COULOMBE, K. L. K. 2020. Engineering a collagen matrix for cell - instructive regenerative angiogenesis. *Journal of Biomedical Materials Research Part B: Applied Biomaterials*, 108, 2407-2416.
- MOGILNER, I. G., RUDERMAN, G. & GRIGERA, J. R. 2002. Collagen stability, hydration and native state. *Journal of molecular Graphics and Modelling*, 21, 209-213.
- MONTALBANO, G., TOMASINA, C., FIORILLI, S., CAMARERO-ESPINOSA, S., VITALE-BROVARONE, C. & MORONI, L. 2021. Biomimetic Scaffolds Obtained by Electrospinning of Collagen-Based Materials: Strategies to Hinder the Protein Denaturation. *Materials*, 14, 4360.
- MORSHED, M., HASAN, A., SHARIFI, M., BABADAEI, M. M. N., BLOUKH, S. H., ISLAM, M. A., CHOWDHURY, E. H. & FALAHATI, M. 2020. Non-viral delivery systems of DNA into stem cells: Promising and multifarious actions for regenerative medicine. *Journal of Drug Delivery Science and Technology*, 60, 101861.
- MOSLEH, Y., VAN DIE, M., GARD, W., BREEBAART, I., VAN DE KUILEN, J.-W., VAN DUIN, P. & POULIS, J. A. 2023. Gelatine adhesives from mammalian and fish origins for historical art objects conservation: How

- do microstructural features determine physical and mechanical properties? *Journal of Cultural Heritage*, 63, 52-60.
- MURPHY, S., BOYD, D., MOANE, S. & BENNETT, M. 2009. The effect of composition on ion release from Ca–Sr–Na–Zn–Si glass bone grafts. *Journal of Materials Science: Materials in Medicine*, 20, 2207-2214.
- NAIR, M., JOHAL, R. K., HAMAIA, S. W., BEST, S. M. & CAMERON, R. E. 2020. Tunable bioactivity and mechanics of collagen-based tissue engineering constructs: A comparison of EDC-NHS, genipin and TG2 crosslinkers. *Biomaterials*, 254, 120109.
- O'NEILL, E., AWALE, G., DANESHMANDI, L., UMERAH, O. & LO, K. W.-H. 2018. The roles of ions on bone regeneration. *Drug discovery today*, 23, 879-890.
- OLDE DAMINK, L. H. H., DIJKSTRA, P. J., VAN LUYN, M. J. A., VAN WACHEM, P. B., NIEUWENHUIS, P. & FEIJEN, J. 1995. Glutaraldehyde as a crosslinking agent for collagen-based biomaterials. *Journal of materials science: materials in medicine*, 6, 460-472.
- OLE, J., MIKE, B., LU, F. A. N., FABIAN, K., CUIFENG, Z., RUMEN, K., SVEN, P. & XIN, X. 2023. Republication: In Vitro and Ex Vivo Analysis of Collagen Foams for Soft and Hard Tissue Regeneration. *In Vivo*, 37, 320.
- OLIVEIRA, É. R., NIE, L., PODSTAWCZYK, D., ALLAHBAKHS, A., RATNAYAKE, J., BRASIL, D. L. & SHAVANDI, A. 2021. Advances in growth factor delivery for bone tissue engineering. *International journal of molecular sciences*, 22, 903.
- OLSEN, E. G. & RINGVOLD, A. 1982. HUMAN CORNEA ENDOTHELIUM AND ULTRAVIOLET RADIATION. *Acta Ophthalmologica*, 60, 54-56.
- OOSTERLAKEN, B. M., VENA, M. P. & DE WITH, G. 2021. In Vitro Mineralization of Collagen. *Advanced Materials*, 33, 2004418.
- ORYAN, A., KAMALI, A., MOSHIRI, A., BAHARVAND, H. & DAEMI, H. 2018. Chemical crosslinking of biopolymeric scaffolds: Current knowledge and future directions of crosslinked engineered bone scaffolds. *Int J Biol Macromol*, 107, 678-688.
- PARK, J.-Y., JUNG, I.-H., KIM, Y.-K., LIM, H.-C., LEE, J.-S., JUNG, U.-W. & CHOI, S.-H. 2015. Guided bone regeneration using 1-ethyl-3-(3-dimethylaminopropyl) carbodiimide (EDC)-cross-linked type-I collagen membrane with biphasic calcium phosphate at rabbit calvarial defects. *Biomaterials Research*, 19, 15.
- PATEL, J. M., JACKSON, R. C., SCHNEIDER, G. L., GHODBANE, S. A. & DUNN, M. G. 2018. Carbodiimide cross-linking counteracts the detrimental effects of gamma irradiation on the physical properties of collagen-hyaluronan sponges. *Journal of Materials Science: Materials in Medicine*, 29, 1-8.
- PEHRSSON, M., MORTENSEN, J. H., MANON-JENSEN, T., BAY-JENSEN, A.-C., KARSDAL, M. A. & DAVIES, M. J. 2021. Enzymatic cross-linking of collagens in organ fibrosis–resolution and assessment. *Expert Review of Molecular Diagnostics*, 21, 1049-1064.
- PEREZ, R. A., KIM, J.-H., BUITRAGO, J. O., WALL, I. B. & KIM, H.-W. 2015. Novel therapeutic core–shell hydrogel scaffolds with sequential delivery

- of cobalt and bone morphogenetic protein-2 for synergistic bone regeneration. *Acta Biomaterialia*, 23, 295-308.
- PETRE, D. G. & LEEUWENBURGH, S. C. G. 2022. The Use of Fibers in Bone Tissue Engineering. *Tissue Eng Part B Rev*, 28, 141-159.
- PFEIFFENBERGER, M., DAMERAU, A., LANG, A., BUTTGEREIT, F., HOFF, P. & GABER, T. 2021. Fracture Healing Research—Shift towards In Vitro Modeling? *Biomedicines* [Online], 9.
- PIEPER, J. S., HAFMANS, T., VEERKAMP, J. H. & VAN KUPPEVELT, T. H. 2000. Development of tailor-made collagen–glycosaminoglycan matrices: EDC/NHS crosslinking, and ultrastructural aspects. *Biomaterials*, 21, 581-593.
- POPOK, V. 2012. Ion implantation of polymers: formation of nanoparticulate materials. *Reviews on advanced materials science*, 30, 1-26.
- RAISKUP, F. & SPOERL, E. 2013. Corneal crosslinking with riboflavin and ultraviolet A. I. Principles. *Ocul Surf*, 11, 65-74.
- RAMACHANDRAN, G. N. & KARTHA, G. Studies on collagen: I. Structure of the collagen group of proteins. 1955 1955. Springer, 215-234.
- RAYMOND J FONSECA, D. M. D. 2017. *Oral and Maxillofacial Surgery - Inkling Enhanced E-Book: 3-Volume Set*, Elsevier Health Sciences.
- REGINSTER, J.-Y. & MEUNIER, P. J. 2003. Strontium ranelate phase 2 dose-ranging studies: PREVOS and STRATOS studies. *Osteoporosis international*, 14, 56-65.
- REN, Y., FAN, L., ALKILDANI, S., LIU, L., EMMERT, S., NAJMAN, S., RIMASHEVSKIY, D., SCHNETTLER, R., JUNG, O., XIONG, X. & BARBECK, M. 2022. Barrier Membranes for Guided Bone Regeneration (GBR): A Focus on Recent Advances in Collagen Membranes. *International Journal of Molecular Sciences* [Online], 23.
- ROBINSON, J., RUSSELL, T., XU, Z. & YUN, Y. 2022. Mechanically Tunable Extracellular Matrix of Genipin Crosslinked Collagen and Its Effect on Endothelial Function. *Applied Sciences* [Online], 12.
- ROWE, P., KOLLER, A. & SHARMA, S. 2018. Physiology, bone remodeling.
- SARRIGIANNIDIS, S. O., REY, J. M., DOBRE, O., GONZÁLEZ-GARCÍA, C., DALBY, M. J. & SALMERON-SANCHEZ, M. 2021. A tough act to follow: collagen hydrogel modifications to improve mechanical and growth factor loading capabilities. *Materials today. Bio* [Online], 10.
- SCHATKOSKI, V. M., DO AMARAL MONTANHEIRO, T. L., DE MENEZES, B. R. C., PEREIRA, R. M., RODRIGUES, K. F., RIBAS, R. G., DA SILVA, D. M. & THIM, G. P. 2021. Current advances concerning the most cited metal ions doped bioceramics and silicate-based bioactive glasses for bone tissue engineering. *Ceramics International*, 47, 2999-3012.
- SHELL, H., DUDA, G. N., PETERS, A., TSITSILONIS, S., JOHNSON, K. A. & SCHMIDT-BLEEK, K. 2017. The haematoma and its role in bone healing. *Journal of Experimental Orthopaedics*, 4, 5.
- SEL, S., NASS, N., PÖTZSCH, S., TRAU, S., SIMM, A., KALINSKI, T., DUNCKER, G. I. W., KRUSE, F. E., AUFFARTH, G. U. & BRÖMME, H.-J. 2014. UVA irradiation of riboflavin generates oxygen-dependent hydroxyl radicals. *Redox Report*, 19, 72-79.

- SEOL, Y.-J., PARK, J. Y., JUNG, J. W., JANG, J., GIRDHARI, R., KIM, S. W. & CHO, D.-W. 2014. Improvement of bone regeneration capability of ceramic scaffolds by accelerated release of their calcium ions. *Tissue Engineering Part A*, 20, 2840-2849.
- SHARIF, R., HJORTDAL, J., SEJERSEN, H., FRANK, G. & KARAMICHOS, D. 2017. Human in vitro Model Reveals the Effects of Collagen Cross-linking on Keratoconus Pathogenesis. *Scientific Reports*, 7, 12517.
- SHARIFI, R., YANG, Y., ADIBNIA, Y., DOHLMAN, C. H., CHODOSH, J. & GONZALEZ-ANDRADES, M. 2019. Finding an Optimal Corneal Xenograft Using Comparative Analysis of Corneal Matrix Proteins Across Species. *Scientific Reports*, 9, 1876.
- SHI, M., ZHOU, Y., SHAO, J., CHEN, Z., SONG, B., CHANG, J., WU, C. & XIAO, Y. 2015. Stimulation of osteogenesis and angiogenesis of hBMSCs by delivering Si ions and functional drug from mesoporous silica nanospheres. *Acta biomaterialia*, 21, 178-189.
- SHOULDERS, M. D. & RAINES, R. T. 2009. Collagen structure and stability. *Annual review of biochemistry*, 78, 929-958.
- SIONKOWSKA, A. 2005. Thermal stability of UV-irradiated collagen in bovine lens capsules and in bovine cornea. *Journal of Photochemistry and Photobiology B: Biology*, 80, 87-92.
- SPECE, H., YU, T., LAW, A. W., MARCOLONGO, M. & KURTZ, S. M. 2020. 3D printed porous PEEK created via fused filament fabrication for osteoconductive orthopaedic surfaces. *Journal of the mechanical behavior of biomedical materials*, 109, 103850.
- SPOERL, E., HUHLE, M. & SEILER, T. 1998. Induction of cross-links in corneal tissue. *Experimental eye research*, 66, 97-103.
- SPOERL, E., MROCHEN, M., SLINEY, D., TROKEL, S. & SEILER, T. 2007. Safety of UVA-riboflavin cross-linking of the cornea. *Cornea*, 26, 385-389.
- STUMPTNER, C., PABST, D., LOIBNER, M., VIERTLER, C. & ZATLOUKAL, K. 2019. The impact of crosslinking and non-crosslinking fixatives on antigen retrieval and immunohistochemistry. *New Biotechnology*, 52, 69-83.
- SU, N., YANG, J., XIE, Y., DU, X., CHEN, H., ZHOU, H. & CHEN, L. 2019. Bone function, dysfunction and its role in diseases including critical illness. *International journal of biological sciences*, 15, 776.
- SU, Y., CAPPOCK, M., DOBRES, S., KUCINE, A. J., WALTZER, W. C. & ZHU, D. 2023. Supplemental mineral ions for bone regeneration and osteoporosis treatment. *Engineered Regeneration*, 4, 170-182.
- SUBASINGHE, S. K., OGBUEHI, K. C. & DIAS, G. J. 2018. Current perspectives on corneal collagen crosslinking (CXL). *Graefe's Archive for Clinical and Experimental Ophthalmology*, 256, 1363-1384.
- SUN, Y., LIU, X., ZHU, Y., HAN, Y., SHEN, J., BAO, B., GAO, T., LIN, J., HUANG, T. & XU, J. 2021. Tunable and controlled release of cobalt ions from metal-organic framework hydrogel nanocomposites enhances bone regeneration. *ACS Applied Materials & Interfaces*, 13, 59051-59066.
- SUTTHAVAS, P., SCHUMACHER, M., ZHENG, K., HABIBOVIĆ, P., BOCCACCINI, A. R. & VAN RIJT, S. 2022. Zn-Loaded and Calcium

- Phosphate-Coated Degradable Silica Nanoparticles Can Effectively Promote Osteogenesis in Human Mesenchymal Stem Cells. *Nanomaterials* [Online], 12.
- SZWED-GEORGIU, A., PŁOCIŃSKI, P., KUPIKOWSKA-STOBBA, B., URBANIAK, M. M., RUSEK-WALA, P., SZUSTAKIEWICZ, K., PISZKO, P., KRUPA, A., BIERNAT, M., GAZIŃSKA, M., KASPRZAK, M., NAWROTEK, K., MIRA, N. P. & RUDNICKA, K. 2023. Bioactive Materials for Bone Regeneration: Biomolecules and Delivery Systems. *ACS Biomaterials Science & Engineering*, 9, 5222-5254.
- TAUBENBERGER, A. V., WOODRUFF, M. A., BAI, H., MULLER, D. J. & HUTMACHER, D. W. 2010. The effect of unlocking RGD-motifs in collagen I on pre-osteoblast adhesion and differentiation. *Biomaterials*, 31, 2827-2835.
- THOMPSON, J. M. T. & HING, K. A. 2004. Bone repair in the twenty-first century: biology, chemistry or engineering? *Philosophical Transactions of the Royal Society of London. Series A: Mathematical, Physical and Engineering Sciences*, 362, 2821-2850.
- TOOSI, S. & BEHRAMAN, J. 2020. Osteogenesis and bone remodeling: A focus on growth factors and bioactive peptides. *Biofactors*, 46, 326-340.
- TUCKER, E. C., ROBERTS, M. B., SWEENEY, N. A. & GORDON, D. L. 2018. Chapter 25 - Miscellaneous Antibacterial Drugs. In: RAY, S. D. (ed.) *Side Effects of Drugs Annual*. Elsevier.
- UDHAYAKUMAR, S., SHANKAR, K. G., SOWNDARYA, S., VENKATESH, S., MURALIDHARAN, C. & ROSE, C. 2017. l-Arginine intercedes bio-crosslinking of a collagen-chitosan 3D-hybrid scaffold for tissue engineering and regeneration: in silico, in vitro, and in vivo studies. *Rsc Advances*, 7, 25070-25088.
- UEMURA, R., MIURA, J., ISHIMOTO, T., YAGI, K., MATSUDA, Y., SHIMIZU, M., NAKANO, T. & HAYASHI, M. 2019. UVA-activated riboflavin promotes collagen crosslinking to prevent root caries. *Scientific Reports*, 9, 1252.
- UTAMI NIKE, D., MD FADILAH, N. I., SALLEHUDDIN, N., NOR AZLAN, A. Y. H., IMRAN, F. H., MAAROF, M. & FAUZI, M. B. 2022. Genipin-Crosslinking Effects on Biomatrix Development for Cutaneous Wound Healing: A Concise Review. *Frontiers in Bioengineering and Biotechnology*, 10.
- VALLECILLO-RIVAS, M., TOLEDANO-OSORIO, M., VALLECILLO, C., TOLEDANO, M. & OSORIO, R. 2021. The Collagen Origin Influences the Degradation Kinetics of Guided Bone Regeneration Membranes. *Polymers* [Online], 13.
- VO, N. T. N., HUANG, L., LEMOS, H., MELLOR, A. L. & NOVAKOVIC, K. 2021. Genipin-crosslinked chitosan hydrogels: Preliminary evaluation of the in vitro biocompatibility and biodegradation. *Journal of Applied Polymer Science*, 138, 50848.
- VÝBORNÝ, K., VALLOVÁ, J., KOČÍ, Z., KEKULOVÁ, K., JIRÁKOVÁ, K., JENDELOVÁ, P., HODAN, J. & KUBINOVÁ, Š. 2019. Genipin and EDC crosslinking of extracellular matrix hydrogel derived from human umbilical cord for neural tissue repair. *Scientific Reports*, 9, 10674.

- WANG, J., PENG, Y., CHEN, M., DAI, X., LOU, L., WANG, C., BAO, Z., YANG, X., GOU, Z. & YE, J. 2022. Next-generation finely controlled graded porous antibacterial bioceramics for high-efficiency vascularization in orbital reconstruction. *Bioactive Materials*, 16, 334-345.
- WANG, P., PERCHE, F., MIDOUX, P., CABRAL, C. S. D., MALARD, V., CORREIA, I. J., EI-HAFICI, H., PETITE, H., LOGEART-AVRAMOGLU, D. & PICHON, C. 2021. In Vivo bone tissue induction by freeze-dried collagen-nanohydroxyapatite matrix loaded with BMP2/NS1 mRNAs lipopolyplexes. *Journal of Controlled Release*, 334, 188-200.
- WANG, W. & YEUNG, K. W. K. 2017. Bone grafts and biomaterials substitutes for bone defect repair: A review. *Bioactive Materials*, 2, 224-247.
- WISSINK, M. J. B., BEERNINK, R., PIEPER, J. S., POOT, A. A., ENGBERS, G. H. M., BEUGELING, T., VAN AKEN, W. G. & FEIJEN, J. 2001. Immobilization of heparin to EDC/NHS-crosslinked collagen. Characterization and in vitro evaluation. *Biomaterials*, 22, 151-163.
- WOJTOWICZ, A. M., SHEKARAN, A., OEST, M. E., DUPONT, K. M., TEMPLEMAN, K. L., HUTMACHER, D. W., GULDBERG, R. E. & GARCÍA, A. J. 2010. Coating of biomaterial scaffolds with the collagen-mimetic peptide GFOGER for bone defect repair. *Biomaterials*, 31, 2574-2582.
- WOLLENSAK, G., SPOERL, E. & SEILER, T. 2003. Riboflavin/ultraviolet-A-induced collagen crosslinking for the treatment of keratoconus. *American journal of ophthalmology*, 135, 620-627.
- WONG, H. M., WU, S., CHU, P. K., CHENG, S. H., LUK, K. D. K., CHEUNG, K. M. C. & YEUNG, K. W. K. 2013. Low-modulus Mg/PCL hybrid bone substitute for osteoporotic fracture fixation. *Biomaterials*, 34, 7016-7032.
- WU, C., ZHOU, Y., FAN, W., HAN, P., CHANG, J., YUEN, J., ZHANG, M. & XIAO, Y. 2012. Hypoxia-mimicking mesoporous bioactive glass scaffolds with controllable cobalt ion release for bone tissue engineering. *Biomaterials*, 33, 2076-2085.
- WU, R.-X., XU, X.-Y., WANG, J., HE, X.-T., SUN, H.-H. & CHEN, F.-M. 2018. Biomaterials for endogenous regenerative medicine: coaxing stem cell homing and beyond. *Applied materials today*, 11, 144-165.
- WU, X., GUO, W., WANG, L., XU, Y., WANG, Z., YANG, Y., YU, L., HUANG, J., LI, Y. & ZHANG, H. 2022. An injectable asymmetric-adhesive hydrogel as a GATA6+ cavity macrophage trap to prevent the formation of postoperative adhesions after minimally invasive surgery. *Advanced Functional Materials*, 32, 2110066.
- XYNOS, I. D., EDGAR, A. J., BUTTERY, L. D. K., HENCH, L. L. & POLAK, J. M. 2001. Gene-expression profiling of human osteoblasts following treatment with the ionic products of Bioglass® 45S5 dissolution. *Journal of Biomedical Materials Research*, 55, 151-157.
- YAMAGUCHI, M., IGARASHI, A. & UCHIYAMA, S. 2004. Bioavailability of zinc yeast in rats: stimulatory effect on bone calcification in vivo. *Journal of health science*, 50, 75-81.
- YAMAUCHI, M. & SHIIBA, M. 2008. Lysine hydroxylation and cross-linking of collagen. *Post-translational modifications of proteins: tools for functional proteomics*, 95-108.

- YAMAUCHI, M. & SRICHOLPECH, M. 2012. Lysine post-translational modifications of collagen. *Essays in biochemistry*, 52, 113-133.
- YAN, M., AN, X., JIANG, Z., DUAN, S., WANG, A., ZHAO, X. & LI, Y. 2022. Effects of cross-linking with EDC/NHS and genipin on characterizations of self-assembled fibrillar gel prepared from tilapia collagen and alginate. *Polymer Degradation and Stability*, 200, 109929.
- YANG, Y., XIONG, X., CHEN, J., PENG, X., CHEN, D. & PAN, F. 2021. Research advances in magnesium and magnesium alloys worldwide in 2020. *Journal of Magnesium and Alloys*, 9, 705-747.
- YANNAS, I. V. & TOBOLSKY, A. V. 1967. Cross-linking of Gelatine by Dehydration. *Nature*, 215, 509-510.
- YI, B., XU, Q. & LIU, W. 2022. An overview of substrate stiffness guided cellular response and its applications in tissue regeneration. *Bioactive Materials*, 15, 82-102.
- YOSHIDA, Y. G., YAN, S., XU, H. & YANG, J. 2023. Novel metal nanomaterials to promote angiogenesis in tissue regeneration. *Engineered regeneration*.
- YU, H., PEI, T., REN, J., DING, Y., WU, A. & ZHOU, Y. 2018. Semaphorin 3A enhances osteogenesis of MG63 cells through interaction with Schwann cells in vitro. *Mol Med Rep*, 17, 6084-6092.
- YUAN, Z., WEI, P., HUANG, Y., ZHANG, W., CHEN, F., ZHANG, X., MAO, J., CHEN, D., CAI, Q. & YANG, X. 2019. Injectable PLGA microspheres with tunable magnesium ion release for promoting bone regeneration. *Acta biomaterialia*, 85, 294-309.
- ZANDRINI, T., FLORCZAK, S., LEVATO, R. & OVSIANIKOV, A. 2022. Breaking the resolution limits of 3D bioprinting: future opportunities and present challenges. *Trends in Biotechnology*.
- ZARRINTAJ, P., KHODADADI YAZDI, M., YOUSSEFI AZARFAM, M., ZARE, M., RAMSEY, J. D., SEIDI, F., REZA SAEB, M., RAMAKRISHNA, S. & MOZAFARI, M. 2021. Injectable cell-laden hydrogels for tissue engineering: recent advances and future opportunities. *Tissue Engineering Part A*, 27, 821-843.
- ZHANG, Q., BEI, H.-P., ZHAO, M., DONG, Z. & ZHAO, X. 2022a. Shedding light on 3D printing: Printing photo-crosslinkable constructs for tissue engineering. *Biomaterials*, 286, 121566.
- ZHANG, X., NAN, K., ZHANG, Y., SONG, K., GENG, Z., SHANG, D. & FAN, L. 2024. Lithium and cobalt co-doped mesoporous bioactive glass nanoparticles promote osteogenesis and angiogenesis in bone regeneration. *Frontiers in Bioengineering and Biotechnology*, 11.
- ZHANG, X., XU, L., HUANG, X., WEI, S. & ZHAI, M. 2012. Structural study and preliminary biological evaluation on the collagen hydrogel crosslinked by γ -irradiation. *Journal of Biomedical Materials Research Part A*, 100A, 2960-2969.
- ZHANG, Y., CONRAD, A. H. & CONRAD, G. W. 2011. Effects of ultraviolet-A and riboflavin on the interaction of collagen and proteoglycans during corneal cross-linking. *Journal of Biological Chemistry*, 286, 13011-13022.

- ZHANG, Y., WANG, K.-C., CHANG, C.-K. & LIN, J.-T. 2016. Analysis of the effective dose of ultraviolet light in corneal cross-linking. *International Journal of Ophthalmology*, 9, 1089.
- ZHANG, Y., ZHANG, W., SNOW, T., JU, Y., LIU, Y., SMITH, A. J. & PRABAKAR, S. 2022b. Minimising chemical crosslinking for stabilising collagen in acellular bovine pericardium: Mechanistic insights via structural characterisations. *Acta Biomaterialia*, 152, 113-123.
- ZHAO, Q., NI, Y., WEI, H., DUAN, Y., CHEN, J., XIAO, Q., GAO, J., YU, Y., CUI, Y. & OUYANG, S. 2023. Ion incorporation into bone grafting materials. *Periodontology 2000*.
- ZHENG, Y., LIN, C., HOU, X., MA, N., YU, W., XU, X., LOU, Y., FEI, H., SHEN, Y. & SUN, X. 2017. Enhancing the osteogenic capacity of MG63 cells through N-isopropylacrylamide-modified polyethylenimine-mediated oligodeoxynucleotide MT01 delivery. *RSC advances*, 7, 27121-27127.
- ZHONG, Z., WU, X., WANG, Y., LI, M., LI, Y., LIU, X., ZHANG, X., LAN, Z., WANG, J., DU, Y. & ZHANG, S. 2022. Zn/Sr dual ions-collagen co-assembly hydroxyapatite enhances bone regeneration through procedural osteo-immunomodulation and osteogenesis. *Bioact Mater*, 10, 195-206.
- ZHOU, Q., LYU, S., BERTRAND, A. A., HU, A. C., CHAN, C. H., REN, X., DEWEY, M. J., TIFFANY, A. S., HARLEY, B. A. C. & LEE, J. C. 2021. Stiffness of nanoparticulate mineralized collagen scaffolds triggers osteogenesis via mechanotransduction and canonical wnt signaling. *Macromolecular bioscience*, 21, 2000370.
- ZHU, G., ZHANG, T., CHEN, M., YAO, K., HUANG, X., ZHANG, B., LI, Y., LIU, J., WANG, Y. & ZHAO, Z. 2021. Bone physiological microenvironment and healing mechanism: Basis for future bone-tissue engineering scaffolds. *Bioactive Materials*, 6, 4110-4140.
- ZHU, T., JIANG, M., ZHANG, M., CUI, L., YANG, X., WANG, X., LIU, G., DING, J. & CHEN, X. 2022. Biofunctionalized composite scaffold to potentiate osteoconduction, angiogenesis, and favorable metabolic microenvironment for osteonecrosis therapy. *Bioactive Materials*, 9, 446-460.

7. Declaration

I declare that the doctoral thesis submitted is my original work, completed under the mentorship of Dr. Xin Xiong and Prof. Dr. Katja Schenke-Layland. This thesis exclusively includes manuscripts where I have been the principal author, significantly contributing to the experimental design, execution, evaluation, data analysis, visualization, and the drafting and revising of the manuscript. It has not been submitted, in whole or in part, for any other degree. This thesis has not been previously submitted, either in full or in part, for any degree. All sources have been duly cited and acknowledged, and any content not personally created by me has been clearly indicated.

Reutlingen, 15th April 2024

Lu Fan

8. Author Contribution

Publication 1. Evaluation of Injectable Composite Material Comprising Biphasic Bone Substitutes and Crosslinked Collagen

Advanced Engineering Materials, 2023, 2300508.

The conceptualization of the study was performed by Dr. Mike Barbeck, Dr. Xin Xiong, and Lu Fan.

The formal analysis was done by Lu Fan, and Dr. Ole Jung.

The investigation was carried out by Lu Fan, Yanru Ren, Dr. Claus Burkhardt, and Prof. Reinhard Schnettler.

Resources were provided by Dr. Xin Xiong, Dr. Mike Barbeck and Dr. Steffen Schröter.

The manuscript was written and prepared by Lu Fan.

Review and editing of the manuscript were performed by Dr. Xin Xiong.

Visualization was carried out by Lu Fan.

The supervision was achieved by Dr. Xin Xiong, Prof. Reinhard Schnettler and Prof. Katja Schenke-Layland.

Dr. Mike Barbeck and Dr. Xin Xiong were involved in the funding acquisition and responsible for the project administration.

Publication 2. Deciphering UVA/Riboflavin Collagen Crosslinking: A Pathway to Improve Biomedical Materials

Advanced Functional Materials. 2024, 2401742.

The conceptualization of the study was performed by Lu Fan, Dr. Mike Barbeck, Dr. Xin Xiong, and Prof. Katja Schenke-Layland.

The formal analysis was done by Lu Fan, Dr. Ole Jung, Markus Herrmann, Marina Shirokikh, Dr. Sanja Stojanovic, and Dr. Stevo Najman.

The investigation was carried out by Lu Fan, Markus Herrmann, Marina Shirokikh, Fabian Körte, and Dr. Xin Xiong.

Resources were provided by Dr. Xin Xiong, Dr. Mike Barbeck and Prof. Katja Schenke-Layland.

The manuscript was written and prepared by Lu Fan.

Review and editing of the manuscript were performed by Dr. Xin Xiong, Markus Herrmann, Marina Shirokikh, Dr. Mike Barbeck and Prof. Katja Schenke-Layland.

Visualization was carried out by Lu Fan and Marina Shirokikh.

The supervision was achieved by Dr. Xin Xiong, and Prof. Katja Schenke-Layland.

Dr. Xin Xiong and Dr. Mike Barbeck was responsible for the project administration.

Dr. Mike Barbeck, Dr. Xin Xiong, and Prof. Katja Schenke-Layland were involved in the funding acquisition.

Publication 3. Encapsulated vaterite-calcite CaCO₃ particles loaded with Mg²⁺ and Cu²⁺ ions with sustained release promoting osteogenesis and angiogenesis

Frontiers in Bioengineering and Biotechnology, 2022, 10: 983988.

The conceptualization of the study was performed by Dr. Xin Xiong, Lu Fan and Dr. Fabian Körte.

The formal analysis was done by Lu Fan, Dr. Claus Burkhardt, and Dr. Fabian Körte.

The investigation was carried out by Lu Fan, Dr. Fabian Körte, Dr. Claus Burkhardt, Alexander Rudt, Dr. Ole Jung, and Dr. Xin Xiong.

Resources were provided by Dr. Xin Xiong, and Dr. Mike Barbeck.

The manuscript was written and prepared by Lu Fan.

Review and editing of the manuscript were performed by Dr. Xin Xiong, and Dr. Mike Barbeck.

Visualization was carried out by Lu Fan.

The supervision was achieved by Dr. Xin Xiong and Prof. Katja Schenke-Layland.

Dr. Mike Barbeck and Dr. Xin Xiong were involved in the funding acquisition and responsible for the project administration.

9. Acknowledgements

I might have begun with "time flies," yet the reality is, finally, finally I have arrived at this moment. It is only in drafting these acknowledgments that I sense the journey's culmination. These past three years and five months have seemingly passed in an instant, but reflecting on those twelve hundred days, every single one stands out vividly. I am profoundly grateful to myself and to everyone who has supported and nurtured my growth along the way.

Foremost, I extend my heartfelt thanks to my primary supervisor, Prof. Katja Schenke-Layland, an extraordinary female scientist, who has been an unwavering source of inspiration. I am immensely grateful for the opportunity she gave me to study in Tübingen, this enchanting university town, and to pursue my PhD project at the Faculty of Medicine and NMI Natural and Medical Sciences Institute at the University of Tübingen, surrounded by a rich academic atmosphere. Her encouragement during my initial struggles and her invaluable, constructive guidance on my project have been pivotal.

I would also like to express my profound gratitude to another two doctoral committee members, Prof. Ulrich Rothbauer and Prof. Peter Loskill for their invaluable guidance and support throughout my PhD studies. Their insightful feedback on my annual reports and their scholarly advice have significantly contributed to the rigor and quality of my research.

Special appreciation goes to my project supervisor, Dr. Xin Xiong, for his significant support throughout my PhD journey. Our endless discussions, debates, and occasional disagreements, though challenging at times, fostered my growth, deepening my critical thinking and exploration. Special gratitude is also due to another important person, Xin's wife, Cuifeng Zhao, and their two delightful daughters, who became my family away from home. Their warmth and selfless care have meant a lot to me.

I am thankful for my wonderful colleagues at NMI, especially Markus Herrmann, Fabian Körte, Anastasia Binder, and Marina Shirokikh, for their endless kindness and support. Their presence made my research journey

smoother and less lonely. Thankfully, it's not yet time for farewells, softening the sadness of parting.

I owe a debt of gratitude to my dear parents for respecting my freedom to choose my own path and for instilling in me the independence and responsibility to make my own decisions from a young age. The resilience—or perhaps stubbornness—I observed and learned from them has empowered me to face and overcome numerous challenges. My brother and sister-in-law also deserve my great thanks for their unwavering support and encouragement as I navigated the unknown and ventured into new realms.

I extend my heartfelt gratitude to my partner, Tarjar Bunke Risstad, whose unwavering support and understanding have been the beacon guiding me through periods of uncertainty and despair. It was Tarjar who rekindled my passion for discovery, who helped me find back my ability to express and stand on myself with confidence during moments of doubt and despondency, and who reminded me of the strength that lies in genuine curiosity. May we always carry this enthusiasm for our future adventure, unafraid of challenges and changes.

Lastly, I thank myself for persevering through the ups and downs of PhD life to reach this milestone. This is not the endpoint but rather a new beginning. I hope to continue facing the unknown fearlessly, to remain curious in my explorations, and to seek knowledge humbly. I also extend my thanks to everyone who has journeyed through this path, those who are currently on it, and everyone who has made or continues to make an effort.

10. Appendix

10.1 Ethical Statement

The conduct of all animal experiments involved in this research was rigorously overseen by Dr. Sanja Stojanovic, Dr. Stevo Najman, and Dr. Mike Barbeck, with explicit authorization granted by the Local Ethical Committee of the Faculty of Medicine at the University of Niš, Serbia. This approval was contingent upon the consent from the Veterinary Directorate of the Ministry of Agriculture, Forestry, and Water Management of the Republic of Serbia, under the approval number 323-07-01762/2019-05/9, issued on 01 March 2019. Data analysis and visualization tasks were undertaken by Lu Fan and Dr. Mike Barbeck.

10.2 Proof of Author Contribution Agreement


Declaration of Contributions of All Authors

Herewith I, Lu Fan declare, that I have contributed to the major part of the following publications:

1. Fan, L., Körte, F., Rudt, A., Jung, O., Burkhardt, C., Barbeck, M., and Xiong, X., "Encapsulated vaterite-calcite CaCO₃ particles loaded with Mg²⁺ and Cu²⁺ ions with sustained release promoting osteogenesis and angiogenesis." *Frontiers in Bioengineering and Biotechnology*, 10 (2022): 983988. Impact factor: 5.7

The authors contributed to this publication as indicated in the following table (indicated in %):

Contribution	Lu Fan, Author 1	Fabian Körte, Author 2	Alexander Rudt, Author 3	Ole Jung, Author 4	Claus Burkhardt, Author 5	Mike Barbeck, Author 6	Xin Xiong, Author 7
Research concept	50%	5%		10%		15%	20%
Selection of methods	60%	5%	5%	5%	10%		15%
Data acquisition	100%						
Data analysis	80%				10%		10%
Interpretation of results	80%					5%	15%
Preparation of Manuscript	80%						20%

Signature of the doctoral candidate:

Lu Fan (Author 1)

As supervisor, I agree with the declarations by the candidate:

Prof. Katja Schenke-Layland

As corresponding authors, we agree with the declarations by the candidate:

Dr. Dr. Mike Barbeck

Dr. Xin Xiong (Author

As co-authors, we agree to the declarations above:

Dr. Fabian Körte (Author 2)

Alexander Rudt (Author 3)

Dr. Dr. Ole Jung (Author 4)

Dr. Claus Burkhardt (Author 5)



2. Fan, L., Ren, Y., Burkhardt, C., Jung, O., Schnettler, R., Barbeck, M., & Xiong, X.
 "Evaluation of Injectable Composite Material Comprising Biphasic Bone
 Substitutes and Crosslinked Collagen." *Advanced Engineering Materials*, 2023,
 2300508. Impact factor: 4.1

The authors contributed to this publication as indicated in the following table (indicated in %).

Contribution	Lu Fan, Author 1	Yanru Ren, Author 2	Claus Burkhardt, Author 3	Ole Jung, Author 4	Reinhard Schnettler, Author 5	Mike Barbeck, Author 6	Xin Xiong, Author 7
Research concept	50%			10%		20%	20%
Selection of methods	60%	5%	10%		5%	10%	10%
Data acquisition	75%		5%	10%		10%	
Data analysis	75%	5%				10%	10%
Interpretation of results	80%					10%	10%
Preparation of Manuscript	80%					10%	10%

Signature of the doctoral candidate:

Lu Fan (Author 1)

As supervisor, I agree with the declarations by the candidate:

Prof. Katja Schenke-Lay

As corresponding author, I agree with the declarations by the candidate:

Dr. Dr. Mike Barbeck (Author 6)

Dr. Xin Xiong (Author 7)

As co-authors, we agree to the declarations above:

Yanru Ren (Author 2)

Dr. Claus Burkhardt (Author 3)

Dr. Dr. Ole Jung (Author 4)

Prof. Reinhard Schnettler (Author 5)



3. Fan, L., Herrmann, M., Körte, F., Barbeck M., Xiong X., Schenke-Layland, K. "Exploring the Mechanism of UVA/Riboflavin Crosslinked Collagen for Biomedical Applications", *Under Submission*

The authors contributed to this publication as indicated in the following table (indicated in %):

Contribution	Lu Fan, Author 1	Markus Herrmann, Author 2	Fabian Körte, Author 3	Mike Barbeck, Author 4	Xin Xiong, Author 5	Katja Schenke- Layland, Author 6
Research concept	50%	5%	5%	10%	15%	15%
Selection of methods	60%	10%		10%	15%	5%
Data acquisition	80%	10%		10%		
Data analysis	80%	5%		5%	5%	
Interpretation of results	80%			5%	10%	5%
Preparation of Manuscript	80%				5%	5%

Signature of the doctoral candidate:

Lu Fan (Author 1)

As supervisor, I agree with the declarations by the candidate:

Prof. Katja Schenke-Layland (Author 6)

As corresponding authors, we agree with the declarations by the candidate:

Dr. Xin Xiong (Author 5) ✓

Prof. Katja Schenke-Layland (Author 6)

As co-authors, we agree to the declarations above:

Markus Herrmann (Author 2)

Dr. Fabian Körte (Author 3)

Dr. Dr. Mike Barbeck (Author 4)